ProQuest LLC.
789 East Eisenhower Parkway
P.O. Box 1346
Ann Arbor, MI 48106 – 1346

Evaluation of Tests for Porosity and Defects in PVD and Electroless Coatings

Petra Ernst

A thesis submitted in partial fulfilment of the requirements of Sheffield Hallam University for the degree of Master of Philosophy

December 1995

Collaborating Organisation: A.T. Poeton (Gloucester Plating) Ltd

Sponsoring Establishment: Material Research Institute Sheffield Hallam University

Statement

The research was carried out during the period from October 1994 to December 1995 in the Material Research Institute and the School of Engineering at Sheffield Hallam University.

Post-Graduate courses in Surface Engineering at the School of Engineering and Crystallography, Surface Engineering Part I (PVD-coatings) and Electron Microscopy and X-Ray Techniques Part I (Electron Microscopy) were attended and the appropriate examinations passed in the Material Research Institute. In addition research seminars organised by the School of Science and the Material Research Institute / Sheffield Hallam University were attended.

I would like to give special thanks to Dr. G.W. Marshall for his guidance, support and encouragement during this course. I also would like to thank Dr. I. Wadsworth for his contribution and assistance. Furthermore special thanks go to Anthony Earnshaw for his effort and support, especially throughout the experimental period.
I would like to thank the staff of the Material Research Institute and School of Engineering for their help and support.

The results obtained and the theories developed are to the best of my knowledge original, except where references are made to the work of others. No part of this thesis has been submitted for a degree at any other university.

Petra Ernst
December 1995

Abstract

The porosity of electroless nickel, (TiAl)N, TiN and CrN PVD coatings on mild steel having different surface roughnesses was investigated using porosity/corrosion tests. The tests used were the neutral salt spray test, ferroxyl test, sulphur dioxide test and the copper cementation test. Additionally the effect of radii on the corrosion resistance and porosity of electroless nickel coatings was examined. Electron optics, GDOES and ICP were used to evaluate the limits of their applicability to extend porosity/corrosion tests used on coated specimen. A marking technique was developed which enabled individual features on coated surfaces to be examined by SEM before and after porosity/corrosion tests.

The neutral salt spray test was used to rank electroless nickel coated mild steel specimens according to their corrosion resistance. However the test did not provide any detailed information on the porosity of the coatings. The ferroxyl test was found to be applicable to all the coatings on mild steel investigated but only macrodefects could be observed. With the help of the SO_2 test the origin of defects in electroless nickel coatings was examined using SEM techniques. Furthermore the test was used to observe the formation of corrosion products at defect sites as a function of exposure time. A ranking according to the corrosion resistance depending upon defects present was made. The SO_2 test was not applicable to (TiAl)N, TiN and CrN PVD coatings since the defect density in these coatings was too high and any corrosion products formed during the test spread over their surface thus hiding smaller defects as a result of the test's high sensitivity. In copper cementation tests on PVD coatings, copper did not preferentially precipitate at large defect sites but precipitated randomly on the coated surface. The amount of copper precipitated, its distribution and size was used to provide information concerning the defect density in PVD coatings. A mechanism has been suggested which explains how copper is deposited on the top of coatings rather than in the bottom of defects during cementation tests. The relationship between porosity, substrate roughness and coating thickness has been established, and it is suggested how the relationship might be used in industry as a quality control tool.

Introduction and Objectives

Protective metal coatings are used to extend and improve the industrial application and service lifetime of components. Therefore the main purpose of protective metal coatings is to increase the wear and corrosion resistance of the components.

In corrosive environments protective metal coatings act as a barrier between the corrosive medium and the substrate metal. Depending upon the nobility of the coating with respect to the substrate, the coatings provide either cathodic or anodic protection. Coatings which are less noble than the substrates corrode galvanically and hence provide sacrificial cathodic protection at defects in the coating. Coatings with a greater corrosion resistance than the substrate provide protection by forming a barrier between the corrosive environment and the substrate. Defects in such coatings give rise to galvanic corrosion of the substrate which can lead to either flaking of the coating or its failure due to catastrophic pitting at isolated spots. Hence the corrosion resistance of such substrate/coating systems is mainly determined by the integrity of the coatings, particularly in the case of thin coatings, where the possibility of defects extending through the whole coating is high.

The detection and evaluation of defects in coatings, their origin and development, is of great practical interest to the coater as well as to the user.

Most industrial porosity tests are standardised and relate to the particular type of coating being examined e.g. see BS 5466-1979 and ASTM B765-1993. Often standard porosity/corrosion test procedures allow variations, by agreement between the coater and user, in the way the results are to be evaluated in particular cases .

Porosity tests can be divided into various classes, i.e. long term and accelerated or direct and indirect. Indirect tests such as those involving electrical/electrochemical methods are often very complicated and are not always suitable for use in industrial testing. Furthermore these tests do not usually provide information concerning both the size and distribution of any defects present. In fact the presence of defects is often inferred from the measurement of a current, rather than from direct observation of the defects. Direct tests involve chemical reaction of the test medium with the exposed substrate. The results of such reactions are visible to the naked eye, sometimes assisted by a magnifying glass, due to the presence of coloured corrosion products on the corroded surface e.g. as in the sulphur dioxide test [1] or ferroxyl tests [2]. A problem with these tests is that the corrosion products initially formed at defect sites in the coating may subsequently spread out. Then the apparent size of the defect observed, as represented by the corrosion products, appear to be larger than their true size. Another

problem with such test is often the lack of comparability in the results obtained using different tests, or associated with different test solutions. These difficulties may relate either to a test carried out on different substrate/coating systems or to a test done on the same substrate/coating system but using different test solutions. Thus a substrate/coating system may perform well under one set of test conditions and poorly under another test.

The ***objective of this study*** was to investigate different kinds of porosity/corrosion test as applied to electroless nickel and PVD coatings ((TiAl)N, TiN and CrN) on mild steel substrate. The aim of the work was to demonstrate the limits and accuracy of the tests investigated in both their ´standardised` forms and as modified in the light of experiences gained in their use. An additional aim of the work was to investigate whether modern electron optical techniques could be successfully employed to extend the usefulness of standard tests. It was thought such an extension might form a valuable tool in understanding how pores and defects in coatings are formed and lead to service failure. To this end, and to fully evaluate the full scope of the tests, coatings of different thicknesses on substrates having different surface roughnesses were studied.

Contents

1 Literatur Review

1.1 Corrosion and Porosity of Substrate/Coating Systems

The exposure of a component to a corrosive environment can lead to uniform or local corrosion attack. The latter is the most dangerous form of corrosion because the lifetime of the component cannot easily be estimated. Such estimations are usually made by calculating the weight loss of the coating per unit area over a period of time assuming that the protective coating corrodes uniformly.

The corrosion resistant of coated components is mainly determined by their metallurgical composition and structure, prefinishing of the substrate material, nature of the corrosive environment and the kind and thickness of the coating as well as its structure, integrity and any post coating treatment received. Metallic coatings can be anodic or cathodic with respect to the substrate. Their application depends upon the function which the coating is providing. Anodic coatings provide cathodic protection of the substrate at breaks in the coating. Cathodic coatings act as a barrier between the environment and the substrate. Consequently breaks, such as pores, in cathodic coatings may lead to corrosion of the substrate in a corrosive environment. Sometimes pores are formed during the coating process as a result of substrate surface defects as will be discussed in sections 1.2.5 and 1.3.4. The porosity of coatings can reflect failures in the coating process and can therefore be used as a parameter to control and monitor the coating process.

The porosity of a coating can be defined as the ratio of the exposed base material to its total area or the number of defects per unit area.

Large defects can be detected by visual examination. However in many cases the defects are microscopically small and special corrosion tests are needed to detect them. Hence, it is useful to divide the porosity of coatings into two broad categories, those showing only intrinsic porosity and those showing gross defects in addition to the intrinsic porosity [2]. The intrinsic porosity indicates small deviation from ideal coating conditions and/or substrate surface conditions, and generally shows an inverse relationship with coating thickness for coatings produced by wet finishing processes. The gross defects may result from the coating of a dirty substrate surface or mechanical damage. Examples of such defects are mechanical damage to the coating through mishandling or wear resulting in the presence of networks of micocracks. The size of gross defects is usually greater than that of intrinsic pores [2]. Defects may extend throughout the coating and act as a pathway for a rapid corrosion attack, especially if the

coating is more noble than the substrate and the potential difference between them is high. With this combination a small anodic area is associated with a large cathodic area. Hence the anodic current density is high and leads to a rapid corrosion attack of the substrate. Figure 1 illustrates diagrammatically the difference between aqueous corrosion of a cathodic and an anodic coating (top and bottom respectively) in contact with a substrate.

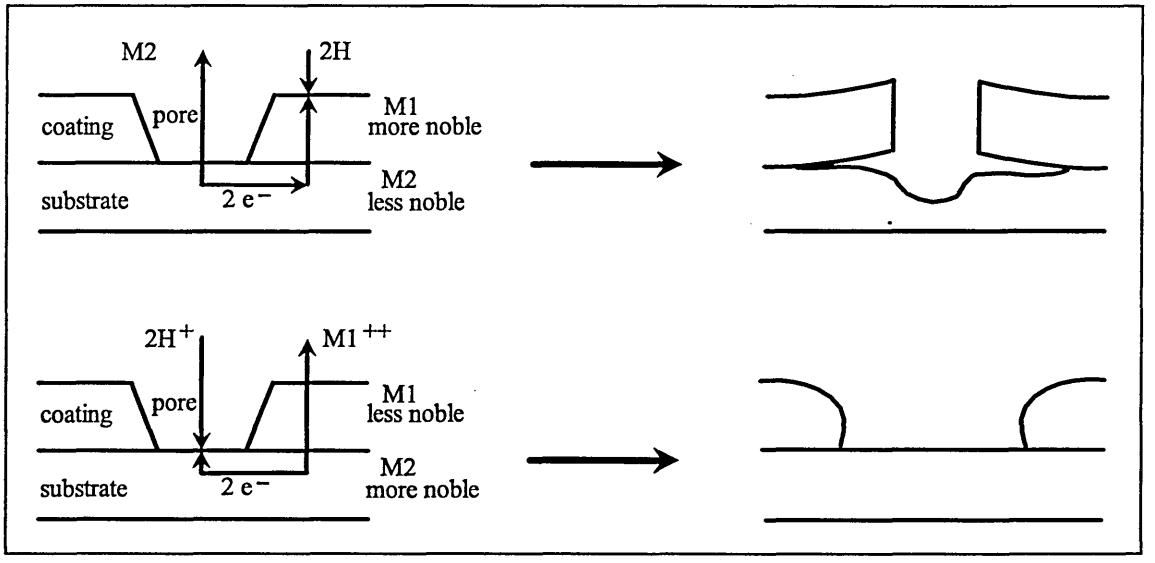

Figure 1 Galvanic effects produced at pores in a coating. On the top: A pore in a cathodic coating leads to a corrosion attack of the substrate and flaking of the coating. Bottom: The anodic coating protects the substrate [3]

The driving force for corrosion reaction is the difference in the potential between the two metals. The corrosion resistance of materials in general depends upon the corrosive environment, as well as any bimetallic contact present in a component exposed to the environment.

Corrosion behaviour in basic coating systems, i.e. those having a single coating on a substrate, resulting from porosity and defects, may be reduced by a number of strategies.

In the case of tradition coatings, i.e. electroplated and paint coatings etc., the simplest way to reduce corrosion is to increase the coating thickness thereby reducing its porosity. This approach is not so readily applicable to some PVD coatings which can only be produced as thin coatings e.g. TiN. An alternative strategy in such cases is to place a corrosion resistant intermediate layer between the substrate and the coating. Thus, intermediate layers of electroless nickel or nickel palladium alloy have been used with TiN coatings [4, 5, 6, 7]. Finally passivation of either the substrate, prior to

coating, or the coating itself has been attempted as a general method of increasing the corrosion resistance of coating systems [8, 9].

1.1.1 Electrochemical Aspects

The possibility always exists that when a metal is immersed in a solution then atoms from the metal will pass into solution as ions in accordance with the reaction:

$$Me - ne^{n+} \rightarrow Me^{n+}$$

This is termed the anodic reaction and is central to corrosion. Thus when iron or mild steel rusts the initial reaction involves the dissolution of ferrous ions, i.e.

$$Fe - 2e^{-} \rightarrow Fe^{2+}$$

Further reactions in solution result in the initial precipitation of this iron as ferrous hydroxide which then undergoes further reaction to produce hydrated ferric oxide ($Fe_2O_3 * xH_2O$) familiar to us as red rust.

The electrons 'freed' at the anode cannot accumulate and are conducted through the metal(s) surface to cathodic regions where they are involved in a suitable cathodic reaction. The actual cathodic reaction involved depends upon the corrosive environment but is usually one of the following :

i) Hydrogen evolution

$$2H^{+}_{(aq)} + 2e^{-} \rightarrow H_{2(g)}$$

ii) Oxygen reduction (acid solution)

$$O_{2(g)} + 4H^{+}_{(aq)} + 4e^{-} \rightarrow 2H_2O$$

iii) Oxygen reduction (basicly , neutral solution)

$$O_{2(g)} + 2H_2O + 4e^{-} \rightarrow 4OH^{-}_{(aq)}$$

The overall corrosion reaction involves two half reactions, that taking place at the anode (associated with a negative potential), together with that taking place at the cathode (associated with a positive potential, i.e. noble). Combining the two reactions involved

gives the overall initial corrosion reaction. Thus the initial reaction for the corrosion of iron or mild steel in a neutral solution can be presented as:

Anodic reaction	$2Fe - 4e^- \rightarrow 2Fe^{2+}_{(aq)}$
Cathodic reaction	$O_{2(g)} + 2H_2O + 4e^- \rightarrow 4OH^-_{(aq)}$
Initial corrosion reaction	$2Fe + O_{2(g)} + 2H_2O \rightarrow 2Fe(OH)_{2(s)}$

1.1.2 Pourbaix Diagrams

Pourbaix diagrams are often used to predict the behaviour of a metal in water. The lines in the Pourbaix diagrams represent the equilibrium potential dependency upon the pH-value of a metal in a solution, based on thermodynamic data and the Nernst equation. Superimposed upon the diagrams are the lines representing the hydrogen and oxygen reactions under equilibrium conditions (figure 2).

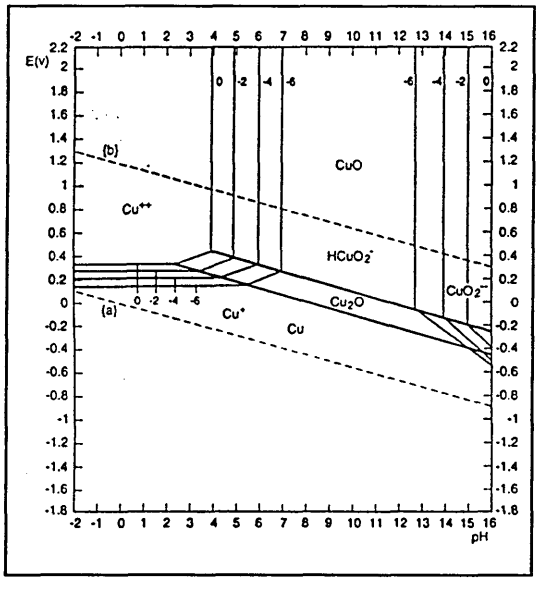

{a} $2H_2O + 2e \Leftrightarrow H_2 + OH^-$

$E = -0.059 * pH$

{b} $O_2 + 2H_2O + 4e^- \Leftrightarrow 4OH^-$

$E = 1.23 - 0.059 * pH$

Figure 2 Potential-pH-diagram for copper [10]

The diagrams represent the metallic species stable at 25 °C and different potentials under different conditions of acidic. The solubility limit is taken as 10^{-6} mol/l when

constructing these diagrams. In applying these diagrams it is assumed, that an equilibrium between the different phases exists, which is not always true. Some metals undergo a passivation process, which slows their corrosion rate and thus gives them protective properties which are disregarded in these diagrams. A prediction of the kinetic of a reaction, i.e. whether it is slow or fast, cannot be made from the diagrams. Another problem is that the diagrams only exist for relatively simple solutions which do not contain complexes which thus limit their usefulness.

1.1.3 Porosity/Corrosion Tests

Porosity/corrosion tests are used to highlight all pores which are sources of corrosion action. Until now there have been no methods available which detect and satisfactorily describe totally the porosity of coatings [11, 12, 13, 14].

Defects in coatings can be investigated by SEM observations which do not take subsurface defects into consideration [15, 16]. Additionally a complete analysis of the defects present in a coating is not always easy and depends upon the magnification used.

A summary of porosity tests which are most used in industry is given in [11, 14, 17, 18, 19, 20]. Two types of tests are generally applied, outdoor long term field or site tests, and accelerated tests. Outdoor exposure tests for example are conducted over long periods and the conditions are not reproducible. However these tests do show the corrosion behaviour of a component in its actual working environment. Although such tests have the advantage that they measure the rate of the type of corrosion found in service, which may not be the case in accelerated tests, they do take a long time to complete.

The choice of the accelerated porosity test depends upon what kind of defects are expected to be present in a given coating. For measuring the intrinsic porosity of electrodeposits the ferroxyl and the CASS test are preferred and for gross defects the hot water test [2] is used.

Where the coating is cathodic with respect to the substrate under the test conditions then the test should show the following characteristics if optimum results are to be obtained [14].

i) Effective penetration of pores by the fluid .
ii) Creation of a visible corrosion product .
iii) Whilst the product from the smallest pore should spread enough to be visible, that from the largest should not produce general staining .

iv) During the test corrosion should not produce any defects or modify the size and shape of pores present.

Porosity tests can be divided into qualitative and quantitative methods. Qualitative tests, for example the salt spray test, exposes the samples to a fluid (gas or liquid) which penetrates through the defects and attacks the substrate over time. The corrosion products formed, or the corrosion attack itself, is visible to the naked eye or with the use of a microscope. Some tests use special chemicals which combine with the corrosion products to form coloured spots, as for example in the ferroxyl test. In general gel and liquid immersion tests are suitable for detecting gross defects only since surface tension and viscosity of the corrosive media reduce their penetration into defects. Hence these tests often show a low porosity. In comparison, gaseous tests using a corrosive vapour or gas show high porosity since the vapour or gas is able to penetrate even 'narrow' defects more easily than liquids or gels.

The defects can be counted and related to the area examined. Another possible method of evaluation is to rank the surfaces according to the degree of corrosion attack, or their weight losses, following the test. However the comparison of different porosity/corrosion tests used on one type of coating is not always possible, as some investigators have shown [12, 21, 22], since the corrosion attack depends upon the corrosive environment and the evaluation method used.

Some quantitative methods measure the electrochemical behaviour between the coating and the substrate [23, 24, 25]. The porosity can be measured in three ways [26]:

i) Measurement of the corrosion potential, E_{corr}.
ii) Measurement of the corrosion current, I_{corr}.
iii) Measurement of the polarisation resistance, $\Delta I/\Delta E$.

These methods are often very complex, involve the use of expensive equipment which can only be operated by highly trained workers, and do not provide information on pore size and distribution.

Some of the qualitative tests used more frequently are described in the next paragraphs.

Salt Spray Tests

Three different salt spray tests exist:

- NSS-Test (Neutral Salt Spray Test)
- AASS-Test (Acetic Acid Salt Spray Test)
- CASS-Test (Copper-Accelerated-acetic acid Salt Spray Test)

Details of these tests have been described [27].

In these tests the samples to be tested are hung in a salt spray cabinet and exposed to a very fine mist. During the test the samples are not permitted to dry and no drops of the test solution should settle on the test samples. For the **NSS-Test** a 0.5 % solution of sodium chloride having a pH-value between 6.5 and 7.2 is used. The NSS-Test is applied to certain anodic and cathodic coatings. For the **ASS-Test** an addition of glacial acetic acid is made to the salt spray solution until its pH-value is between 3.1 and 3.3. This test is especially useful in the testing of decorative coatings such as those consisting of multilayers of copper+nickel+chromium. The solution used for the **CASS-Test** contains hydrated copper II chloride ($CuCl_2 * 2H_2O$). Glacial acetic acid is used to adjust the pH-value to within a range of 3.1 to 3.3. This test is more severe than the NSS test. The CASS-Test is used for decorative coatings and to evaluate the intrinsic porosity of electroless nickel coatings.

According to Yajima et al., the results of the salt spray test used on electroless nickel coatings cannot be compared with those from outdoor exposure tests since the specimens are always wet in the salt spray test and the corrosion can be concentrated at certain points [28]. This effects can also be seen with other coatings

Ferroxyl Tests

Apart from the ferroxyl test described in ASTM B765-1993 and BS 4758-1986 numerous similar, but modified, ferroxyl tests are available. The standards lay down three solutions which are used by dipping a special test paper, successively, in the solutions, at specific points throughout the test. Solution A contains sodium chloride and white gelatine, solution B contains sodium chloride and a non-ionic wetting agent and solution C potassium hexacyanoferrate (III). The paper is soaked in solution A and dried. Then the paper is immersed in solution B and firmly pressed onto the sample surface. After ten minutes the paper is removed and immediately dipped in solution C which results in the formation of cyanoferric complexes, visible as blue spots. Saubestre

and Hajdu used 5 % HCl (37 %) instead of the standard solution B [21]. Bergmann et al. used only one solution containing 10 g/l potassium hexacyanoferrate (III) and 20 g/l sodium chloride [12]. The resulting blue colouration then occurred directly on the sample surface. This work postulated that the test solution progressively opens and produces new pores. A similar test, the authors called it ferricyanid test, used a solution containing 6 % sodium chloride and 0.05 % potassium hexacyanoferrate (III). A filter paper is dipped in the solution and then pressed on the sample surface for five minutes. Tomlinson and Mayor used this test to assess porosity in a qualitative way [29]. A further variation of the ferroxyl test solution contains $K_3Fe(CN)_6$, $K_4Fe(CN)_6*3H_2O$ and NaCl [30]. A filter paper is soaked in the reagent and laid upon the sample surface, the number of the blue spots on the filter paper is then measured.

The basis of all ferroxyl tests is the formation of blue iron cyanoferrate complexes which have a low solubility and are therefore precipitated at pore site. In all variations of the test the reagent from solution B is absorbed into pores by capillary force and attacks the iron substrate to produce a mixture of ferrous and ferrics ions. These cations diffuse to the surface of the filter paper and then, if the paper is dipped in solution C, they react with the potassium hexacyanoferrate to produce blue iron complexes according to the following equations.

$$4Fe^{2+} + 4[\,Fe^{(3+)}(CN)_6]^{3-} \rightarrow [Fe^{(2+)}(CN)_6]^{4-} + Fe_4^{(3+)}[Fe^{(2+)}(CN)_6]_3\downarrow$$

or

$$4Fe^{3+} + 3[Fe^{(2+)}(CN)_6]^{4-} \rightarrow Fe_4^{(3+)}[Fe^{(2+)}(CN)_6]_3\downarrow$$

The final blue products are the same when it is produced from either ferrous or ferric cations originating from pore sites.

A modified ferroxyl test, using only potassium ferricyanide, was used by Nazarenko et al. to correlate the number of pores completely penetrating the coating to the results of electrochemical tests on nitride coatings [31]. According to Uergen the ferroxyl test gives only a rough indication of the macrodefects present in coatings [32].

Sulphur Dioxide Tests

These tests were developed for predicting the corrosion behaviour of materials exposed in industrial areas in which a high level of sulphur dioxide exists. Some of these tests may also be used to detect defects in coatings. Sulphur dioxide tests can be divided into two main categories, those involving condensation, e.g. the Kesternich test [33] and those without condensation, e.g. the Clark and Leeds test [34].

In the Kesternich test [17, 33], the samples are exposed to an atmosphere containing sulphur dioxide gas in a Kesternich chamber. This special chamber also contains distilled water. The Kesternich test operates at a temperature of 40 °C. After the samples have been exposed to a relative humidity of 100 % for eight hours they are left in the chamber under the test conditions for another sixteen hours. The Kesternich test gives information only relating to the corrosion resistance of a material or a coating system to atmospheres containing sulphur dioxide. Prediction of service lifetime cannot be made from Kesternich tests. This test is not suitable for the detection of defects in coatings since the corrosion products formed during the test spread over the surface and thus mask the precise size and position of defects. According to Tang et al. it is not possible to distinguish between corrosion resulting from low porosity in electroless nickel coatings and that resulting from general corrosion of the coating itself using a moist SO_2 test [35]. However the test is sometimes used to detect defects in electroless nickel coatings [15].

In the Clarke and Leeds test coated samples are placed in a desiccator which contains a mixture of sodium thiosulphate, sulphuric acid and distilled water [1]. This test was modified by Clark and Sansum using the same solution but at a higher temperature, 60 °C [36]. Both tests are included in BS 6670:Part 2-1986. In the presence of sulphuric acid the sodium thiosulphate decomposes mainly to water, sulphur dioxide and sodium sulphate and generates a fixed concentration of sulphur dioxide in the atmosphere above the solution. The sulphur dioxide concentration in the atmosphere is about 10 % and can be altered by altering the sulphuric acid concentration since the sulphur dioxide is soluble in both water and sulphuric acid. The residual solution comes to equilibrium with an atmosphere having a relative humidity of 86 %. The atmosphere thus obtained is very stable and only slightly effected by changes in room temperature. Since no condensation occurs and the corrosion products, mainly sulphides, do not spread over the surface of the exposed coated sample, the test is used to make defects visible as a result of the formation of dark brown spots of iron sulphides. Since the reactions occurring are electrochemical in nature only coated samples in which the coatings are more noble than the substrate can be tested.

Copper Cementation Tests

Cementation is defined as the precipitation of a metal from a solution of its salt onto a less noble metal. With this technique it is possible to show defects of noble coatings on less noble substrates [32, 37].

Cementation reactions can be described in terms of two half reactions, one cathodic and one anodic, in the same way as described for corrosion reactions above (section 1.1.1). Thus solid copper is precipitated onto the surface of mild steel exposed to a solution containing the more noble metal copper. Iron from the surface of the mild steel passes into solution, i.e. corrodes, simultaneously copper precipitation occurs and the whole process can be represented as:

Anodic reaction $Fe_{(s)} - 2e^- \rightarrow Fe^{2+}_{(aq)}$

Cathodic reaction $Cu^{2+}_{(aq)} + 2e^- \rightarrow Cu_{(s)}$

Cementation reaction $Fe_{(s)} + Cu^{2+}_{(aq)} \rightarrow Fe^{2+}_{(aq)} + Cu_{(s)}$

Whether or not cementation will occur between a solid metal immersed in a solution containing a second metal depends to a large extend upon the relative values of the electrode potentials of the two metals involved. If the metal in solution is more noble than the solid metal then cementation may occur. Some standard electrode potential which are of interest to the present study are summarised in table 1

Table 1 Standard potentials of elements important to this work [38]

Metal	Standard potential E° volt vs. SHE
Al / Al^{3+}	-1.66
Ti / Ti^{2+}	-1.63
Cr / Cr^{3+}	-0.74
Fe / Fe^{2+}	-0.44
Cu / Cu^{2+}	+0.33

Hence the following cementation reactions relevant to the present work are possible in theory during cementation tests

$$3Cu^{2+}_{(aq)} + 2Al_{(s)} \rightarrow 2Al^{3+}_{(aq)} + 3Cu_{(s)}$$

$$Cu^{2+}_{(aq)} + Ti_{(s)} \rightarrow Ti^{2+}_{(aq)} + Cu_{(s)}$$

$$3Cu^{2+}_{(aq)} + 2Cr_{(s)} \rightarrow Cr^{3+}_{(aq)} + 3Cu_{(s)}$$

$$Cu^{2+}_{(aq)} + Fe_{(s)} \rightarrow Fe^{2+}_{(aq)} + Cu_{(s)}$$

An additional way in which metal from a solid surface might enter solution, especially in acidic solution, is via a reaction involving hydrogen, e.g.

$$mM_{(s)} + nH^{+}_{(aq)} \rightarrow H_{2(g)} + mM^{n+}_{(aq)}$$

or in the case of mild steel

$$Fe_{(s)} + 2H^{+}_{(aq)} \rightarrow H_{2(g)} + Fe^{2+}_{(aq)}$$

This type of reaction, when occurring in parallel to the cementation reaction, can be very important since it maintains an active rather than an inactive and passivated surface which might hinder the cementation reaction.

Uergen et al. successfully investigated the detection of porosity in TiN and CrN coated carbon steel and ZrB and ZrBN coated steel using copper cementation [32, 37]. These authors used a copper sulphate solution containing 0.1 g/l Cu^{2+} at a pH-value of 1. The test samples were dipped in this solution for 60 seconds at room temperature.

In recent work, the copper cementation technique was used to study the porosity of (TiAl)N coated mild steel [39]. In this work copper sulphate solution was used at two different pH-values (1 and 5.5) and two different exposure times (60 and 300 seconds). The authors discovered that copper precipitation occurred randomly on the surface of the coating and that the amount of precipitation was governed both by the exposure time and solution acidity.

It is useful to consider the Pourbaix diagrams for aluminium, titanium, iron, chromium and for titanium nitride (figures 3 and 4) in order to predict how the relevant metals might behave in copper cementation tests. The diagrams suggest an unreactive layer of TiO_2 is formed on the surface of titanium in highly acidic solution (pH = 1) but that Al, Cr and Fe surfaces are all active and hence corrode in such solutions. In contrast the diagrams suggest that Ti, Al and Cr surfaces are inactive in less acidic

solutions (pH = 5) and that this acidity represents the boundary conditions for the transition from an active to passive behaviour for iron surfaces.

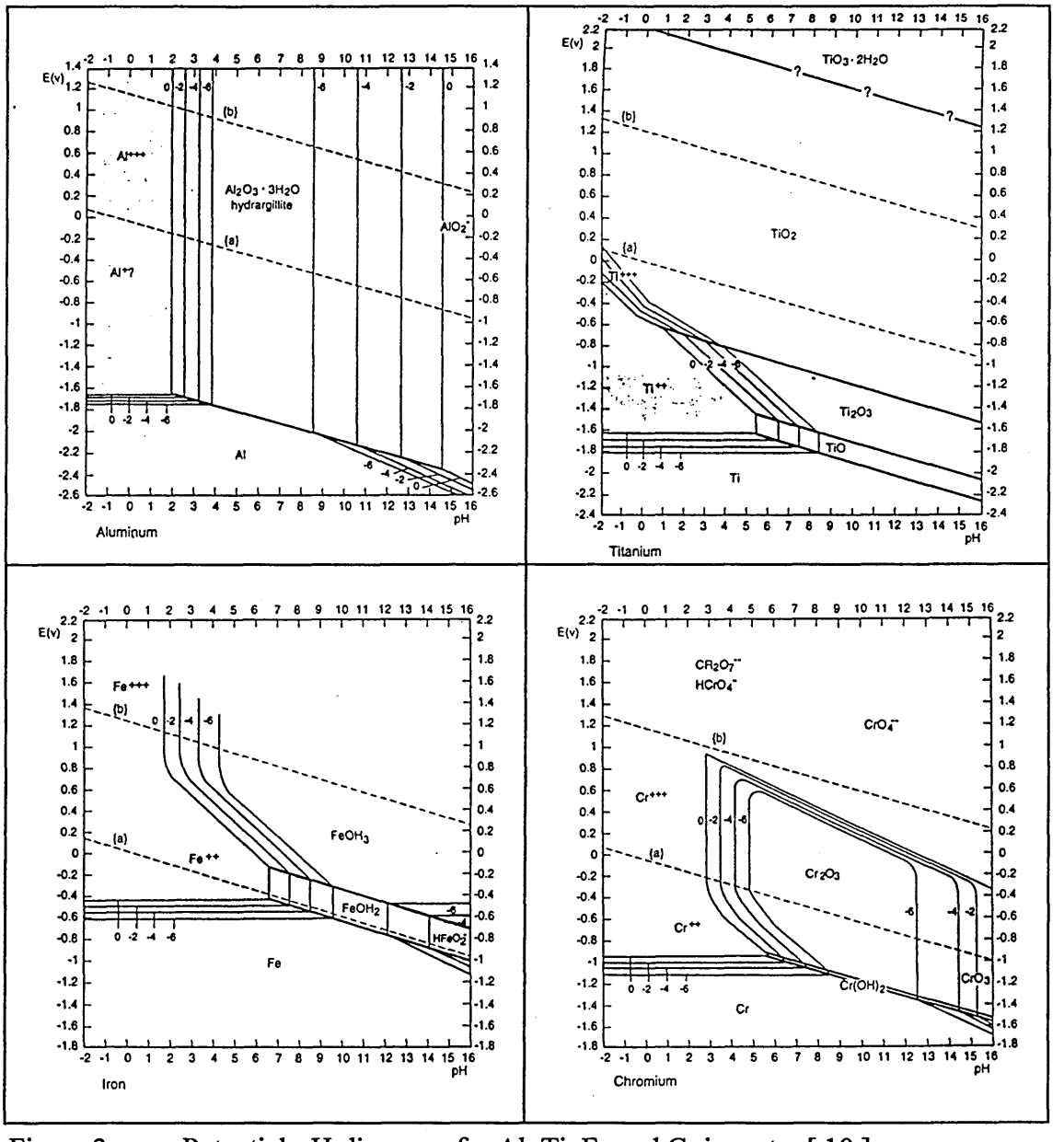

Figure 3 Potential-pH-diagrams for Al, Ti, Fe and Cr in water [10]

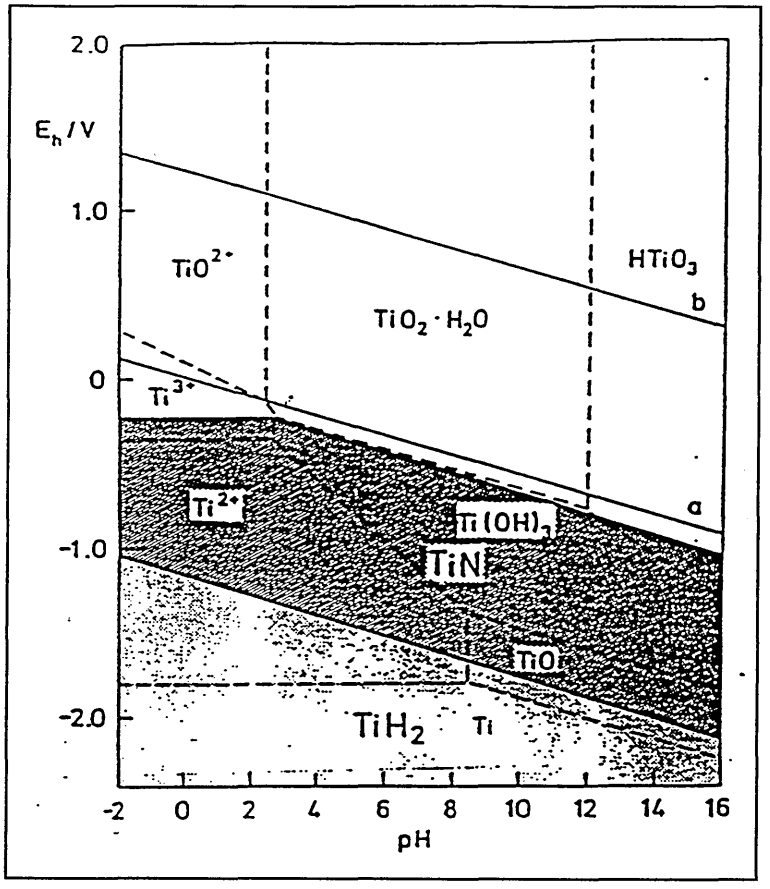

Figure 4 Potential-pH-diagram for TiN in water [7]

Some information is available concerning the actual corrosion behaviour of PVD coatings in acidic solutions. According to Chyou the corrosion resistance of TiN coatings in sulphuric acid strongly depends upon their concentration [40]. TiN dissolves in 0.1 - 16N H_2SO_4 forming titanium oxy cations ($Ti(OH)^{2+}$ and $Ti(OH)_2^{2+}$) and NO_2, NO or N_2 which was observed as brown bubbles. In 20 - 36N H_2SO_4 it was found that the corrosion rate is lower. Ward investigated the corrosion resistance of TiN, (TiAl)N and ZrN coated stainless steel in H_2SO_4 solutions, some containing NaCl additions [41]. Titanium nitride was found to passivate in 1N H_2SO_4 which Ward attributed to the formation of TiO_2 due to the replacement of nitrogen present in the coating by oxygen, as suggested by Milošev and Navinšek [24]. Forsén et al. considered the formation of titanium oxide or hydroxy-oxide layers on TiN coatings in the pH range 1-12 leading to their passivation [7].

Electrographic Tests

In this test a special test paper is immersed in a corrosive electrolyte containing an 'indicator' reagent. The coated specimen is made anodic and the impregnated wet test paper is laid on the surface of the coating with a metal cathode, which also acts as an additional weight, on top. The substrate exposed through defects in the coating dissolves and cations travel through the defects and react with the 'indicator' reagent to form coloured spots on the test paper.
As in the ferroxyl test the supposition for detecting the true porosity of the coating is that the wet paper must be in good contact with the coated surface being examined. The number of the pores detected depends upon the type and composition of the solution used and any additives, such as gel, as well as on the applied pressure and operating conditions used [14].

1.2 Electroless Nickel

Electroless deposition is based on a chemical reaction occurring at a solution metal interface without the application of an external current. The formation of electroless coatings is a reduction process involving a chemical reducing agent. This process can only occur spontaneously if a catalytically active surface is immersed in a solution containing ions of the metal to be deposited and a reducing agent. The reaction which results in formation of the deposit may be represented as :

$$R^{n+}_{(aq)} + M^{z+}_{(aq)} \rightarrow \quad R^{(n+z)}_{(aq)} + M_{(s)}$$

where R^{n+} is the reducing agent and M the metal

Not all surfaces are catalytically active but fortunately the most commonly plated material, mild steel, is catalytic. For baths containing hypophosphites only metals of group VIII of the periodic table are catalytically active.

The nickel bath contains several ingredients and can be operated under appropriate conditions to produce dense and coherent coatings.

1.2.1 Bath Constitution

All baths used for chemical nickel deposition contain a number of essential ingredients as follows:

- Nickel-ions which are necessary for the deposition of nickel and are added to the bath in form of salts e.g. nickel chloride, nickel sulphate or nickel acetate.
- Reducing agents e.g. hypophosphite, borohydride or hydrazine. Sodium hypophosphite is the most common reducing agent used.
- Complexants.
- pH regulators.
- Stabilisers.

Each of the above components has a special function and influences both the bath operation and the deposit properties. Ninety percent of baths used for electroless nickel deposition are hypophosphite baths [11].

1.2.2 Hypophosphite Baths

The reaction for nickel deposition may be presented overall as:

$$Ni^{++}_{(aq)} + H_2PO_2^-{}_{(aq)} \xrightarrow{\text{catalytic surface}} Ni^{\circ}_{(s)} + H_2PO_3^-{}_{(aq)} + 2H^+_{(aq)} \qquad (1)$$

However this is an oversimplification since deposits consists of nickel-phosphorus alloy. The process is not fully understood and various suggestions for the mechanism of deposition have been made [11, 42, 43] but none of the proposed mechanisms has been fully accepted. The following intermediate stages can explain how nickel-phosphorus coatings are formed [11].

$$H_2PO_2^-{}_{(aq)} + H_2O_{(aq)} \xrightarrow{\text{catalytic surface}} H^+{}_{(aq)} + HPO_3^-{}_{(aq)} + 2H_{(ads)} \quad (2)$$

$$Ni^{++} + 2H_{(ads)} \rightarrow Ni^\circ{}_{(s)} + 2H^+{}_{(aq)} \quad (3)$$

$$2H_{(ads)} \rightarrow H_{2(g)} \quad (4)$$

$$H_2PO_2^-{}_{(aq)} + H_2O_{(aq)} \xrightarrow{\text{catalytic surface}} H_2PO_3^-{}_{(aq)} + H_{2(g)} \quad (5)$$

$$H_2PO_2^-{}_{(aq)} + H_{(ads)} \rightarrow H_2O_{(aq)} + OH^-{}_{(aq)} + P_{(s)} \quad (6)$$

$$3H_2PO_2^-{}_{(aq)} \xrightarrow{\text{catalytic surface}} H_2PO_3^-{}_{(aq)} + H_2O_{(aq)} + 2OH^-{}_{(aq)} + 2P_{(s)} \quad (7)$$

The intermediate stages take place simultaneously and their rates depend mainly upon the bath constitution, the temperature and the pH-value, as well as other factors. Equations 6 and 7 show how both nickel and phosphorus are produced in the coating. Coating growth starts at catalytic sensitive areas which then, being catalytic themselves, become the centre for further growth.

The hypophosphite baths for nickel deposition are of two types, acidic and alkaline. It has been claimed that the deposition mechanism is the same in both types of baths [11, 22], but their working conditions and the properties of deposits obtained from each type of bath are different.

The acid hypophosphite baths offer a number of advantages in comparison to the alkaline (ammonia) baths. Acid hypophosphite baths are simpler to control, the deposition speed is higher and their stability greater. In general the properties of the nickel coatings produced by an acid hypophosphite bath are better than those from alkaline baths. The pH-value of acid baths is normally held between 4 and 5, bath temperatures range from 85 to 95 °C and the deposition rate is between 10 and 30 µm/h.

Alkaline Hypophosphite baths are only used for special applications. In comparison to the acid solution, the deposition rate of the alkaline solution, as well as the phosphorus content of the coating, is lower. The coatings obtained are more porous and less corrosion resistant, except perhaps in strongly alkaline conditions, than those obtained from acid baths. However the alkaline baths are more stable, the solubility of the nickel phosphite is greater, the working temperatures are lower, and in general they are easier to control than the acid baths [11, 22].

1.2.3 Microstructure of Electroless Nickel Coatings

The microstructure of coatings determines their properties. As noted above, the microstructure is influenced by the plating bath's composition and its working conditions. The growth of the coating, its grain size and shape, is also influenced by the substrate surface. The composition and the developing phases can be predicted from the nickel-phosphorus phase diagram (figure 5) although this diagram is only valid for equilibrium conditions.

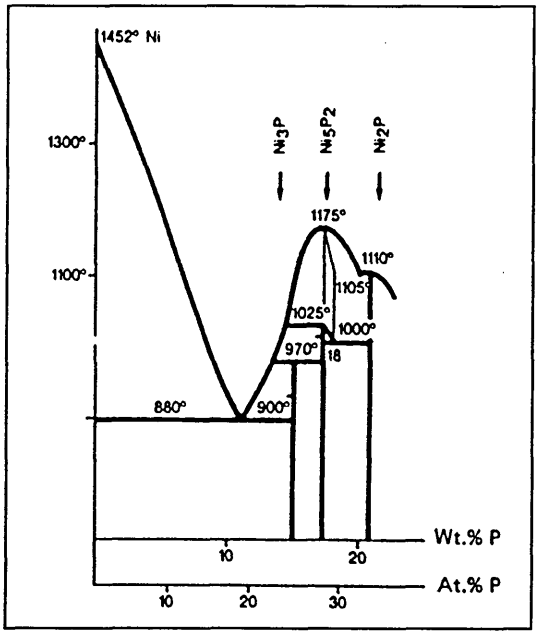

Figure 5 Phase diagram of nickel and phosphorus [11]

The most commonly used electroless nickel phosphorus coatings contain between 4 and 14 mass percent phosphorus. The structure and the transformation of supersaturated electroless nickel phosphorus coatings are not fully understood. Untreated nickel-phosphorus coatings with more than 7 mass percent phosphorus are amorphous like metallic glasses or have extremely fine microcrystalline structures; alloys with less than 7 mass percent phosphorus are crystalline [44, 45, 46]. In both numerous finely distributed inclusions of Ni_5P_4, $Ni_{12}P_5$ and Ni_5P_2 can be found [11, 22]

Macroscopic examination of the coatings shows a lamellar structure parallel to the substrate. The laminae occur as a result of different phosphorus deposition rates occurring throughout the deposition process due to depletion and replenishment of bath ingredients and fluctuating temperature which results in differences in the phosphorus content of individual lamina. In comparison to coatings from acid solutions coatings

from an alkaline solution contain more laminae per unit thickness. The coating structure is dense and homogeneous [11].

If a nickel-phosphorus coating is heated to temperatures above 200 °C the microstructure changes. During the transformation distinct particles of Ni_3P and other intermetallic phases are formed in accordance with the phase diagram. With continued heating the intermetallic particles agglomerate and, a dispersion hardened, two phase alloy is formed. Thus the original amorphous structure changes to a crystalline one. The proportion of the amorphous to crystalline structure depends upon both the temperature and time of the heat treatment. During the heat treatment a diffusion zone develops between the substrate and deposit.

The structural transformation is achieved with a minimal reduction in volume (0.1 - 1.3 %) [47], and accordingly an increased coating density, therefore the number of cracks resulting from the transformation is low. As a result of the formation of a two phased system involving intermetallic phases, especially Ni_3P, the effect of heating the coatings is to decrease their corrosion resistance . The intermetallic and associated nickel phases form corrosion cells. During heat treatment and transformation both the hardness and the wear resistance of the coating is increased whereas the ductility is reduced.

1.2.4 Properties and Applications of Electroless Nickel

The properties of electroless nickel depend strongly upon the substrate material since its condition and type affects the initial nucleation process. Another factor which influences the coating properties is their phosphorus content. Therefore the coatings are often classed as low, medium and high with respect to their phosphorus contents. Some important engineering properties are summarised in table 2.

Table 2 Properties of electroless nickel coatings as a function of their phosphorus content [48]

	low phosphorus	medium phosphorus	high phosphorus
nickel content	96 to 99 %	92 to 95 %	88 to 91 %
phosphorus content by weight	1 to 4 %	5 to 8 %	9 to 12 %
hardness VHN_{100}			
as-plated	650 to 750	500 to 550	450 to 500
heat treated	1000 to 1050	900 to 950	850 to 900
abrasion resistance	superior similar to hard chrome	very good	very good
wear / galling	superior	excellent	excellent
porosity	some porosity	some porosity	generally non-porous
corrosion	best in alkaline environments; poor in acid environments	generally suited for mild corrosive environments	best in acid environments; fair to excellent in alkaline environments
stress	compressive in some cases	tensile	compressive in some cases
magnetic properties	magnetic	slightly magnetic	non magnetic

Advantages of electroless nickel coatings over conventionally plated nickel ones are their uniform thickness, even at corners and in holes, and their solderability. The uniform thickness results from the high throwing power and non-directional nature of the electroless nickel process

On account of the properties described above, electroless nickel coatings are used in many branches of industry, including the automobile, oil, gas, chemical, paper and textile sectors for all kinds of applications requiring their wear and corrosion resistant. When applied to less noble substrates the service life of components is, among other things, determined by their corrosion resistance and hence the presence of defects which extend right through the coatings. Thus it is essential that electroless nickel coatings be pore free if they are to be used to extend the life of components manufactured from mild steel and other low corrosion resistance materials.

1.2.5 Factors Effecting Defects in, and Corrosion Resistance of, Electroless Nickel Coatings

Since initiation of electroless nickel plating involves the adsorption of hydrogen, which creates a catalytic spot receptive to nickel deposition, [42] the substrate surface morphology and its metallurgical condition plays an important role not only in the initiation of coating defects but also in their growth and morphology [49].

Large non-metallic inclusions in the substrate surface can result in pore formation and non-uniform coatings due to the reduced catalytic activity in the region of the inclusion [12, 29, 50].

Localised deformation, resulting from the manufacturing process, can be associated with reduced catalytic surface activity of components and cause pore formation during coating [50, 51]. Lubricants, including any additives, used during component manufacturing can form adherent surface films which can additionally help 'key in' particles to holes or rebates present. This can increase or decrease the catalytic effect of parts of the surface as well as result in pore formation due to the adherence of hydrogen bubbles on the surface [50, 51].

Increasing surface roughness increases the porosity of the coating [15]. This effect was considered by Bergmann to only apply to a coating thickness under 50 µm [12]. According to Tomlinson and Carrol the corrosion potential and corrosion current are independent of surface roughness for coatings over 10 µm thick [13]. The porosity of electroless nickel coatings depends not only on their surface roughness but also on their surface morphology [15, 49] which can in turn be influenced by any mechanical and chemical pretreatment i.e. sand blasting, grinding, rolling, electrochemical polishing or etching.

The precleaning and degreasing of the substrate surface can significantly influence pore formation since it affects not only substrate morphology but also that of the coating, including nodule formation, during subsequent plating [21, 49]. For example anodic cleaning using alkaline solutions tends to increase porosity whereas cathodic cleaning decreases porosity but has the additional disadvantage of hydrogen embrittlement of steel substrates [51]. A nickel strike applied between the precleaning and the electroless plating produces a uniform catalytic surface and leads to the formation of a denser defect free electroless nickel coating with improved corrosion resistance [49].

Both the composition and operating parameters affect the incidence of pore formation during electroless nickel plating. Agitation is an important parameter in the formation of defects during plating. Agitation accelerates the transport of the reactants to the growing

surface and the removal of the reaction products and thus ensures uniform and reproducible coatings [52]. Furthermore, with agitation, coating growth is not disturbed by the formation of hydrogen bubbles adhering to the growing surface [29].

The porosity of electroless nickel coatings decreases with increasing coating thickness [29] since new catalytic sites for nickel deposition occur as the coating thickness increases.

The way in which grooves, i.e. in rough surfaces, and the presence of both conducting and non-conducting particles on the surface can give rise to defects is shown in figure 6.

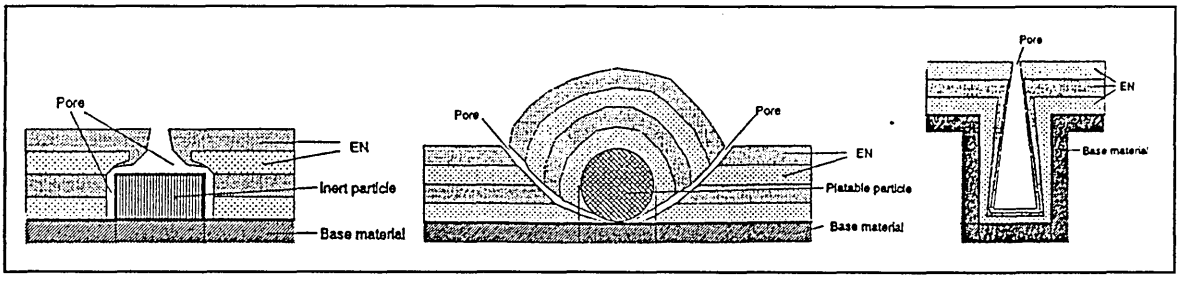

a) Inert particle b) Conducting particle c) Deep groove

Figure 6 Formation of pores caused by particles or grooves present in the growing surfaces [15]

In case a), metal ions from the bulk of the bath are not able to diffuse to the regions adjacent to inert particles and cannot be discharged on the particle itself but only on the substrate. This results in pore formation at the particle/coating interface as plating proceeds. In the case of conducting particles (case b), only diffusion processes hinder the growth process and formation of pores occurs simultaneously to growth of the conducting particle. In case c), the transport of the chemical reactants and products to and from the inside and the bottom of the groove respectively is difficult. Instead of plating the groove uniformly with nickel, a pore is formed. The deeper and narrower the groove the more difficult is diffusion of reactants and products and hence the more likelyhood a pore will be formed. Once a pore is formed it is difficult for it to become filled or covered during further deposition since the original factors giving rise to its initial formation are still present. Nevertheless in most cases coatings beyond a certain thickness do appear to be pore free since none of the pores present penetrate the full thickness of the coating.

Another factor contributing to the corrosion resistance of electroless nickel coatings is the fact that insoluble corrosion products containing phosphorus, i.e. from the coating, deposit in pores and on the surface causing passivation [53].

Heat treatment of electroless nickel coatings causes their crystallisation and the formation of intermetallic phases, in accordance with the phase diagram, and which are accompanied by a volume change (see section 1.2.3), which increases the porosity of the coating. Tomlinson and Mayor obtained maximum porosity in electroless nickel-phosphorus coatings following heat treatment at 400 °C for 24 hours which they attributed to cracks due to transformation stress [29].

1.3 PVD Processes

PVD covers three main techniques namely evaporation, sputtering and ion plating. These techniques differ in the way the coating material is transferred from a source (i.e. cathode) into the gaseous state. In general PVD involves the deposition of thin layers of material and involves the following three steps which take place in a vacuum:

i) Transport of the condensed film material, which may be solid or liquid, into a gaseous state i.e. due to evaporation, sputtering or sublimation.
ii) Transport of the vapour from the source to the substrate.
iii) Condensation of the gaseous metallic species and any reacting gas present to form a thin film through nucleation and growth.

The advantage of PVD techniques is that the three steps can be indepently controlled and varied. Hence the nucleation and growth of the films can be controlled to some extend and different films, having different properties, can be produced. Therefore PVD techniques are used to obtain coatings with advanced technological properties in a reproducible and flexible manner [54].

1.3.1 Basic Principles of PVD Processes

During the **evaporation process** the material which later forms the coating is evaporated using an arc, electron beam or simply by heating. Since the evaporative yield for pure metals is a function of their vapour pressure and the temperature of the solid source material, it is difficult to deposit alloys. The kinetic energy of the evaporated materials is very low (0.1 - 0.2 eV per atom for operating temperatures between 1500 K and 2000 K) and therefore the substrate surface is not changed. Thus the condition of the substrate surface plays an important role in the film growth process [55].

The **sputtering process** involves surface bombardment of a target material, with high energy particles (usually Ar^+ ions), in a vacuum. During this process some atoms of the target surface are ejected (sputtered) in all directions and deposit on surfaces near to the target. A plasma, produced by for example diode, triode, UBM (Unbalanced Magnetron Mode) or RF (Radio Frequency) techniques, is required to produce high energy particles which then are accelerated towards the target under the influence of an electrical field set up between the target (cathode) and the substrate (anode). Only 1% of the bombardment energy results in sputtered atoms and about 75% causes heating of the target [56]. The target particles which are ejected have an average energy of between 5 and 20 eV, are mainly neutral (more than 90%), and form the film on the substrate [54]. The principal advantage of the sputtering process is that almost any material, including alloys or compounds, can be deposited because the material is evaporated by impulse transmission and not by heating.

Adding an active gas to the 'atmosphere' (i.e. as in *reactive sputtering*) induces a reaction with the sputtered target material to form, for example, nitrides films if nitrogen is added as a reactive gas. It has been found that sputtered films have compressive stresses whereas films formed by evaporation have tensile stresses. Compressive stress may reduce cracking in the coating whereas low stress in general is good for adhesion which means an optimum stress value is often aimed for in practice [57].

The **ion plating process** combines elements of both the evaporation and the sputtering techniques. In contrast to sputtering the workpiece is made the cathode in ion plating, consequently the substrate surface may be sputter cleaned prior to coating. The whole ion plating process consists of three stages, preplating, ion plating and evaporation [58]. The *preplating* process, surface ion bombardment (i.e. sputtering), removes surface contamination. Penetration of argon ions into the substrate surface disrupts its structure and introduces a high defect concentration in its surface, which improves the adhesion of the film formed. Within the *ion plating* process both sputtering and deposition takes place simultaneously. During the *evaporation* process at low pressures the atoms travel directly from the target to the substrate and form the coating on condensation.

1.3.2 Microstructure of PVD Coatings

A significant advantage of the PVD technique is that it allows the possibility to alter the deposit properties over a wide range by changing the condensation conditions. Therefore it is important to understand the interrelationship between the nucleation

process, the microstructure and the properties of the coating in relation to the operating parameter of the process.

If atoms hit a solid material they may be reflected or condense as adatoms, thereby transferring energy to the lattice. The adatoms migrate over the surface until they are either desorbed or condensed at growth sites on stable nuclei. The likelihood of surface migration taking place depends upon the kinetic energy of the migrating species, substrate temperature and interaction between the adatoms and the surface. A high interaction between the latter two causes a high nucleation density. The nucleation density is also influenced by the gas atmosphere, ion bombardment, surface pollution, substrate surface defects and surface roughness. The stable nuclei grow into small isolated 'islands' which, with the addition of further adatoms, grow until they impinge upon each other to give complete coverage of the surface. This initial film, once formed, will take on the appropriate orientation as it grows relating to the operating parameters. The nucleation process effects the grain orientation and size, the defect density as well as the film growth. Since PVD coatings are formed from a influx of atoms the microstructure tends to be columnar in nature and hence the film has anisotropic properties [59, 60]. Movchan and Demchishin were the first to recognize that the structure of evaporated thick films depends upon the ratio between the working temperature, T, and the substrate's melting temperature, Tm [61]. Their structural model contains three zones, one, two and three. Later Thornton demonstrated the additional influence of sputtering gas pressure and established another zone T, which was included in the model shown in figure 7 [59]. The original zone T has been named zone T' in the present work to avoid any confusion with the temperature symbol T.

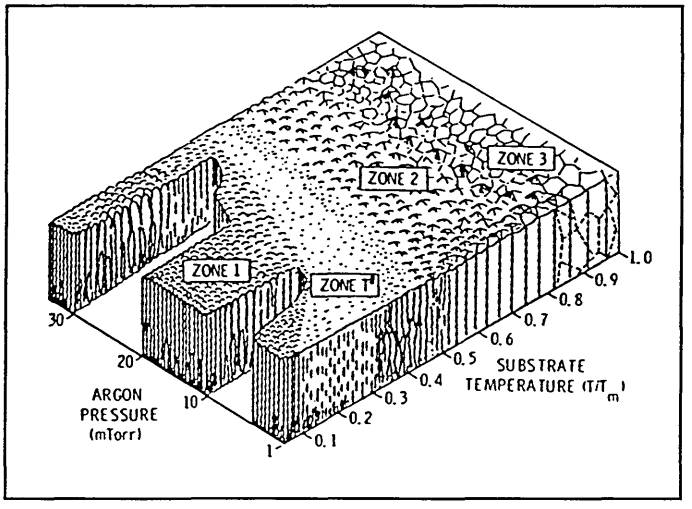

Figure 7 Structure model according to Thornton [59]

The low temperature zone, 1, is associated with a porous structure. Here the mobility of adatoms is low and is affected by shadowing effects which cannot be eliminated. In addition the nucleation density is low. The structure consists of tapered columns with domed tops. In zone T' adatoms are able to avoid shadowing effects by surface diffusion. The structure obtained then is fibrous and more dense than in zone 1. In zone 2 the rate of surface diffusion determines the growth of the film. The structure obtained in zone 2 is of a vertical columnar nature. The diameter of the 'columns' increases, and the film porosity decreases with increasing temperature. In addition surface topography is smoother than for zone 1. In zone 3 bulk diffusion is the dominant process. The structure associated with zone 3 is dense, corresponding to the structure of a recrystallized metal, and is equaxed in nature. Undesired structures as found in zone 1 can be avoided by increasing the process temperature, as explained above, or by ion bombardment of the surface as demonstrated by Messier et al. [62]. A higher ion bombardment (i.e. obtained using higher bias voltages) of the surface produces defects, and thus increases the nucleation rate which leads to a smaller grain size and coatings having higher hardnesses. As a result of the higher bias voltage used, a high compressive stress is introduced into the coating which then has lower porosity [60, 63]. The condition of the substrate surface is a major determinant in film nucleation and thus influences the orientation and the size of growing crystallites. The difference in the thermal expansion coefficients between the substrate material and that of the film causes an internal stress (tensile or compressive) in the interfacial zone. Internal stress is also created by structural disorder caused by the presence of foreign argon atoms. This kind of stress can be influenced by the process parameters used to form the coating. In zone 1 there are gaps between individual columns, hence the internal stress is low whereas in the zone T' the columnar structure is more dense and therefore the internal stress is high.

The PVD process can be described as 'atomistic deposition' at a low temperature. The coatings obtained are, in general, non-equilibrium in nature. Atoms of different elements initially condense in a random manner on the substrate surface to give an unstable structure, which is then stabilised to some extend through surface diffusion. Complete stabilisation is not possible since the rate of arrival of new material at the surface, resulting from the high quench rate, 10^{13}K/s, precludes species already on the surface diffusing very far, i.e. distances in the region of nanometers only. Surface atoms would have to travel greater distances in order to form ordered or two phase systems which explains why metastable coatings, having thermodynamically unstable phases (e.g. TiZrN) are so often produced in practice [64, 65].

1.3.3 Properties and Applications of PVD Coatings

Titanium nitride coatings are relatively hard (2300 HV 0.025), exhibit very low friction and very good resistance against abrasive wear. They are also resistant to high temperatures, up to 600 °C [66]. Eighty to ninety percent of all PVD coated tools and components are coated with TiN, CrN and TiC_XN_y, with $(TiAl_X)N$ coatings taking the remainder of the market. Titanium nitride coatings are often applied to components for wear resistance in the textile and printing industries, whilst TiN and (TiAl)N are applied to drills and rotary grinders. As TiN coatings can be produced in different colours, depending upon the PVD processing parameters used, these coatings are also applied for decorative purposes. Titanium nitride coatings combine a high specific surface area, good passivation properties, electric and thermal conductivity, as well as a high bio-compatibility. These coatings are therefore used for dental applications, surgical implants and electrodes for pacemakers on account of their favourable properties [65].

1.3.4 Factors Effecting Defects in, and Corrosion Resistance of, PVD Coatings

The corrosion resistance of PVD coatings is very poor due to the presence of pores (pinholes) which extend right through the coatings to the substrate [67], and is also influenced by the nature of the substrate/coating interface [68] and the coating's adherence [32]. The rate of corrosion of the substrate depends upon the quantity, size and depth of penetration of any defects present. However the use of PVD coatings is limited by their corrosion resistance in some cases.

Since some PVD coatings can only be grown having limited thickness (5-6 μm), due to high internal stresses which causes cracking and decreased adhesion [3, 67], their corrosion resistance cannot be improved by simply increasing coating thickness. The limited thicknesses which can be obtained with these coatings also prevents grooves, or particles on the surface, being uniformly and effectively covered during coating [67]. In addition the shadowing effect and the directional nature of growth in PVD coatings coupled to their interaction with surface contaminants and defects may produce pores as illustrated in figure 8 and 9 respectively.

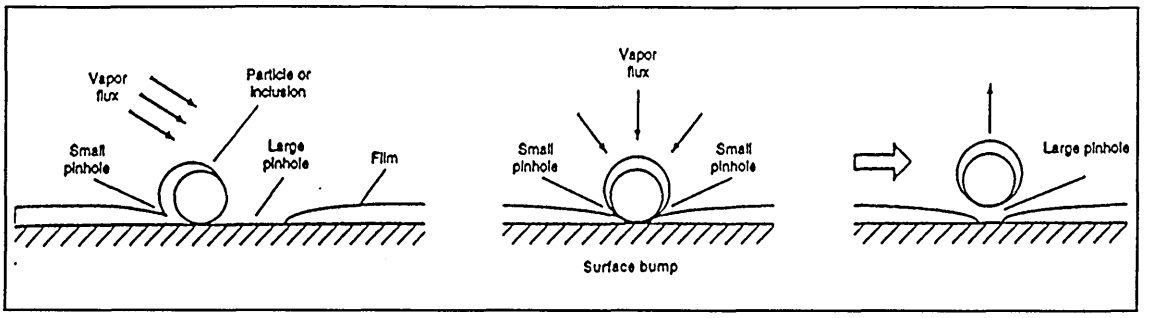

Figure 8 Pinholes formed by a surface bump [69]

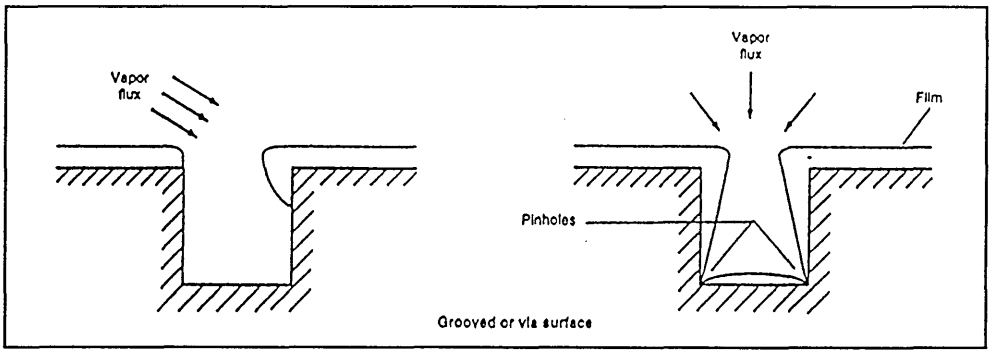

Figure 9 Pinholes formed by a groove [69]

In view of this surface roughness and substrate precleaning are an important factor in determining pinhole density [70]. According to Munemasa and Kumakiri pinhole density decreases with decreasing surface roughness and increasing coating thickness and there exists, depending upon the coating's composition, a critical roughness, i.e. Rmax of ≥ 2 µm and ≥ 5 µm for Ti and TiN coatings respectively, above which the incidence of pinholes drastically increases [30].

The porosity and corrosion resistance of PVD coatings are also affected by deposition parameters which can modify coating morphology as explained in section 1.3.2 [3, 31]. The main factors affecting porosity are bias voltage, substrate temperature, film growth rate and the substrate current density [25, 71, 72]. The orientation of the substrate being coated with respect to the target also effects the porosity of the film formed [73].

Coating surfaces often contain irregularities i.e. depressions, nodules and droplets. Droplets are inhomogenities found in the coating and can give rise to microcracks [74] and pinholes [75] which influence the coated component's behaviour in corrosive environments. Droplet formation during the arc evaporation process is not influenced by surface roughness [25]. Droplets are usually weakly bonded to the substrate surface where the solid particles settle during coating. As illustrated in figure 10 the growing

coating can lift up droplets thus forming a voided region between the coating and droplet.

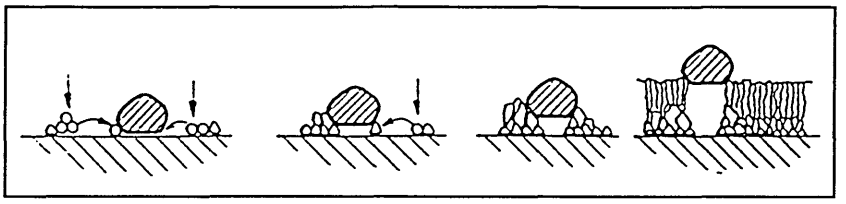

Figure 10 The influence on film growth of droplets on a cold substrate surface [76]

In addition droplets result in shadowing effects such as those illustrated in figure 8 above.

The interrelationship between defects and their cause associated with substrates and coatings are given in table 3.

Table 3 Defects in TiN coatings [37]

origin of defect	cause of defect	defect
substrate	structure of the substrate	cracks
	mechanical surface treatment	surface roughness
	chemical or electrochemical surface treatment	inclusion cavities
coating	structural	porosity pinholes
	coating technique	bare patches in homogeneous coating droplets fallen droplet crater pinholes
	physical damage	scratches cracks

1.3.5 The Arc Bond Sputtering Process (ABS^{TM}-Process)

The ABS^{TM}-Process combines the advantages of the cathodic arc process with those of the unbalance magnetron mode (UBM) sputtering process, i.e. produces denser, stress free films with good adhesion. [77]

The good adhesion of ABS films results from surface etching during the cathodic arc process in which the substrate surface is bombarded with titanium ions. The substrate/coating interface is smooth and consists of a recrystallized zone of only some nanometers in thickness.

The UBM-mode allows the use of various kinds of target materials. The formation of droplets is reduced compared to that achieved using the normal arc mode [78], even in cases where targets consist of a combination of high and low melting point materials. These are some advantages of the UBM sputtering process. A typical ABS^{TM}-process sequence is outlined in figure 11

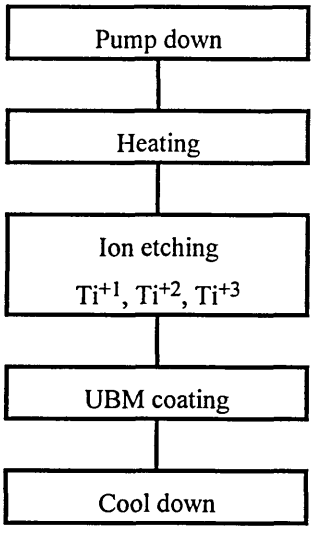

Figure 11 Typical ABS^{TM}-process sequence [79]

The arc mode is an evaporative process where a high current electrical discharge acts as a heat source. Due to the high energy at the cathodic discharge spot the source material sublimes. The vapour generated consists of highly ionised and neutral particles as well as microdroplets of the source material. The flux generated has a high kinetic energy and is used for the etching process.

The UBM mode is a sputtering process, as explained in section 1.3.1, where argon ions are accelerated towards the target (cathode) and eject electrons, charged and

neutral particles. These particles condense on the substrate, to which a bias voltage can be applied to enhance the ion bombardment.

2 Experimental Work

2.1 Material and Sample Preparation

Mild steel samples (type EN3B) 6.5 mm thick and cut from 31.5 mm diameter bar were used as substrates for a variety of coatings. The chemical composition of the steel was analysed using GDOES and is given in table 4. The structure of the mild steel consists of ferrite and perlite with small inclusion of MnS (figure 12).

Samples to be coated with electroless nickel-phosphorus were prepared by grinding and polishing using standard metallographic techniques. Three different grinding, and one polishing, parameters were chosen (60, 120 , 1200 grit and 6 μm diamond paste). Some samples contained holes, having different radii on the shoulders of the holes (0, 0.5, 1.0, 1.5 and 2.5 mm), in their centres produced using a lathe.

Specimens to be coated with (TiAl)N were prepared by automatic grinding and polishing with a BUEHLER® Automet2® Power Head / Ecomet 3® Grinder/Polisher. Three different polishing parameters were chosen (25, 14 and 6 μm). An additional set of six samples was prepared manually to a 6 μm finish.

The TiN and CrN coatings were provided by Hauzer[1]. The substrate used for these coatings was a rolled mild steel sheet (55 × 20 × 2 mm).

Following grinding and polishing the surface roughness of all specimens was measured using a Rank Taylor Hobson Laser Form Talysurf Series 120 L instrument. To describe the surface, the arithmetic mean of the departure of the roughness profile from the mean line (Ra) and the distance between the maximum height above the mean line and the maximum depth below the mean line within the measurement distance (Rt) was chosen.

The values quoted below are the highest of three values measured for each specimen. The measuring direction was perpendicular to the grinding tracks. The measurement of the radii proved to be more difficult than expected since the results depended upon the sample's orientation and adjustment to the measuring equipment as well as the measured length calculated from the expected radius. Furthermore, the results differed with the evaluating parameter, i.e filters, chosen for the measurement.

[1]Hauzer Techno Coating, Venlo, Netherland

2.2 Electroless Nickel Coating

All electroless nickel coating was carried out by A.T. POETON[2].

A specially made jig, figure 13, was used to carry the samples to be plated through the different cleaning and plating process steps. The length of the jig was approximately 500 mm enabling it to fit into the plating bath which had a maximum depth of 600 mm. Suspending the jig using two hooks reduced the tendency for it to swing or move in the plating bath. Each of the four jigs used held twenty-four samples, in batches of six, with each batch having different surface roughnesses.

The tapped and ground samples were screwed onto the jigs which ensured that they were held firmly during immersion in the vigorously agitated processing solutions.

The process used to clean the samples consisted of the following six main steps.

1) Degrease using trichlorethylene
2) Soak and clean in an alkaline solution (ATOTECH X40, 75 g/l) at a temperature of 70 °C.
3) Etch in hydrochloric acid (50% per volume).
4) Electrolytically treat in ATOTECH ALKAN DERUSTER (150 g/l) at 60 °C using periodic reverse current. The cleaning cycle consisted of alternate periods of anodic and cathodic current for twenty and five seconds respectively over a total time of two minutes. The process was always ended using anodic current.
5) Wash in hydrochloric acid (50% per volume) for thirty seconds.
6) A nickel strike in a Woods (high chloride nickel) solution at an applied voltage of four volts for between two and three minutes.

The samples were washed thoroughly in water between each of the above stages.

The samples were then coated with electroless nickel using a high phosphorus (≈ 12% P) plating bath, Lea Ronal NPA 5011. The bath temperature was maintained at 91 °C and the pH-value at 4.7. The bath used had already been operated for one metal turnover, i.e. 6g/l nickel replenishment, and was therefore stable. The plating rate was 12.5 μm/h. The specimens coded B, C, D and E were plated to nominal thicknesses of 3.4, 5.4, 12.0 and 22.1 μm respectively. The samples coded F and G were plated to a nominal thickness of 4.5 μm using a bath which had been operated for 0.4 metal turnover.

[2] A. T. Poeton (Gloucester Plating) Ltd, Gloucester, England

The composition and the profile of the electroless nickel coatings was determined using GDOES. In order to observe the appearance of the coated surfaces as a function of substrate surface roughness and coating thickness the SEM together with special metallographic preparation and etching techniques were used.

2.3 PVD Coating

A Hauzer HTC 1000-4 ABS^{TM} coater was used to coat the mild steel samples with (TiAlY)N, and (TiAl)N by means of a ABS^{TM}-process.

Before the specimens were coated, cleaning was necessary. In order to determine the optimum precleaning procedure for the main investigation and to observe the influence of the surface cleaning process on the porosity and the quality of PVD coatings, coated mild steel samples were subjected to three different cleaning procedures. Mild steel samples were prepared by manual grinding and polishing to 1 μm (Ra = 0.007 μm) and then exposed to the following three cleaning procedures:

1. Standard cleaning schedules:

- Alkaline wash, BALZER (proprietary) at 70 °C, for 2 minutes.
- Mains water rinse.
- Alkaline wash, BALZER (proprietary) at 70 °C, for 2 minutes.
- Mains water rinse.
- Wash in ultrasonic bath (deionisied water), for 1 minute.
- Wash in deionisied water for 1 minute.
- Rinse with acetone.
- Hot air dry.

2. Cathodic cleaning schedules:

- Cathodic cleaning in a cyanide based bath (Kleenex), operated at 40 °C, for 2.5 minutes using a current density of 0.24 A/cm^2.
- Static wash in deionisied cold water.
- Wash in running cold water.
- Wash in cold deionisied water.
- Rinse with acetone.
- Hot air dry.

3. Cathodic cleaning plus etching:

- Cathodic cleaning in a cyanide based bath (Kleenex),operated at 40 °C, for 2.5 minutes using a current density of 0.24 A/cm^2.
- Static wash in cold deionisied water.
- Wash in running cold water.
- Wash in cold deionisied water.
- Etch in Activator No. 2, LEA RONAL at room temperature for 1.5 minutes.
- Static wash in deionisied water.
- Wash in deionisied water.
- Rinse with acetone.
- Hot air dry.

The deposition parameters used during (TiAlY)N coating are summarised in table 5. Ferroxyl tests (both standard and the modified version described in section 2.5) and GDOES analysis were carried out on coatings formed on specimens following each of the three pretreatments investigated.

In order to measure the adhesion between the coatings and substrates scratch tests were carried out using a Megatech Model ST-200. With this technique a Rockwell diamond was drawn at a controlled speed (10 mm/min) over the coated surface in which an applied normal force (Fn), was increased continuously from 0 to 100 N. The critical force (Fn_c), at which the adhesion fails, is indicative of the coating's integrity. Evaluation of Fn_c was made, using a microscope, on the basis of an examination of the scratch made on the coating during the test. The critical normal force was estimated from a knowledge of the test parameters such as speed and loading rate. Different types of coating damage have been related to possible detachment mechanisms [80].

Results of trials

The scratch tests gave no indication whether or not the adhesion was influenced by the cleaning process since the substrate used was relatively soft and the indenter was pressed into the coating and deformed the substrate (figures 14 a, b, c). Furthermore, these figures show the change in appearance of the coating resulting from the different cleaning procedures.

The GDOES analyses provided no decisive conclusion with regard to any change in the composition of the bulk coating or at the substrate/coating interface zone.

The modified ferroxyl test indicated that samples cleaned using the standard cleaning procedure were more porous than those cathodically cleaned. It was also found that etching after cathodic cleaning increases porosity compared to cathodically cleaning alone. This was probably due to the fact that the etchant preferentially attacked sulphide inclusions in the surface. In fact dark browny streaks were observed on the mild steel surfaces after etching.

In view of these results it was decided to use cathodic cleaning (procedure 2) as the standard pretreatment of further samples to be coated with (TiAl)N for use during the project.

The deposition parameters for (TiAl)N deposition are summarised in table 5. The targets used in the process consisted of a TiAl-alloy. Hauzer's standard processing parameters were used for TiN and CrN coating. The thicknesses and compositions of the coatings investigated were estimated using GDOES.

2.4 Neutral Salt Spray Tests

The neutral salt spray test was carried out using an ASCOTT S 1000 A salt spray cabinet. The salt solution used contained 50 g/l sodium chloride and was sprayed continuously at a flow rate of 12 ml/min. The pH-value of the solution was adjusted from 2.7 to 7 using analytical grade sodium hydroxide. The temperature of the chamber was held at 35 °C and that of the humidifier at 50 °C. The air used to atomise the solution was preheated and moistened. Using an air pressure of 0.14 MPa (1.4 bar) gave a salt fog discharge rate of 1.0 ml/h.

A trial run, without samples, was conducted for approximately ten minutes to collect the sprayed salt solution in order to adjust the pH and ensure that all tubes were clean and free of any precleaning solutions.
The samples were ultrasonically cleaned in methanol for five minutes and then rinsed with acetone before mounting in special sample holders ready for positioning in the NSS chamber. In line with normal industrial test procedure, the edges of the samples were protected against the salt fog using adhesive tape .

2.5 Ferroxyl Tests

Preliminary trials were carried out on mild steel samples electroplated with nickel in order to determine the optimum test procedure. The round samples were prepared with different surface roughnesses (120 grit, 320 grit and 1 μm diamond paste) and plated with approximately 3, 6 and 19 μm of nickel from a commercial Watts nickel bath (Schlöter). Two variations of the ferroxyl test were investigated in order to determine which one gave the best result when applied to the nickel coated specimen. The standard ferroxyl test solutions used were as specified in ASTM B 689-1981 and BS 4758:1986. All samples were ultrasonically cleaned in methanol for five minutes and then rinsed with acetone before being subjected to ferroxyl tests.

Standard ferroxyl test:

Solution A
- 50 g/l Sodium chloride
- 50 g/l White gelatine

Solution B
- 50 g/l Sodium chloride
- 1 g/l Non-ionic wetting agent / Tween (Polyoxyethylene sorbitan monolaurate)

Solution C
- 10 g/l Potassium hexacyanoferrate (III), $K_3[Fe(CN)_6]$

The results of these trials established that the following procedure gave good results. Whatman No. 1 filter paper was soaked in solution A at 35 °C and allowed to dry without rinsing. Shortly before the test the dried paper, impregnated with solution A, was immersed in a fresh sample of solution B for ten seconds after which it was placed

on an untreated filter paper. The coated sample was then laid, coating down, on the test paper and a pressure of 0.13 N/mm^2 was applied using a 10 kg weight, as shown in figure 15. After ten minutes the test paper was removed from beneath the coated sample and immersed in a quantity of solution C for ten seconds. After removal from solution C the test paper was allowed to dry, first on a glass plate, and later on a sheet of paper. It was found that best results were obtained using the above procedure using freshly prepared test papers. Figure 16 shows the results of porosity tests carried out using optimum and non-optimum procedures.

Modified ferroxyl test [30]

In this modified version of the standard ferroxyl test a single solution was used having the following composition :

10 g/l $K_3Fe(CN)_6$
10 g/l $K_4Fe(CN)_6 * 3H_2O$
60 g/l NaCl

A Whatman 'Ashless 42' filter paper was soaked in the solution for ten seconds and then laid on the surface of the coated sample for five minutes. In another trial the sample was placed, coated surface down, on the soaked paper which was then placed on top of an untreated filter paper.

It was found that the contrast and 'spreading' of the blue spots and thus the results of both modified techniques are dependent on the coating morphology and wetting characteristic as shown in figures 17 and 18.

'Spreading' of the blue coloration at the edges of the samples, which may hide the existence of pores, depends upon the amount of dissolved iron, as well as on the water content of the filter paper. If the filter paper is too wet a blurring of the blue colouration occurs, but if the filter paper is too dry there may not be enough solution available to indicate the presence of smaller pores.

The intensity of the blue spots changes after a period of time and thus it is necessary to evaluate the results from the test papers immediately following the test.

Result of the trials

Figures 17 and 18 show that the modified test is more sensitive than the standard test and identifies both the large and small pores more effectively. In view of this it was decided to use the modified test in the main work in which the coated samples were laid face down on the soaked test papers. The number of blue spots formed during the tests were counted using an optical image analyser (see section 2.10)

2.6 Sulphur Dioxide Tests

Before starting the test, the samples to be examined were ultrasonically cleaned in methanol for five minutes and then placed in sample holders. The edges of the samples were protected against the atmosphere using adhesive tape.
In order to generate the SO_2 atmosphere a solution consisting of a mixture of four volumes of 20 % sodium thiosulphate and one volume of 50 % sulphuric acid was used [1, 34]. The total volume of this solution occupied 1/40 of the test chamber's volume. When using a glass desiccator of ten litres capacity, as in the present work, the mixture contained

200 ml of 20 wt% $Na_2SO_2O_4$ * 5 H_2O (40 g)
and 50 ml of 50 vol% conc. H_2SO_4

This solution was mixed in an acrylic beaker already positioned in the base of the desiccator. This beaker was then covered with a perforated acrylic sheet on which the prepared samples were placed in a holder which supported them at an angle of 30°. The desiccator was closed as soon as possible following the positioning of the samples. A maximum of eight samples was used per test.

The samples were exposed to the SO_2 atmosphere for 24 hours as was recommended by Clarke and Leeds [1] and is laid down in BS 6670:Part2-1986 since the atmosphere remains constant over this time period.

In order to observe the development of pores and the corrosion attack on samples having the same surface preparation and coating thickness, different exposure times were used in the tests. All samples tested were manually ground under the same conditions using silicon carbide paper (120 grit) prior to electroless nickel coating and 6 μm diamond paste was used for samples to be coated with (TiAl)N. Before the coated

samples were exposed to the SO_2 test they were prepared for examination under the SEM using the procedure described in section 2.11. After the samples had been exposed to the SO_2 test for an appropriate time, their surfaces were sputter coated with platinum. This ensured that no electric charge developed during the SEM investigation since sulphide corrosion products are non conducting.

The application of electroless nickel on an industrial scale often requires deposition on shielded edges and rebates. In order to examine the effects of these features on pore formation, samples with edges having different radii (0, 0.5, 1.0, 1.5 and 2.5 mm) as described in section 2.1 were exposed to the SO_2 atmosphere test for 40/45 hours.

2.7 Copper Cementation Tests

Coated specimens were prepared as described in 2.11 prior to cementation tests. The back, side and a part of the surface of these samples were lacquered using Lacomet so that the surface remaining exposed to the test solution was approximately 490 mm^2.

The specimens were dipped at room temperature in 50 ml of a $CuSO_4$ solution, containing 0.1 g/l Cu, for 300 seconds and then immediately rinsed with 10 ml of deionised water which was added to the initial solution. This procedure ensured that no test solution remained on the sample surface. Afterwards the samples were rinsed with methanol and air dried. Two different solution pH-values, 1.1 and 5.2, adjusted with concentrated sulphuric acid and concentrated sodium hydroxide respectively, were tested. During immersion the samples were well agitated to remove hydrogen bubbles and undesired reaction products which might inhibit the cementation reactions by remaining on the surface.

The test solutions were analysed before and after the tests using ICP (see section 2.9)

2.8 Glow Discharge Optical Emission Spectroscopic (GDOES) Analysis

The Glow Discharge Optical Emission Spectroscopy (GDOES) technique relies on the principles of atomic spectroscopy which are based on the fact that if energy is supplied to an atom then the energy levels of its electrons are raised as a result of the adsorption of that energy. The resulting excitation state is unstable and the electrons revert to a

lower energy level whilst emitting radiation. The emitted radiation has a particular wavelength which is characteristic of the element concerned.

The GDOES technique involves sputtering of the surface being investigated using a plasma. The surface atoms knocked out by sputtering are excited by the plasma. The resulting radiation emitted is detected by photosensors.

With this technique it is not only possible to analyse bulk material but also to produce quantitative depth versus elemental concentration profiles of coatings. In this work a LECO® GDS-750 QDP instrument was used to measure depth profiles and carry out bulk analyses.

2.9 Inductive Coupled Plasma Spectroscopic (ICP) Analysis

Inductive Coupled Plasma Spectroscopy (ICP) is based on the principles of atomic spectroscopy similar to those for GDOES. In the ICP technique a high temperature argon plasma is used as the excitation source. The argon plasma is created and controlled by a radiofrequency field which maintains a working temperature between 5000°C-10 000°C. The samples to be analysed, usually in liquid form, are introduced into the ICP source as an aerosol mist. Droplets from this sample undergo various stages such as desolvation, decomposition, atomisation and excitation as well as ionisation and excitation. The atomic and ionic emission characteristic of the elements concerned are detected by a spectrometer and analysed by a suitable computer. With the ICP technique it is possible to carry out elemental analyses in concentration ranges from ppm to ppb. The instrument used in this work was a ICP Model P (Spectro Analytic Instrument).

2.10 Image Analysis

The image analyser program SEESCAN IMAGING, Task Programming package, was used to quantify the number of visible spots on the test paper from ferroxyl tests. A calibration circle (∅ 25 mm) was placed under a video camera with a macrolense which is connected to the computer. This circle was focused and a circular frame on the screen was calibrated to represent an area of 490 mm^2. Then the filter paper was laid under the macrolense, without changing the focus, and the calibrated frame was positioned in the middle of the image. This package was used to count defect sites highlighted by the staining using a threshold function to differentiate them from the

background. All samples were examined and analysed under the same magnification and image conditions i.e. contrast and threshold levels.

2.11 Scanning Electron Microscopy (SEM)

A Philips XL 40 SEM was used to locate, examine and analyse the topography, surface and defects of coated samples prior to their exposure to the porosity tests. Some samples were marked with a waterproof pen as shown in figure 19. The square areas were marked out such that each area would occupy a complete microscope screen when using low magnification (x10-20). The square areas were examined before and after porosity tests in the manner described below in order to compare the unattacked and attacked surfaces. An identification line at the edge of the samples ensured that they were placed in the microscope chamber with the same orientation both before and after testing.

Examination of these areas at low magnification gave an initial view of the surface. Visible features were then positioned at the centre of the field of view and examined at higher magnification. Another feature was then chosen and brought into the middle of the screen and investigated at higher magnification. This procedure was repeated until the image clearly showed pore/defect sites. In order to precisely relocate each area after the applied test, video prints were taken at each stage.

With this technique it was possible to assess whether the test applied generated, opened or enlarged pores. Using the cementation test it was possible to investigate whether all pores had been covered with copper or whether other reactions had taken place such as oxidation of parts of the coating.

3 Results

3.1 Electroless Nickel Coating

The composition and profile of a nominally 22.1 μm thick electroless nickel coating is shown in figure 20. The profile shows that the phosphorus content is evenly distributed throughout the coating thickness and its concentration is about nine mass percent.

Figures 21 a and b, 22 a and b show the effects of surface roughness and coating thickness on the surface morphology of electroless nickel coatings. The grinding tracks on polished samples (i.e. to 6 μm) could be seen under the SEM (x100 magnification) prior to, but not after, coating with electroless nickel. In contrast the grinding tracks on coarse ground samples (i.e. 60 grit) could be seen (x100 magnification) both prior to, and after coating, even when the electroless nickel coating was 22.1 μm thick. However the grinding tracks became less defined as the coating thickness increased (see figures 21 a and 22 a).

The effect of electroless nickel coating on the surface roughness is given in table 6 in which the surface roughnesses of uncoated and electroless nickel coated specimen are listed. The results from typical individual measurements are shown in figures 23 and 24 which show surface roughness readings of a 6 μm polished substrate and an electroless nickel coating on a 6 μm polished substrate respectively. The surface of the electroless nickel coating contains surface peaks which lead to the high Ra and Rt values found for coated samples on polished substrates. The influence of the electroless nickel coating on the surface roughness is better expressed in figures 25 and 26.

The surface roughness of the substrate also seems to affect the growth of the electroless nickel coating. A few isolated nodules are visible primarily along the grinding tracks of thinly coated samples. These nodules increase in number and size with increasing coating thickness (see figures 21 and 22). Higher magnification shows that thick coatings contain depressions and grain boundary like features, where nodules have apparently 'grown together' (figure 27). Closer examination of a thick coating on a smooth substrate shows that the coating consisted of small depressions and 'hummocks' (figure 28 a). At higher magnification, coatings on polished substrates also showed circular areas containing irregular shaped black features (figure 28 b). It was originally thought that these might be due to surface dirt but the fact that thorough washing failed to remove them suggests otherwise. These features were visible, on both thick and thin coatings, only on polished substrates.

Unetched and etched metallographic cross-sections of a thick coating are shown in figures 29 and 30. The coating is generally uniform, even at sharp edges. Anodic etching in 10% chromium acid revealed the laminar structure of the electroless nickel coatings.

3.2 PVD Coating

Compositional profiles obtained by GDOES for (TiAl)N, TiN and CrN coatings are shown in figures 31, 32 and 33 respectively. It can be seen that in all cases the composition of the coating varies throughout their thickness. This is true of all coatings with respect to the substrate coating interfaces and in the outer surface of (TiAl)N and TiN. The thicknesses of (TiAl)N, TiN and CrN coatings are approximately 1.5, 2.2 and 2.8 μm, respectively.

All the PVD coatings obtained appeared dense and adherent on visual examination. The (TiAl)N, TiN and CrN coatings were dark blue, gold and silver coloured respectively. However more detailed examination of their surface morphologies using the SEM showed that the (TiAl)N and TiN coatings contained many droplets whilst the CrN coatings showed only a few droplets (figures 34, 35 and 36). Scanning electron microscopic examination of a cross-section, prepared from a fractured sample coated with (TiAl)N, showed a gap between the coating and substrate, possibly indicating poor adhesion (figure 37). Careful examination of figure 37 also reveals a crack present between a droplet and the bulk coating.

3.3 Neutral Salt Spray Tests

The neutral salt spray test carried out on electroless nickel coated samples were terminated after 300 hours . The results obtained from this test are significant. The degree of corrosion observed visually on individual specimens was used to rank their performance in the test with respect to corrosion resistance. The results of this ranking are shown in table 7. In the ranking system used the specimen showing the most corrosion has been designated 1, that showing the second worst resistance to corrosion has been designated 2 and so on down to specimens designated 9 which showed no corrosion. Figure 38 shows specimen B3 and B8 (see table 7) which had been subjected to the salt spray test and subsequently designated 1 and 2 respectively in the ranking used. It can be seen that the corrosion products had spread over the surfaces of

the specimens designated 1 and 2 in the ranking system. Consideration of table 7 indicates that in general the corrosion resistance of the coated specimens increased as coating thickness increased.

3.4 Ferroxyl Tests

As shown in figure 39 the porosity of electroless nickel coatings decreases with increasing surface roughness and decreasing coating thickness. The tiny red marks on test papers from samples B1, B19, E1 and E19, and shown in figure 39 resulted from the areas marked red for SEM examination. Table 8 gives the numbers of blue spots per unit area (i.e. 490 mm^2) obtained on coated samples using ferroxyl tests. The result suggests that the most important parameter determining porosity is the original surface roughness of the substrate, and that the influence of coating thickness on porosity is of only secondary importance (see also figure 40).

SEM examination of coated samples, both before and after ferroxyl tests, showed that attack by the test solution had revealed the presence of sub-surface pores which had not been detected prior to the test (figures 41 a and b). Hence the results of ferroxyl tests depend upon the relative rates of attack by the test solution on both the substrate and coating.

Table 9 gives the results of tests on samples coated with (TiAl)N, TiN and CrN using the ferroxyl test. Figure 42 shows the results of tests on (TiAl)N coated specimens. The results obtained in this test cannot readily be related to substrate roughness.

SEM examination of the surfaces of coated samples following ferroxyl tests produced interesting results (see figures 43 and 44 a and b). Thus no corrosion products were seen on the perimeters of droplets which is unexpected in view of the accepted association of porosity with droplets [67, 74, 75]. It therefore seems that the ferroxyl test is not sensitive enough to indicate the presence of such defects associated with droplets.

3.5 Sulphur Dioxide Tests

During SO_2 tests corrosion attack and development of pores can be observed visually and a judgement made as to the relative corrosion resistance of the different samples being tested.

In table 10 the results of ranking test samples according to the way in which visible corrosion occurred during the test are given. It was not possible to evaluate these tests quantitatively using image analysis since sufficient contrast could not be achieved between corroded and uncorroded areas due to differences in both brightness and roughness of the surfaces being tested. However visual examination showed that the corrosion of specimens exposed to the test atmosphere did increase with increasing surface roughness and decreasing coating thickness.

Figures 45 a and b show electroless nickel samples after exposure to the SO_2 atmosphere for 24 hours along with a sample exposed for 72 hours (figure 45 c). The corrosion products on all these samples were rust red in colour. Unfortunately the black and white photographs do not show this and thus perhaps falsely give the impression that the corrosion products on different samples had different colours. In all cases electroless nickel samples exposed to the SO_2 test became dull and tarnished with a colourless film (see figure 45 b) prior to the formation of any red rust.

To investigate both the formation of the tarnish film and corrosion process further, a number of samples, having a 120 grit finish and 4.5 μm coatings, were exposed to the SO_2 test for different times ranging from half an hour to sixteen hours.

Figures 46 a and b show a sample before and after exposure to the SO_2 test for two hours. Although the initial corrosion of specimens was of a general nature there was a tendency for above average corrosion to occur along the lines of grinding tracks in the specimen surface (figure 46 b). After longer test times, thin tarnish films grew on the electroless nickel surfaces. Figure 47 shows in detail the appearance of a electroless nickel surface exposed to the SO_2 test for three hours and which is covered with a thin tarnish film. According to a GDOES analysis made on the same sample, the thin film consist of mainly sulphur (figure 48).

After 15 hours exposure to the SO_2 test nickel surfaces showed the first signs of localised corrosion which appeared as spots to the naked eye. SEM examination of these spots showed them to be small hummock like formations associated with apparent localised cracking of the surface (figure 49 and 50). Closer examination revealed that these hummocks had formed in places where the coating contained nodules, possibly resulting from the presence of inclusions in the coating (figure 50). EDX analysis of

these coatings showed that the coating consisted mainly of nickel and phosphorus (see figure 51) and that the hummock like formations contained mainly iron and sulphur (see figure 52) presumably attributable to the formation of corrosion products. Although figures 49 and 50 might give rise to the assumption that the integrity of the electroless nickel coatings has been destroyed as the 'hummocks' formed, examination of metallographic cross-sections showed that this is not the case. Thus figure 53 shows that the 'hummock' seen on a coating actually consist of fairly loose material lying on top of the still intact electroless nickel coating, which now spans a gab between the substrate and coating directly below the position of the 'hummock'. Analysis of this loose material using EDX and GDOES showed it to consist of mainly iron and sulphur (figures 54 and 55) and the material in the gap between the electroless nickel coating and the mild steel substrate to consist of iron and sulphur (figure 56). The apparent cracks in the electroless nickel coatings (see figures 49 and 50) are in fact most likely cracks in the thin sulphur containing outer tarnish film present, as confirmed by GDOES analysis (figure 55) and noted earlier with respect to figures 47 and 48.

Further tests on specimens with thicker coatings (22.1 μm) for 72 hours resulted in the localised formation of red corrosion products. Figure 57 shows the surface of a specimen subjected to the test for 72 hours. It can be seen that the corrosion products occur as isolated roundish formations and the sulphur containing film, formed at the beginning of the test, has flaked away around the heavy corrosion sites. Back scattered electrons were used to produce the image of the same area shown in figure 57. The resulting back scattered image is shown in figure 58 where the black areas probably indicate the presence of high sulphur concentration. Elemental profiles obtained by GDOES on these samples clearly show the presence of iron in the outer surfaces of the coatings, suggesting that iron from the substrate has somehow passed through the coating defects (see figure 59). Figures 59 and 60 confirm the present of sulphur on both sides of the coating in the corroded regions.

In order to investigate the 'edge effect' during SO_2 corrosion tests a number of samples, each having a 'shoulder' with a different radius, were submitted to the test for 40 hours. It was observed that the heaviest incidence of corrosion always occurred at the point of transition from the flat to the curved surface regardless of the actual 'shoulder radius' involved. However the general corrosion of the curved surfaces increased as the 'shoulder radii' decreased (see figures 61 a and b). Metallographic cross-sections of untested as-plated specimens having curved surfaces showed that some faults were already present at the curved substrate/coating interface (figure 62). Cross-sections of specimens subjected to the SO_2 test for 40 hours showed substantial corrosion attack at

the curved substrate/coating interface (figure 63). This corrosion was heavier than that observed at the adjacent flat substrate/coating interface (figure 64). Comparing figures 63 and 64 suggests that the coating had been almost completely lifted from the curved surface by the interfacial corrosion products, but essentially remained in contact with the flat section of the substrate surface. These results might suggest that the coating is more porous on the curved, than the flat, sections of specimens. However the differences observed might also reflect differences in surface preparation.

Mild steel samples coated with (TiAl)N, TiN and CrN all corroded when subjected to the SO_2 test (see figures 65 and 66). As in the case of electroless nickel coated samples subjected to the test, initially the samples became dull, due to the formation of a thin tarnish film, before the formation of any red rust. In order to study the way in which the test affected PVD coatings a number of (TiAl)N coated specimens were exposed to the SO_2 test for different periods of time varying in length between one and 24 hours.

A (TiAl)N coated sample was exposed to the SO_2 test for one hour after which a thin tarnish film on its surface was visible to the naked eye. The results of a more detailed SEM examinations of the specimen are shown in figures 67 a and b. By comparing figures 67 a and b it can be seen that little change in the general appearance of the surface has taken place as a result of the test. However closer observation suggests that a droplet, originally present in the coating, has dropped out prior to the test and that corrosion has occurred at the remaining pit site during the SO_2 test. However no red rust was observed at this stage.

A (TiAl)N coating subjected to the SO_2 test for two hours showed indications of red rust in localised areas. Figure 68 shows that the coating appeared to have remained intact even in the areas where corrosion products had been formed. This was confirmed by preparing a metallographic cross-section (figure 69) which shows that the corrosion products on the surface are associated with large defects related to nodules/droplets contained in the coating. Furthermore it can be seen from figure 69 that corrosion appears to have spread laterally along the coating/substrate interface from such a defect. Figure 70 also shows these phenomena and in addition shows a break in the coating.

The amount of red rust observed on (TiAl)N coated mild steel specimens exposed to the SO_2 test for periods longer than two hours became heavier. Further investigations confirmed that, as in the case of specimens exposed for two hours, corrosion products were formed both above and below the coating. Figure 71 obtained using GDOES profile analysis confirms this and clearly shows the presence of iron both above the coating and in the gap between the coating and the substrate.

3.6 Copper Cementation Tests

Figure 72 shows the results of a cementation test on an uncoated, polished mild steel sample. As expected, copper had precipitated on the surface generally and around the MnS inclusions. It can be see from figure 72 that some of the MnS inclusions had been dissolved out by acid from the cementation solution. During all tests gas bubbles, presumable hydrogen, were observed to be formed on the surface of the test specimens.

Figures 73 a and b show the same surface region on a (TiAl)N coated specimen both before and after subjection to the copper cementation test at a pH of 1.1. It can be seen from figure 73 b that the copper has been precipitated out randomly as 'spots' on the coating's surface. Comparison of figures 73 a and b show that copper precipitation is not confined to surface droplets or flatter areas nor is there particular evidence for precipitation at the peripheries of droplets. Furthermore the precipitation which has occurred generally on the flatter areas of the surface is not preferentially sited along the lines of the grinding tracks.

Reducing the cementation solution's acidity from a pH of 1.1 to 5.5 did not alter the way in which cementation occurred. Thus comparison of figures 74 a and b obtained on a (TiAl)N coated specimen before and after cementation test at a pH of 5.5 with the corresponding photomicrographs (figures 73 a and b) obtained for cementation at a pH of 1.1 shows very similar features in relation to the cementation behaviour. Examination at higher magnification of individual mounds of copper obtained on the surface of (TiAl)N coatings during precipitation showed that they had a characteristic cauliflower like shape (figure 75).

The results from tests carried out on both TiN and CrN coatings showed similar cementation behaviour to that observed for (TiAl)N coatings as can be seen from figures 76 a and b and figures 77 a and b respectively when compared to figures 73 a and b. It was noticeable that no excessive precipitation was associated with relatively large defects present in any of the coatings tested, for example see figures 76 b and 77 b.

The size and distribution of copper precipitates on the three types of coatings examined varied. The precipitates formed on CrN coatings were the largest and those formed on TiN coatings the smallest with precipitates of intermediate size being found on (TiAl)N coatings. In contrast the surface density of precipitates was the greatest for TiN coatings and smallest for CrN.

From the results obtained it is not possible to compare the relative amounts of copper precipitation obtained on the three types of coatings examined in view of the variations in precipitate size and distribution found on the different coatings.

In order to confirm which elements from the test sample entered solution during cementation, analyses were carried out on the aliquots of test solution used for individual tests using ICP. The results of these analyses are given in table 11, 12, 13 and 14. These results, as expected, confirm that generally iron entered solution in all cases but to a significantly lower extend than when a uncoated sample was tested. It is thought that the one exception (CrN1, table 13) resulted from failure of the 'Lacomit' lacquer used to 'stop-off' the back and sides of the test specimen. There is no evidence to suggest that either chromium or titanium from any of the coatings entered the test solution. The analysis results suggest that a trace of aluminium, present in the solution as an impurity, may have been precipitated out along with copper.

4 Discussion

For convenience the tests used in the present work, together with their advantages and disadvantages, will be discussed before a detailed discussion of the results obtained using the tests on electroless nickel and PVD coatings is entered into.

Although the neutral salt spray test (NSS test) is used widely in industry the present work suggests that its use has severe limitations with respect to the understanding of the role played by coating defects in corrosion. Although it is possible to use a ranking system in the evaluation of corrosion resistance such methods are usually carried out in conjunction with relatively large test specimens. The use of large specimens unfortunately precludes the use of advanced electron optic techniques, as used in the present work, to augment the results. Further disadvantages of the salt spray test are that it is difficult to follow its progress visually without disturbing the test and the tendency for any corrosion products formed to spread out, due to the high humidity involved. For these reasons, together with the fact that the NSS test is particularly aggressive towards PVD coatings, relatively little use was made of the test.

The ferroxyl test is a quick, easy and practical method for investigating the porosity of coatings on steel. Reference to the ferroxyl test in the literature is synonymous with the use of solutions containing potassium hexacyanoferrate. In the present work, it was found that, depending upon the test parameters chosen, the tests can give different results. Tests carried out in accordance with BS and ASTM standards involve the use of three solutions which make the test complicated, mainly due to the method require to prepare the test papers. The results of these standard tests depend not only upon the pressure applied during the test but also upon the age of the test paper used. The modified ferroxyl test used in the present work involved only one solution which simplified the test procedure. The blue spots developed during the modified test are more intense than those obtained using the standard tests, presumable due to the absence of gelatine in the modified test solution. Thus the corrosion sites are better defined in the modified test. Additionally the modified test is more sensitive which might also be due to the absence of white gelatine which leads to a less viscose solution. Chloride ions present in both versions of the test attack the substrate through defects in the coating and produce ferrous and/or ferric ions, which then react with the potassium hexacyanoferrate to form blue complexes. In some cases the aggressive nature of the chloride solution may attack the coating itself to open up sub-surface pores (see figures

41 a and b). In such cases a higher value for porosity may be indicated by the test than might otherwise be the case. Other factors found to affect the numbers of pores recorded by the test are the test paper's moisture content and the wettability of the coated surface.

A quantitative assessment of porosity following both standard and modified ferroxyl tests can be made by counting the blue spots formed on the test paper using image analysis. In some cases it is possible to make the evaluation by counting the corrosion sites directly on the test specimens although this is not normal practice. There must be suitable colour and contrast between the corrosion sites and the rest of the coating surface where a direct evaluation is to be made. In the present work it would have been possible to evaluate porosity directly from the electroless nickel coated samples tested but not from the (TiAl)N coated specimens. Therefore the evaluation of porosity of both electroless nickel and (TiAl)N coatings was made from the test papers. In general the evaluation of porosity following ferroxyl tests depends upon a number of factors including: the ability of the test solution to penetrate pores and defects; the extent to which the blue spots formed on the test paper spread out; the extent to which individual pores are associated with single spots on the test paper; and the resolution of the microscope. It is clear from the results obtained that the ferroxyl test is only sensitive to the detection of relatively large pores and defects. Thus ferroxyl tests on (TiAl)N coatings failed to give an indication of the fine background porosity (as can be seen by comparing figure 73 with figure 42). The information gained from the ferroxyl test can be extended by SEM examination of test specimens in addition to any evaluation of porosity based upon optical image analysis. In several instances SEM examination of coated surfaces revealed the presence of defects which had not shown up on the test papers.

The SO_2 test is carried out under standard conditions in a glass desiccator during which the progressive corrosion of the test pieces can be observed directly. The results of tests can be evaluated using a ranking system similar to that used with NSS test results, as for example shown in table 10. Furthermore since the progress of the test can be followed visually, something which cannot be done in the NSS test, the SO_2 test can be terminated as soon as an interesting stage in the corrosion process has been reached in order to investigate the nature of the corrosion in more detail using electron optic techniques. This technique was used in the present work during the testing of electroless nickel specimens. For example see figure 58 obtained from test samples removed at a suitable stage from the test chamber and examined using secondary and backscattered electrons. The actual significance of these figure will be discussed later in relation to the

corrosion behaviour of the relevant coatings. However it should be noted that once interrupted the test cannot be continued [1, 36] as is often the practice in industrial NSS tests. Therefore where there is a requirement to test a number of samples using the SO_2 test then individual batches to be tested should contain test pieces with similar corrosion resistance, i.e. samples with thin or highly defective coatings should not be tested in batches containing thick defect free coatings.

As with all porosity/corrosion tests in which reaction products are formed the presence of any small defects may be obliterated or masked by the reaction products initially formed at large defect sites. In the case of narrow pores 'compact' reaction products initially formed at the base of the pore may prevent further corrosion. Whilst the ferroxyl test can only be used to evaluate pore density of coatings the SO_2 test can be used to investigate both pore density and the way in which corrosion occurs at pores and defect sites. Additionally the SO_2 test is more sensitive than the ferroxyl test, possibly due to the involvement of gaseous media.

Unlike the corrosion and porosity test discussed above, the use of cementation in the identification of defects and evaluation of porosity is a relatively new technique. It has been claimed that the technique is a particularly straightforward one for detecting defects and evaluating porosity in PVD coatings [32, 37, 81, 82]. The method relies on the coating under test being more noble than both the substrate material and the metal, usually copper, being cemented. As discussed earlier, (TiAl)N, TiN and CrN coatings on mild steel all fulfil these requirements with respect to an acidified copper containing solution (see section 1.1.3). Although the potential use of this method is relatively limited, as compared to the NSS, SO_2 and ferroxyl tests, it was considered worthy of further investigations.

Initial trials on electroless nickel coated mild steel samples resulted in the cementation of a uniform copper layer over the whole surface of the exposed sample. This is perhaps understandable, in view of the closeness of the electrode potentials of iron and nickel, and probably of nickel-phosphorus coatings also. In view of these trials no further work was done using cementation tests on electroless nickel-phosphorus coatings.

The results of cementation tests on (TiAl)N, TiN and CrN all resulted in cementation occurring at random sites on the coating surfaces, presumable at pore sites (see figures 73, 76, 77). However in the present work no preferential cementation associated with large defects or droplets in the coating was observed as reported by Uergen et al. [32, 37, 81, 82] (see figure 74). The results of cementation tests on PVD coatings are

discussed in more details below. At this stage however, it is worth noting that several questions concerning the use of cementation tests remain unresolved. In this connection the technique used to identify the same microscopic area for SEM examination on surfaces both before and after cementation tests certainly proved an advance on the previous procedures used. The main advantage being that it allowed the effects of cementation on particular defects, including individual droplets and droplets craters, to be studied (see figure 73 a and b).
Even if these questions concerning cementation test were to be resolved it is unlikely that the test will prove so useful as the other tests dealt with.

The as-plated electroless nickel coatings appeared to be sound and lustrous. This was confirmed from a metallographic cross-section (figure 29) which showed the coating to be of good quality with a laminar structure (figure 30). Schenzel et al. showed that such laminar structures in electroless nickel-phosphorus coatings result from differences in the phosphorus contents of the different laminae present [83]. These differences in phosphorus content are thought to be due to small temperature, concentration and pH fluctuations in the plating bath. The appearance of the electroless nickel coatings at low magnification reflected the surface roughnesses of the original substrates. In general the roughness of the coatings increased with the roughness of the substrate as can be seen in figures 21 and 22 which also show the tendency for nodule formation along the lines of the grinding tracks as previously observed by Tomlinson and Mayor [29]. No nodules were observed to be present in coatings plated onto polished substrates although some small 'hummocks' and depressions were observed (figure 28 a). However the tendency to nodule formation increased as the surface roughness of the substrate increased and there was an increasing tendency for nodules to overlap and grow into each other as the coatings became thicker. Cases have also been reported in the literature where, once formed, nodules became covered and incorporated in the coating as it grows [29]. Comparison of figures 21 a and 22 a suggests that some levelling of the surface occurs during coating resulting in the thicker coatings having smoother surfaces. This was confirmed by surface roughness measurements. Thus the roughness measurements in figures 23 and 24 for a specimen surface having a 6 μm finish, before and after receiving a 22.1 μm thick electroless nickel coating, show that the background roughness is lower after plating but that this generally smoother surface contains randomly scattered protrusions. These protrusions recorded in the roughness measurements obviously result from the presence of the 'hummocks' observed on such surfaces (i.e. see figure 28 a). Consideration of figures 25 and 26 suggest that there are

critical roughness values of the substrate associated with hummock formation which may themselves be associated with the thickness of the coating. For the parameters used in the present work, i.e. Ra between 0.010 and 1.578 μm, Rt between 0.115 and 15.304 μm, and coating thicknesses between 3.4 and 22.1 μm the upper limit of the Ra and Rt values of the substrate associated with hummock formation are 0.055 and 1.6 μm. Thus 'hummocks' were only observed on coated specimens having surface roughness parameters below these two critical values. Although on the macro-scale electroless deposition is associated with uniform coating thickness the levelling effects observed on the micro-scale can be accounted for by oriented crystal growth as used by Raub to explain the same phenomenon during electrodeposition [84]. Raub showed that geometric levelling occurred during the electrodeposition of copper as a result of field oriented growth. This type of microlevelling can be expected during electroless nickel deposition since growth orientation of the deposit, i.e. at right angles to the surface both in the groove and on the flat, will always favour levelling as demonstrated in figure 78.

Electroless nickel coated mild steel specimens were attacked to varying degrees during NSS, ferroxyl and SO_2 tests. The tendency of the corrosion products formed during the NSS tests to spread out over the coatings' surfaces made it difficult to evaluate the test results quantitatively. In this connection it should be remembered that the specimens used in this work were relatively small as compared to those used in industrial tests for which ranking methods are available.

The ferroxyl test produced clearly defined results when applied to electroless nickel coated test specimens. Thus defect sites showed up on the test papers as sharply defined blue spots, which could be counted using optical image analysis. Ranking the performance of the specimens according to the number of defects indicated by the test allowed the relative corrosion resistance of different specimens to be compared (see table 8). The results obtained show that the porosity of the electroless nickel coatings examined decreased with increasing coating thickness. This was also found to be the case in previous work on a) electroless nickel coatings [11, 29, 85] and b) coating of other metals [14, 86, 87, 88]. The results also showed that the porosity of the coatings tested decreased with decreasing substrate surface roughness (see figure 39). This result is also in agreement with previous work [11, 29]. It is worth noting that the small depressions and hummock like features observed on coatings on polished substrates seem not to be associated with porosity.

Few quantitative results concerning the porosity of electroless nickel coatings have been reported in the literature [11, 14]. In fact few quantitative results concerning the

porosity of coatings in general have been reported, perhaps with the exception of gold. A general equation :

$$P = A' * R^{n} * t^{-n} \qquad (i)$$

has been suggested for describing the relation between porosity, substrate roughness and coating thickness. In this equation:

P is the porosity, i.e. pores per unit area,
A' is a constant,
R is the substrate roughness Ra,
t is the nominal coating thickness, and
n is a constant relating to the porosity test used.

This equation was used by Chonglun Fan et al. to evaluate the results of porosity tests carried out on electrodeposited nickel on copper/tin sheets[86].

When the results of porosity measurements obtained in the present work using the ferroxyl test are evaluated using equation (i) then the expression :

$$P = 797 * \left(\frac{R}{t}\right)^{1.38} \qquad (ii)$$

is obtained where; P is the number of pores per 490 mm^2 and the values of 'A'' and 'n' in equation (i) are 797 and 1.38 respectively. Furthermore plotting P against R/t gives figure 79 which shows that porosity increases as the ratio of surface roughness to thickness increases. This quantifies the empirical data from table 6 and shows:

i) how an increase in roughness, at a constant thickness, increases the ratio R/t and increases porosity and,
ii) how an increase in thickness, at a constant roughness, decreases the ratio R/t and decreases porosity.

It is worth noting that this equation does not relate to a pore free coating. Additionally it should be noticed that if R<t then the expression does not apply to the present results. However figure 79 is in effect a calibration chart which can be used to evaluate the

parameters which would be expected to produce pore free coatings in relation to practical electroless nickel coatings.

Although SO_2 atmospheres can attack nickel and nickel alloys the rate of attack on electroless nickel coatings under the conditions found in the SO_2 test is slow. During the initial stages of SO_2 tests nickel plated specimens became dull and tarnished (figure 45 b). Analysis of this surface film showed that it contained sulphur suggesting that the film consisted of a sulphide and/or sulphate of nickel. After longer test periods localised red corrosion products, probably FeS, appeared on the coatings' surfaces. These red corrosion products turned bright red on removal of the coated specimens from the test chamber thereby exposing the corrosion products to a fresh supply of oxygen. The successful use of the SO_2 test to investigate defects in nickel coatings is possible due to the passivating effect of the initial tarnish film formed, and the fact that, the relatively small anodic areas ensure intense attack at defect sites (figure 45 c), with a corresponding disturbance of the surrounding tarnish film (figure 49). Due to insufficient contrast between pore sites and the surrounding surfaces it was not possible to evaluate difference in porosity and hence corrosion resistance, of samples using image analysis. However visual ranking of the nickel coated specimens following SO_2 tests allowed variations in the porosities of different specimens to be made. The results of this process are given in table 10 , from which it can be seen that corrosion resistance increases with decreasing substrate roughness and increasing coating thickness. This confirms the results found using the ferroxyl test although in this case it was not possible to quantify the results.

It had been noticed that in some tests unrepresentative attack at specimen edges had taken place, i.e. where the tape used to stop off areas had failed. For this reason, and the fact that edge protection is normal practice in industrial testing, the effects of tests done on edges having different radii were carried out. These tests showed that the decisive factor determining the degree of edge attack was the sharpness of the transition from a flat to a rounded surface (see figure 61). It is clear that the edges of specimens are more vulnerable to corrosion attack than flat surfaces. Several factors might contribute towards this state, including differences in, substrate roughness, surface energy resulting from differences in mechanical working, surface morphology, coating thickness and adhesion, as well as the operating parameters of the coating process. Although the results obtained in the present work were not conclusive they do suggest that coating adhesion plays an important role in whether or not coatings are corrosion resistant (compare figure 63 and 64).

All the PVD coated mild steel test pieces responded in some manner to NSS, ferroxyl, SO_2 and cementation tests. No further work was done using the NSS test after preliminary studies since the test was considered to be too crude and insensitive for the investigation of PVD coatings on small test samples. Although the remaining tests all had some positive effect, i.e. produced corrosion or cementation, on the PVD coatings the results obtained are open to discussion.

The results of ferroxyl tests shown in table 9 suggest that the porosity of (TiAl)N coatings is not directly related to the roughness of the substrate surface. These results are in agreement with those obtained by Munemasa and Kumakiri who also found a similar result for coatings on surfaces having low roughness values, i.e. below Rmax 5 μm for TiN coatings [30]. These workers however did show that the porosity of TiN coatings on steel surfaces is directly related to roughness for roughness values above Rmax 5 μm.

A characteristic of the SO_2 test when used with (TiAl)N coatings was corrosion emanating from preferential attack through large defects. This type of corrosion appears to be so rapid that it outpaces any corrosion which might have occurred at surrounding fine pore sites, especially those associated with droplets. The resulting interfacial 'void' filled with voluminous corrosion products can produce a loss in the PVD coatings' integrity as can be seen in figures 69 and 70. The practical conclusion to be drawn from this is that any intermediate coating used below a PVD coating to increase its integrity should not only be mechanically suitable but also have a high corrosion resistance.

All the PVD coatings investigated responded to the cementation test (see figures 73, 76 and 77) It is unclear from the literature whether or not the coatings investigated might be expected to react with the acidic cementation solution used in the present work (see section 1.1.3). In particular there is work to suggest that TiN both is [24, 41] and is not [40] active in acidic solutions. The ICP analyses of the aliquots of solutions used in cementation tests help clarify the true situation (see table 11 to 13). In all cases it is clear that the only element entering solution to any significant extent during cementation was iron and that none of the other elements present in the coatings entered solution during the tests. This evidence along with the fact that copper was seen to precipitate onto the test pieces might, at first, suggest cementation involving the following reaction:

$$Cu^{2+}_{(aq)} + Fe_{(s)} \rightarrow Cu_{(s)}\downarrow + Fe^{2+}_{(aq)} \qquad (iii)$$

However a gas, presumable hydrogen, was observed to evolve from both PVD coated and uncoated mild steel specimens during cementation tests. Furthermore observation

showed that, during cementation tests, copper precipitated out on the top of PVD coatings (see figure 75), which would suggest that the chemical reaction occurring during the tests is more complex than that inferred by the simple cementation reaction. The cauliflower like copper precipitates seen were similar to those recorded by earlier workers although they did not explain how they came to be formed on top of the coating [32, 37]. The assumed mode of cementation is that copper is precipitated out directly on the surface of the iron substrate involved in the reaction which would not explain the presence of copper 'humps' formed on the top of the coatings, presumable in the region of defects. This suggests an alternative cementation mechanism is operating. A reaction sequence is suggested below which would explain the observations made during this work. It is proposed that although some copper might have been deposited by reaction (iii) at the bottom of pores, alternative reactions have accounted for copper precipitation on the coatings' surfaces. The course of these reactions is shown schematically in figure 80. This figure illustrates two alternative reaction sequences which would explain the formation of the copper 'humps' formed during cementation tests as follows:

1) (a) in figure 80 $Fe_{(s)} - 2e^- \rightarrow Fe^{2+}_{(aq)}$

(b) in " $2H^+_{(aq)} + 2e^- \rightarrow H_{2(g)}\uparrow$

Overall primary reaction $Fe_{(s)} + 2H^+_{(aq)} \rightarrow Fe^{2+}_{(aq)} + H_{2(g)}\uparrow$

Secondary reaction, i.e. cementation:

(c) in figure 80 $2Fe^{2+}_{(aq)} + Cu^{2+}_{(aq)} \rightarrow 2\,Fe^{3+}_{(aq)} + Cu_{(s)}\downarrow$ (iv)

It is worth noting that not only does the hydrogen reaction play a major role in the cementation mechanism but any gaseous hydrogen produced in a pore would leave the pore and, in doing so, help transport ferrous ions from within the pore and at the same time discourage copper cementation at the bottom of the pore.

2) (a) in figure 80 $Fe_{(s)} - 2e^- \rightarrow 2Fe^{2+}_{(aq)}$

(d) in " $Cu^{2+}_{(aq)} + 2e^- \rightarrow Cu_{(s)}\downarrow$

Overall cementation reaction $Fe_{(s)} + Cu^{2+}_{(aq)} \rightarrow 2Fe^{2+}_{(aq)} + Cu_{(s)}\downarrow$ (v)

An interesting point concerning the results of this, and previous work, is that copper appeared to be only precipitated at small defects whereas previous workers observed

precipitation at both small and large defect sites [32, 37]. Thus figure 74 shows that a large defect in a (TiAl)N coated mild steel specimen was unaffected by the cementation test. The difference in these results might be explained by the fact that the mild steel used in this work was rather dirty and contained numerous large MnS inclusions (see figure 12). It is therefore possible that the large defects in the coatings examined appeared at the sites of, and as result of the presence of, such inclusions. This might be especially true where a large MnS inclusion has been partly or wholly dissolved out from the substrate surface during the acid etching at the pretreatment stage.

If the results of the ferroxyl porosity tests on PVD coatings (see table 9) are considered in conjunction with the carbon and oxygen profiles obtained from these coatings using GDOES (figures 31 to 33), then it would appear that the porosity of the coatings increases as their gas content increases. This would appear consistent with the claim that the defect density in PVD coatings reflects their gas content [89]. The porosity of the PVD coatings also shows differences which might again result from the differences in the gas contents of the different coatings (i.e. (TiAl)N, TiN and CrN). One cannot comment quantitatively on the coatings' total porosities as derived from cementation tests, because of the apparent differences in size and distribution of the defects. However it may be that a large number of small, as in the case of TiN (figure 76) or a small number of large defects, as in the case of CrN (figure 77) are associated with high and low gas contents respectively. To establish the full and exact relationship between absolute porosity, taking into account the number, geometry and size distribution, the results of cementation porosity tests, and gas contents of coatings would involve a detailed study using electron optic techniques (SEM/TEM) and an exact measurement of the amounts of copper precipitated during cementation tests, perhaps using modified ICP analyses.

5 Conclusions

Neutral Salt Spray Test

- This was found to be an insensitive test for corrosion when used to test relatively small coated specimen.

Ferroxyl Test

This was found to be useful for evaluating macroporosity on both electroless nickel and PVD coatings. The results obtained using the test are suitable for evaluation using optical image analysis.

Sulphur Dioxide Test

This was found to be a very sensitive test for examining the corrosion resistance of electroless nickel and PVD coatings. However the corrosion obtained during such tests is associated with the larger defects present and tends to mask the role of smaller defects. The test is extremely useful for studying the mechanism of corrosion in coated samples since the test's progress can be followed visually throughout.

Cementation

It was found that the cementation test could be applied to PVD coatings ((TiAl)N, TiN and CrN) but not to electroless nickel coatings. The test was particular useful for detecting background porosity, evidence for which was not readily available from the other tests investigated. The cementation reaction occurring in the test involves a more complex mechanism than a simple replacement of iron by copper at the substrate surface.

Electron Optic Examination

A locating technique was developed for examining specific surface features on coatings before and after porosity/corrosion tests. The information gained from this technique can be used to augment the results of other tests and provide an insight into how coatings fail during tests.

Universal Porosity/Corrosion Test

As with electrochemical test, none of the tests investigated can be regarded as a universal porosity/corrosion test for use with all coatings.

Porosity/Corrosion of Electroless Nickel

Plots of porosity versus the substrate surface roughness to coating thickness ratio provide a convenient means of relating the porosity of a coating to surface roughness and coating thickness which might be used to predict the corrosion resistance of coated material and as an industrial quality control method.

6 References

1 M. Clarke and J.M. Leeds
A Sulphur Dioxide Porosity Test for Coatings of Gold and Platinum Metals on Substrates of Copper and Nickel and Silver
Transaction Institute of Metal Finishing, 46 (1968) 81-86

2 ASTM B765-1993
Standart Guide for Selection of Porosity Tests for Electrodeposits and Related Metallic Coatings

3 H. A. Jehn and M. E. Baumgaertner
Corrosion Study with Hard Coating-Substrate Systems
Surface and Coating Technology, 54/55 (1992) 108-114

4 J.C. Doong, J.G. Duh, S.Y. Tsai, J.H. Wang and B.S. Chiou
Corrosion Behaviour of Electroless Nickel PLating Modified TiN Coating
Surface and Coating Technology, 58 (1993) 157-161

5 M. Hans and E. Bergmann
Corrosion Behaviour of Steel Coated with an Ni-P/PVD Hybrid Layer
Surface and Coating Technology, 62 (1993) 626-629

6 A. Leyland, M. Bin-Sudin, A.S. James, M.R. Kalantary, P.B. Wells, A. Matthews, J. Housden and B. Garside
TiN and CrN PVD Coatings on Electroless Nickel Coated Mild Steel Substrates
Surface and Coating Technology, 60 (1993) 474-479

7 O. Forsén, M. Turkia, J. Aromaa and M. Tavi
Corrosion Resistance of Zirconium and Titanium Nitride Thin Films
East Conference, November 1993, Schwaebisch Gmuend, Germany

8 W.B. Nowak
Thin Metallic Films for Corrosion Control
Surface and Coating Technology, 49 (1991) 71-77

9 N. Pebere, Th. Picaud, M. Durat and F. Dabost
Evaluation of Corrosion Performance of Coated Steel by the Impedance Technique
Corrosion Science, 29 (1989) 1073-1086

10 D.A. Jones
Principles and Prevention of Corrosion
Published by Macmillan Publishing Company, New York, 1992

11 Wolfgang Riedel
Electroless Nickel Plating
Published by Finishing Publication LTd., Ohio, 1991

12 W. Bergmann, E. Kunze and H. Rabold
Zur Bestimmung der Porositaet von Stromlos Abgeschiedenen Nickel
Neue Huette, 15 (1970) 175-178

13 W. J. Tomlinson and M. W. Carrol
Substrate Roughness, Deposit Thickness and the Corrosion of Electroless Nickel Coatings
Journal of Material Science, 25 (1990) 4972-4976

14 Michael Clark
Porosity and Porosity Tests
In Properties of Electrodeposits Their Measurement and Significance
Editiors: R. Sard, H. Leidheiser Jr. and F. Ogburn
The Electrochemical Society, Inc., Pennington, 1975

15 Hong Deng and Per Moller
Effect of the Substrate Surface Morphology on the Porosity of Electroless Nickel Coatings
Transaction of the Institute of Metal Finishing, 71 (1993) 142-148

16 B. Benmalek, P. Gimenez, J. P. Peyre and C. Tournier
Characterization and Comparison of TiN Layers Deposited by Different Physical Vapour Deposition Processes
Surface and Coating Technology, 48 (1991) 181-187

17 D. R. Gabe
Principles of Metal Surface Treatment and Protection, 2 nd Edition
Published by Pergamon Press, Oxford, 1978

18 V. E. Carter
Corrosion Testing for Metal Finishing
Published by Butterworth Scientific, London, 1982

19 R. L. Sauer
Corrosion Testing - Protective and Decorative Coatings
In Properties of Electrodeposits Their Measurement and Significance
Editor: R. Sard, H. Leidheiser Jr. and F. Ogburn
Published by The Electrochemical Society, Inc., Pennington, 1975

20 ASTM B689-1985
Electroplated Engineering Nickel Coatings

21 E. B. Saubestre and J. Hajdu
Influence de la préparation du substrate à la corrosion des revêtements ?
Oberflaeche-Surface, 9 (1968) 53-57

22 G. G. Gawrilow
Chemical (Electroless) Nickel Plating
Published by Portcullis Press, Redhill, 1979

23 U.K. Wiilala, I.M. Penttinen, A.S Korhonen, J. Aromaa and E. Ristolainen
Improved Corrosion Resistance of Physical Vapour Deposition Coated TiN and ZrN
Surface and Coating Technology, 41 (1990) 191-204

24 I. Milošev and B. Navinšek
A Corrosion Study of TiN (Pysical Vapour Deposition) Hard Coatings Deposited on Various Substrates
Surface Coating Technology 63 (1994) 173-180

25 H. Ronkainen, U. Ehrnstén, R. Zilliacus, J. Saarilahti, A. Mahiout and S.-P. Hannula
Investigation of some Microstructure Features Related to Corrosion Initiation in Titanium-Aluminium Nitride Coated Steel
Thin Solid Films, 220 (1992) 160-165

26 I.M. Notter and D.R. Gabe
Polarisation Resistance Methods for Measurement of the Porosity of Thin Metal Coatings
Corrosion Science, 34, (1993) 851-870

27 ISO 9227-1990 (E)
Salt Spray Tests

28 S. Yajima, Y. Togawa, S.Matsushita and T. Kanbe
Outdoor Exposure and Accelerated Tests of Electroless Nickel Plating
Plating and Surface Finishing, 74 (1987) 66-71

29 W. Tomlinson and J. P. Mayor
Formation, Microstructure, Surface Roughness and Porosity of Electroless Nickel Coatings
Surface Engineering, 4 (1988) 235-238

30 J. Munemasa and T. Kumakiri
Effect of the Surface Roughness of Substrates on the Corrosion Properties of Thin Films Coated by Physical Vapour Deposition
Surface Coating Technology, 49 (1991) 496-499

31 P.V. Nazarenko, A.G. Molyar, I.E. Polishchuk, O.G. Yachinskaya and A.A Il'in
Structural Defects and the Electrochemical Properties of Nitride Coatings
Metal Science and Heat Treatment, 32 (1990) 305-308

32 M. Ürgen, A.F. Çakir, O.L. Eryilmaz and C. Mitterer
Corrosion of Zirconium Boride and Zirconium Boron Nitride Coated Steel
Surface and Coating Technology, 71 (1995) 60-66

33 BS 5466:1979
Corrosion Testing of Metallic Coatings
P4-TAA Test
P5-CORR Test
P6-Corrosion Tests of Metallic Coatings Cathodic to the Substrate
P8-Sulphur Dioxide Tests
P9-SD Test

34 BS 6670:P2-1986
Electroplated Gold and Gold Alloys Coating

35 P. T. Tang, T. Watanabe, J. E. T. Andersen and G. Beck-Nielsen
Improved Corrosion Resistamce of Pulse Plated nickel Through Crystallisation Control
Journal of Applied Electrochmistry, 25 (1995) 347-352

36 M. Clarke and A.J.Sansum
A Two Hours Porosity Test for Gold on Substrates of Copper, Silver and Nickel
Transaction of the Institute of Metal Finishing, 50 (1972) 211-214

37 M. Uergen, A.F. Çakir and O.L. Eryilmaz
Defect Evaluation in Arc PVD TiN and CrN Coated Steel by Copper Cementation Technique
East Conference, November 1993, Schwaebisch Gmuend, Germany

38 K. J. Vetter
Electrochemical Kinetics Theoretical and Experimental Aspects
Published by Academic Press, London, 1967

39 Michael Ludwig
Evaluation of Defects in PVD (TiAl)N Coatings by Copper Cementation
Diplomarbeit
Fachhochschule Osnabrueck, D / Material Research Institute Sheffield, UK, 1994

40 S.D. Chyou, H.C. Shih and T.T. Chen
On the Corrosion Characterization of Titanium Nitride in Sulphuric Acid
Corrosion Science, 35 (1-4) (1993) 337-347

41 L.P. Ward
Corrosion Inhibition by PVD Coatings: Status and Behaviour of Refractory Element Based Coatings Deposited on Stainless Steel and Mild Steel Substrates in Selected Environments
Proceedings of Euroworkshop on Advanced in Material Processing and Characterisation Technologies, August 1995, Dublin, Ireland

42 J. Dugasz and A. Szasz
Factors Effecting the Adhesion of Electroless Coatings
Surface and Coating Technology, 58 (1993) 57-62

43 B. D. Barker
Electroless Deposition of Metals
Surface Technology, 12 (1981) 77-88

44 Su Hoon Park and Dong Nyung Lee
A Study on the Microstructure and Phase Transformation of Electroless Nickel Deposits
Journal of Material Sciene, 23 (1988) 1643-1654

45 K.-H. Hur, J.-H. Jeong and D.N. Lee
Microstructure and Phase Transformation of Electroless Nickel Alloy Deposits
Thin Film and Beam Solid Interactions, 99 (1991) 247-256

46 N.M. Martyak, S. Wetterer, L. Harrison, M. McNeil, R. Heu and A.A. Neiderer
Structure of Electroless Nickel Coatings
Plating and Surface Finishing, 80 (1993) 60-64

47 J.W. Dini
Perspective on Plating for Precision Finishing
Plating and Surface Finishing, 79 (1992) 121-128

48 Robert P. Tracy and Gary J. Shawhan
Practical Guide To Using Ni-P Electroless Nickel Coatings
Material Performance, July (1990) 65-70

49 H. Deng and P. Møller
Effects of Pretreatment on the Structure and Properties of Electroless Nickel Coatings
Plating and Surface Finishing, 81 (1994) 73-77

50 G. Schmitt, E. Schmeling and S. Deussen
Grundmaterial und Schutzschicht-ein Verbundsystem
Oberflaeche-Surface, 26 (1985) 308-313

51 C. F. Beer
Improving the Corrosion Resistance of Electroless Nickel Deposits
Surface Technology, 12 (1981) 89-92

52 K. Sevugan, M. Selvam, K.N. Srinivasan, T. Vasudevan and P. Manisankar
Effect of Agitation in Electroless Nickel Deposits
Plating and Surface Finishing, 80 (1993) 56-58

53 E.T. Van Der Kouwe
EIS as a Mean of Evaluating Electroless Nickel Deposits
Electrochimica Acta, 38 (1993) 2093-2097

54 H.-K. Pulker
Wear and Corrosion Resistant Coatings by CVD and PVD
Published by Ellis Horwood Limited, Chichester, 1989

55 R. W. Berry, P. M. Hall and M. T. Harris
Thin Film Technology
D. Van Nostrand Company, Inc. Princton, New Jersey, 1968

56 M. G. Hocking, V. Vasantasree and P. S. Sidky
Metallic & Ceramic Coatings
Published by Longman Scientific & Technical, Harlow, 1989

57 M.G. Hocking
Production of Corrosion and Wear Resistant Coatings
In Surface Engineering Vol II, Engineering Application
Editors: P.K. Datta and J.S. Gray
Published by The Royal Society of Chemistry, Cambridge, 1993

58 B. N. Chapmann and J. C. Anderson
Science and Technology of Surface Coatings
Published by Academic Press, London, 1974

59 J.A. Thonton
The Mircrostructure of Sputtered Deposition Coatings
Journal of Vacuum Science and Technology, A4 (6) (1986) 3059-3065

60 D.S. Rickerby and S.J. Bull
Engineering with Surface Coatings : The Role of Coating Microstructure
Surface and Coating Technology, 39/40 (1989) 315-328

61 Dr. R.A. Haefer and Dr. B. Ilschner
Beschichtungen von Oberflaechen, (Werkstoff-Forschung und -Technik Bd5)
Springer Verlag Berlin, 1987

62 R. Messier, A.P. Giri and R.A. Roy
Revised Structure Zone Model for Thin Film Physical Structure
Journal of Vacuum Science and Technology, A2 (2) (1984) 500-503

63 D. S. Rickerby and P.J. Burnett
Correlation of Process and System Parameters with Structure and Properties of PVD Hard Coatings
Thin Solid Films, 157 (1988) 195-222

64 H. Holleck
Metastable Coatings-Prediction of Composition and Structure
Surface and Coating Technology, 36 (1988) 151-159

65 J. Vetter and W. Burgmer
Industrielle PVD-Beschichtung auf Werkzeugen und Bauteilen
VDI, 5 (1992) 47-49

66 M. Berger and P. Stokley
PVD Protective Coatings for Wear Parts
In Surface Engineering Vol II, Engineering Application
Editors: P.K. Datta and J.S. Gray
Published by The Royal Society of Chemistry, Cambridge, 1993

67 J. Aromaa, H. Ronkainen, A. Mahiout and S.-P. Hannula
Identification of Factors Affecting the Aqueous Corrosion Properties of Ti(Al)N Coated Steel
Surface Coating Technology, 49 (1991) 353-358

68 I.M. Penttinen, A.S. Korhonen, E. Harju, M.A. Turkia and O. Forsén
Comparison of the Corrosion Resistance of TiN and (Ti,Al)N Coatings
Surface and Coating Technology, 50 (1992) 161-168

69 Dieter Muenz-Private Communication

70 J.P. Celis, D. Drees, E. Maesen and J.R. Roos
Quantitative Determination of Through-Coating Porosity in Thin Ceramic Physically-Vapour Deposited Coatings
Thin Solid Films, 224 (1993) 58-62

71 A.S. Korhonen
Corrosion of Thin Hard PVD Coatings
Vacuum, 45 (1994) 1031-1034

72 G. Håkansson, L. Hultmann, J.-E. Sundgren, J.E. Greene and W.-D. Muenz
Microstructure of TiN Films grown by Various Pysical Vapour Deposition Techniques
Surface and Coating Technology, 48 (1991) 51-67

73 H. Freller and H.P. Lorenz
Electrochemically Measured Porosity of Magnetron Sputtered TiN Films Deposited at Various Substrate Orientation
Journal of Vacuum Science and Technology, A4 (6) (1986) 2691-2694

74 K. Reichel, W. Brandl and H.-D. Steffens
Korrosionsverhalten von ARC-PVD-Schichten
In Beschichten mit Hartstoffen
Editor: VDI
Published by VDI-Verlag, Duesseldorf, 1992, pp273-288

75 H. Ljungcrantz, L. Hultmann, J.-E. Sundgren, G. Håkansson and L. Karlsson
Microstructural Investigation of Droplets in Arc Evaporated TiN-Films
Surface and Coating Technology, 63 (1994) 123-128

76 M. Nishbori
How to Solve Problems of Films Coated by ARC Methods
Surface and Coating Technology, 52 (1992) 229-233

77 W. D. Muenz, F. J. M. Hauzer, D. Schulze and B. Buil
A New Concept for Physical Vapour Deposition Coating Combining the Methods of Arc Evaporation and Unbalanced-Magnetron Sputtering
Surface and Coating Technology, 49 (1991) 161-167

78 W.-D. Muenz, T. Harkmans, G. Geiren and T. Trinh
Comparison of TiAlN-Coatings grown by Unbalanced Magnetron and Arc Bond Sputtering Techniques
Journal of Vacuum Science Technology, A11 (5) (1993) 2583-2589

79 Dr. W.-D. Muenz
The New Way to Hard Coating
Arc Bond Sputtering: ABS^{TM}
Part I The Machine Design HTC 1000-4 ABS^{TM}
Published by Hauzer Techno Coating, Venlo, Netherlands, 1991

80 P. Hedenquist, M. Olsson, S. Jacobson and S. Soederberg
Failure Mode Analysis of TiN Coated High Speed Steel: In Situ Sratch Adhesion Testing in the Scannning Electron Microssope
Surface and Coating Technology, 41 (1990) 31-49

81 M. Uergen, A.F. Çakir, O.L. Eryilmaz and K. Tokmanoglu
Proceedings of 3rd Corrosion Symposium, November 1992, Ankara, 33

82 M. Uergen, A.F. Çakir, O.L. Eryilmaz and K. Tokmanoglu
Proceedings of International Ceramic Congress, October 1992, Istanbul, 530

83 H.-G. Schenzel and H. Kreye
Erhoehung der Korrosionsbestaendigkeit von chemisch abgeschiedenen Nickel-Phosphor-Schichten
Galvanotechnik, 81 (1990) 1655-1658

84 E. Raub
Research on Mirco-Throwing Power and Levelling of Plating Baths
Plating, 45 (1958) 486-492

85 J.P. Celis, J.R. Roos and C. Fan
Porosity of Electrolytic Nickel-Phosphorus Coatings
Transaction of the Institute of Metal Finishing, 69 (1991) 15-19

86 C. Fan, J.P. Celis and J.R. Roos
Effect of Substrate Pretreatment on the Porosity in Thin Nickel Electrodeposits
Surface and Coating Technology, 50 (1992) 289-294

87 K.G. Ashurst and R.W. Neale
The Porosity of Gold Deposits
Transaction of the Institue of Metal Finishing, 45 (1967) 75-82

88 E.J. Kudrak, J.A. Abys, V. Chinchankar and J.J. Maisano
Porosity of Composite Palladium, Palladium-Nickel and Gold Electrodeposits
Plating and Surface Finishing, 79 (1992) 49-55

89 Malcom Ives-Private Communication

7 Tables

Table 4 Chemical composition of mild steel EN3B

Method: STOCKS Date: 29.11.1994 Time: 15:53 Results (%)
SAMPLE ID :

	FE	C	SI	MN	P	S	CR	CR2	MO	NI	PB	TI	CU	SN
1	98.61	0.1558	0.214	0.875	0.0173	0.0149	0.021	0.011	<0.002	0.017	0.0163	<0.000	0.010	0.0072
2	98.61	0.1560	0.215	0.875	0.0174	0.0149	0.020	0.011	<0.002	0.016	0.0161	<0.000	0.010	0.0063
3	98.61	0.1553	0.215	0.875	0.0175	0.0149	0.020	0.011	<0.002	0.018	0.0162	<0.000	0.010	0.0065

	SN2	AL	CO	V	W	B	AS	SB	NB	ZR	CA	N
1	0.0147	0.009	0.004	0.004	0.005	<0.0001	<0.0005	<0.0005	0.001	0.006	0.0005	<0.0005
2	0.0153	0.009	0.004	0.004	0.004	<0.0001	<0.0005	<0.0005	0.002	0.006	0.0005	<0.0005
3	0.0139	0.008	0.004	0.004	0.004	<0.0001	<0.0005	<0.0005	0.001	0.007	0.0005	<0.0005

Method: STOCKS Date: 29.11.1994 Time: 15:53 % Average
SAMPLE ID :

FE	C	SI	MN	P	S	CR	CR2	MO	NI	PB	TI	CU	SN
98.61	0.1557	0.215	0.875	0.0174	0.0149	0.020	0.011	<0.002	0.017	0.0162	<0.000	0.010	0.0067

SN2	AL	CO	V	W	B	AS	SB	NB	ZR	CA	N
0.0146	0.009	0.004	0.004	0.004	<0.0001	<0.0005	<0.0005	0.002	0.006	0.0005	<0.0005

Method: STOCKS Date: 29.11.1994 Time: 15:54 % Average
SAMPLE ID :

FE	C	SI	MN	P	S	CR	CR2	MO	NI	PB	TI	CU	SN
98.61	0.1557	0.215	0.875	0.0174	0.0149	0.020	0.011	<0.002	0.017	0.0162	<0.000	0.010	0.0067

SN2	AL	CO	V	W	B	AS	SB	NB	ZR	CA	N
0.0146	0.009	0.004	0.004	0.004	<0.0001	<0.0005	<0.0005	0.002	0.006	0.0005	<0.0005

Table 5 Process parameters for (TiAlY)N and (TiAl)N coatings

Target Cleaning	Time	10 min
	Pressure total	$1.9*10^{-3}$ mbar
	Cathode power	5 kW
	Heater power	45 %
	Bias voltage	0 V
	Coil current	0 A
	Argon flow	160 sccm
Ion Etching	Time	20 min, 10 cycles 1 min. on, 1 min of
	Heater power	5 %
	Bias voltage	-1200 V
	Bias current	8 - 9 A
	Target current	100 A
	Argon flow	160 sccm
	Temperature	not to exceed 500 °C
Coating	Time	120 min
	Pressure total	$3.4*10^{-3}$ mbar
	Cathode power	8 kW
	Heater power	45 %
	Bias voltage	-75 V
	Bias current	12 - 17 A
	Coil current	8 A
	Argon flow	200 sccm
	Nitrogen flow	≈ 190 sccm
	Temperature	stable ≈ 425 °C

The substrate rotation for the entire process was 80 %

Table 6 The roughness of specimens before and after electroless nickel plating

Sample	Thickness	Roughness of substrate surface (S)		Roughness of electroless nickel coating (E)		Ra(S)/Ra(E)	Rt(S)/Rt(E)
	[µm]	Ra [µm]	Rt [µm]	Ra [µm]	Rt [µm]		
B6	3.4	1.094	11.827	0.599	7.965	**1.826**	**1.485**
B11	3.4	0.283	3.259	0.193	3.320	**1.470**	**0.982**
B12	3.4	0.267	3.077	0.198	3.353	**1.352**	**0.918**
B16	3.4	0.039	0.626	0.044	0.543	**0.891**	**1.153**
B17	3.4	0.042	0.588	0.049	0.680	**0.862**	**0.864**
B23	3.4	0.018	0.158	0.026	0.413	**0.699**	**0.382**
B24	3.4	0.011	0.115	0.027	0.447	**0.406**	**0.257**
C5	5.4	1.493	18.531	1.223	15.605	**1.221**	**1.188**
C6	5.4	0.981	11.043	0.570	8.369	**1.720**	**1.319**
C11	5.4	0.337	5.564	0.222	4.931	**1.516**	**1.128**
C12	5.4	0.264	2.751	0.192	3.127	**1.375**	**0.880**
C16	5.4	0.052	0.661	0.044	0.897	**1.195**	**0.737**
C17	5.4	0.034	0.366	0.041	1.128	**0.824**	**0.324**
C22	5.4	0.017	0.14	0.031	0.633	**0.548**	**0.221**
C23	5.4	0.019	0.164	0.032	0.821	**0.598**	**0.200**
D4	12	1.587	15.304	0.913	12.010	**1.739**	**1.274**
D5	12	1.042	9.525	0.679	9.434	**1.534**	**1.010**
D10	12	0.372	3.382	0.237	4.404	**1.573**	**0.768**
D11	12	0.428	5.856	0.282	4.510	**1.518**	**1.298**
D16	12	0.048	0.601	0.059	0.719	**0.821**	**0.836**
D17	12	0.049	0.500	0.062	0.897	**0.792**	**0.557**
D22	12	0.017	0.134	0.039	0.767	**0.430**	**0.175**
D23	12	0.010	0.153	0.038	1.459	**0.265**	**0.105**
E4	22.1	1.354	12.645	0.801	10.157	**1.689**	**1.245**
E5	22.1	1.142	10.240	0.845	10.596	**1.351**	**0.966**
E10	22.1	0.275	4.841	0.195	2.767	**1.414**	**1.750**
E11	22.1	0.347	5.688	0.245	4.313	**1.413**	**1.319**
E16	22.1	0.051	0.556	0.061	0.790	**0.836**	**0.704**
E17	22.1	0.032	0.378	0.059	0.736	**0.542**	**0.514**
E24	22.1	0.018	0.160	0.039	0.662	**0.456**	**0.242**

Table 7 The results of NSS tests carried out on electroless nickel coated specimens

Sample	grade	Roughness measurement		thickness	Ranking
		Ra [µm]	Rt [µm]	[µm]	visual
B3	60	0.952	8.676	3.4	1
B8	120	0.329	4.054	3.4	2
B14	1200	0.047	0.639	3.4	4
B20	6 µm	0.012	0.113	3.4	6
C2	60	0.884	8.583	5.4	3
C8	120	0.259	3.417	5.4	9
C14	1200	0.039	0.308	5.4	5
C20	6 µm	0.025	0.204	5.4	9
D2	60	0.891	10.806	12.0	7
D8	120	0.301	4.384	12.0	9
D14	1200	0.035	0.372	12.0	8
D20	6 µm	0.014	0.320	12.0	9
E2	60	1.638	13.114	22.1	9
E8	120	0.456	6.346	22.1	9
E14	1200	0.068	0.670	22.1	9
E20	6 µm	0.016	0.211	22.1	9

NB. The higher the ranking awarded the higher the corrosion resistance

Table 8 The porosity of coatings with different surface roughnesses and having different thicknesses of electroless nickel as determined using ferroxyl tests

Sample	grade	Roughness measurement		thickness	Porosity	
		Ra [µm]	Rt [µm]	[µm]	No. of pores per unit	Ranking
B1	60	1.525	12.643	3.4	264	1
B5	60	1.019	11.765	3.4	155	3
B6	60	1.094	11.827	3.4	160	2
B7	120	0.351	3.908	3.4	49	7
B11	120	0.283	3.259	3.4	22	11
B12	120	0.267	3.077	3.4	35	10
B13	1200	0.034	0.406	3.4	37	9
B16	1200	0.039	0.626	3.4	0	21
B17	1200	0.042	0.558	3.4	6	16
B19	6 µm	0.017	0.445	3.4	2	19
B23	6 µm	0.018	0.158	3.4	0	21
B24	6 µm	0.011	0.115	3.4	0	21

Table 8 Continuation

Sample	grade	Roughness measurement		thickness	Porosity	
		Ra [μm]	Rt [μm]	[μm]	No. of pores per unit	Ranking
C1	60	0.862	9.213	5.4	63	5
C5	60	1.493	18.531	5.4	122	44
C6	60	0.981	11.043	5.4	58	6
C7	120	0.453	6.839	5.4	35	510
C11	120	0.337	5.564	5.4	14	13
C12	120	0.264	2.751	5.4	13	14
C13	1200	0.050	0.859	5.4	2	19
C16	1200	0.052	0.661	5.4	2	19
C17	1200	0.034	0.366	5.4	0	21
C19	6 μm	0.022	0.163	5.4	.1	20
C22	6 μm	0.017	0.140	5.4	0	21
C23	6 μm	0.019	0.164	5.4	2	19
D1	60	1.164	13.058	12.0	21	12
D4	60	1.587	15.304	12.0	44	8
D5	60	1.042	9.525	12.0	7	15
D7	120	0.353	4.479	12.0	3	18
D11	120	0.428	5.856	12.0	0	21
D12	120	0.370	4.519	12.0	0	21
D13	1200	0.067	0.930	12.0	0	21
D16	1200	0.048	0.601	12.0	0	21
D17	1200	0.049	0.500	12.0	0	21
D19	6 μm	0.014	0.121	12.0	0	21
D22	6 μm	0.017	0.134	12.0	0	21
D23	6 μm	0.010	0.153	12.0	0	21
E1	60	1.330	15.139	22.1	4	17
E4	60	1.354	12.645	22.1	2	19
E5	60	1.142	10.240	22.1	0	21
E7	120	0.221	1.987	22.1	0	21
E10	120	0.275	4.841	22.1	0	21
E11	120	0.347	5.688	22.1	0	21
E13	1200	0.034	0.434	22.1	0	21
E16	1200	0.051	0.556	22.1	0	21
E17	1200	0.032	0.378	22.1	0	21
E19	6 μm	0.016	0.134	22.1	1	20
E24	6 μm	0.018	0.160	22.1	0	21

Unit = 490 mm^2

NB. The higher the ranking awarded the higher the corrosion resistance

Table 9 The porosity of (TiAl)N, TiN and CrN coatings as determined using ferroxyl tests

Sample	grade	Roughness measurement		thickness	Porosity	
		Ra [μm]	Rt [μm]	[μm]	No. of pores per unit	Ranking
A31	25	0.056	0.469	1.5	631	2
A19	14	0.045	1.024	1.5	655	1
A9	6	0.019	0.367	1.5	455	3
TiN2	rolled	1.090	7.011	2.2	722	
CrN2	rolled	0.922	7.158	2.8	65	

Unit = 490 mm^2

NB. The higher the ranking awarded the higher the corrosion resistance

Table 10 The results of SO_2 corrosion tests on electroless nickel coated specimens having different roughness and thickness

Sample	grade	Roughness measurement		thickness	Porosity test	Ranking
		Ra [μm]	Rt [μm]	[μm]	parameters	visual (72h)
B4	60	1.217	12.784	3.4	SO_2 Test, 24 h	1
B9	120	0.236	2.654	3.4	SO_2 Test, 24 h	2
B15	1200	0.035	0.444	3.4	SO_2 Test, 24 h	3
B22	6 μm	0.018	0.152	3.4	SO_2 Test, 24 h	5
C3	60	1.107	10.955	5.4	SO_2 Test, 24 h	4
C9	120	0.268	3.202	5.4	SO_2 Test, 24 h	7
C15	1200	0.035	0.289	5.4	SO_2 Test, 24 h	6
C21	6 μm	0.015	0.540	5.4	SO_2 Test, 24 h	8
D3	60	1.170	12.584	12.0	SO_2 Test, 24 h	9
D9	120	0.425	6.027	12.0	SO_2 Test, 24 h	10
D15	1200	0.036	0.436	12.0	SO_2 Test, 24 h	11
D21	6 μm	0.014	0.125	12.0	SO_2 Test, 24 h	12
E3	60	1.179	10.510	22.1	SO_2 Test, 72 h	(1)
E9	120	0.330	4.352	22.1	SO_2 Test, 72 h	(2)
E15	1200	0.045	0.475	22.1	SO_2 Test, 72 h	(3)
E23	6 μm	0.017	0.488	22.1	SO_2 Test, 72 h	(4)

NB. The higher the ranking awarded the higher the corrosion resistance

Table 11 ICP results for (TiAl)N coated samples exposed to cementation tests

Coating	Sample	grade	Roughness		Test	ICP [mg/l]		
		[µm]	Ra [µm]	Rt [µm]	Conditions	Fe	Al	Ti
	Blank1				pH 1.1	0.321	0.1259	0.0065
(TiAl)N	A12	6	0.019	0.393	pH 1.1, 300 sec	1.243	0.0855	0.0061
(TiAl)N	A23	14	0.044	0.581	pH 1.1, 300 sec	1.220	0.0891	0.0068
(TiAl)N	A35	25	0.053	0.427	pH 1.1, 300 sec	1.455	0.0882	0.0065
	Blank1				pH 5.5	0.259	0.0722	0.0102
(TiAl)N	A24	14	0.042	0.671	pH 5.5, 300 sec	0.820	0.0977	0.0380

Table 12 ICP results for TiN coated samples exposed to cementation tests

Coating	Sample	grade	Roughness		Test	ICP [mg/l]	
		[µm]	Ra [µm]	Rt [µm]	Conditions	Fe	Ti
	Blank1				pH 1.1	0.321	0.0065
TiN	TiN1	rolled	1,023	7.007	pH 1.1, 300 sec	1.156	0.0093
TiN	TiN3	rolled	0.990	8.150	pH 1.1, 300 sec	1.488	0.0120

Table 13 ICP results for CrN coated samples exposed to cementation tests

Coating	Sample	grade	Roughness		Test	ICP [mg/l]	
(TiAl)N		[µm]	Ra [µm]	Rt [µm]	Conditions	Fe	Cr
	Blank2				pH 1.1	0.186	< 0.0101
CrN	CrN1	rolled	0.916	7.150	pH 1.1, 300 sec	2.468	<0.0101
CrN	CrN3	rolled	1.002	6.925	pH 1.1, 300 sec	1.401	<0.0101

Table 14 ICP results for mild steel sample exposed to cementation tests

Coating	Sample	grade	Roughness		Test	ICP [mg/l]
Non		[µm]	Ra [µm]	Rt [µm]	Conditions	Fe
	Blank2				pH 1.1	0.186
Non	Fe	6	0.018	0.148	pH 1.1, 300 sec	2.292

8 Figures

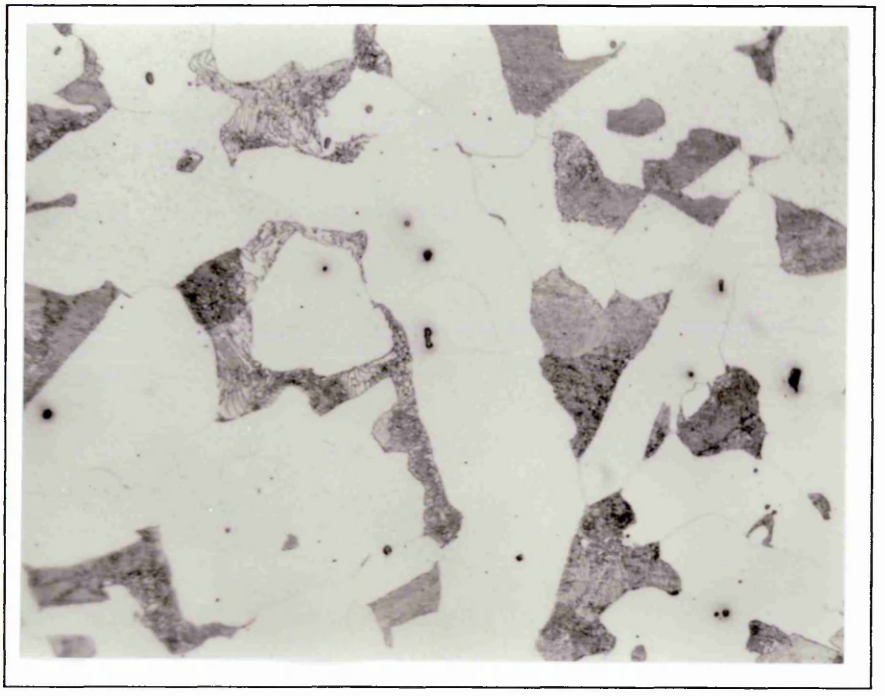

Magn 750 : 1

Figure 12 Microstructure of mild steel EN3B showing small inclusions of MnS in both the ferritic and perlitic phases

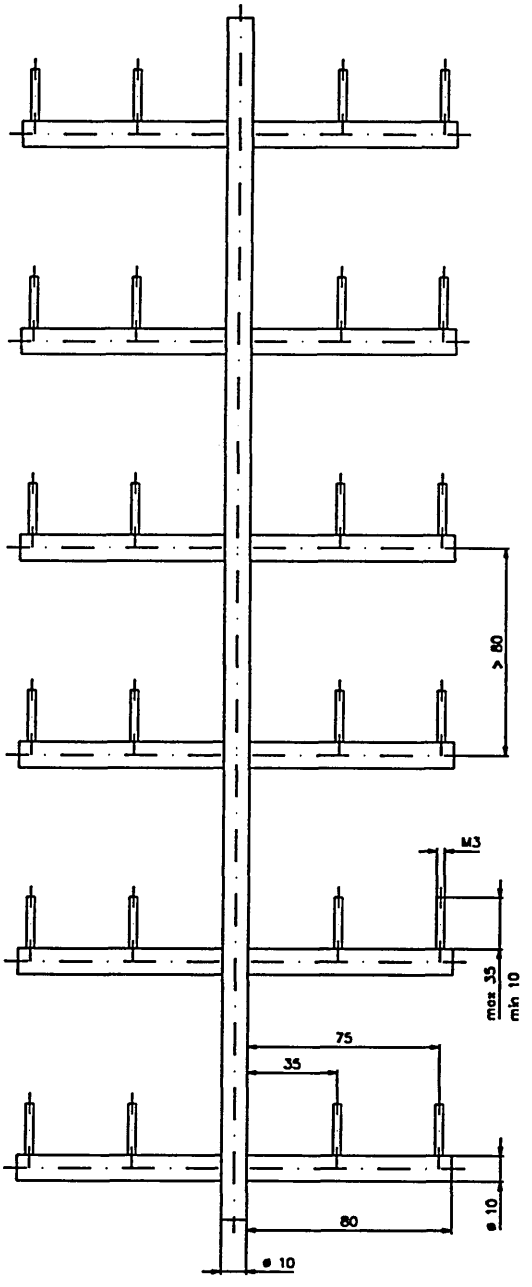

Figure 13 Jig used to carry the electroless nickel samples

a)

b)

c)

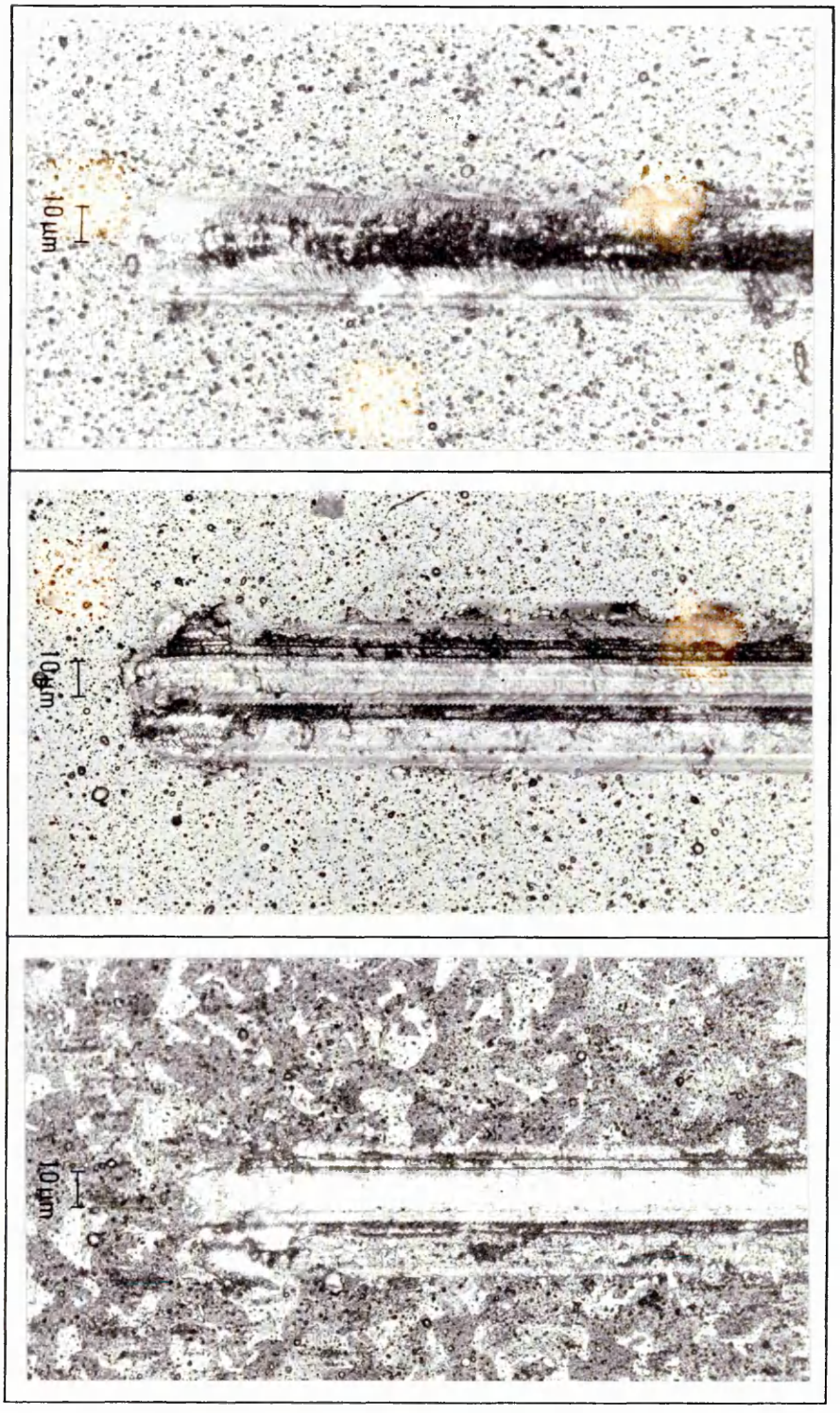

a) precleaning-sequence 1 b) precleaning sequence 2 c) precleaning sequence 3

Figure 14 Grooves obtained on PVD coated mild steel during scratch tests

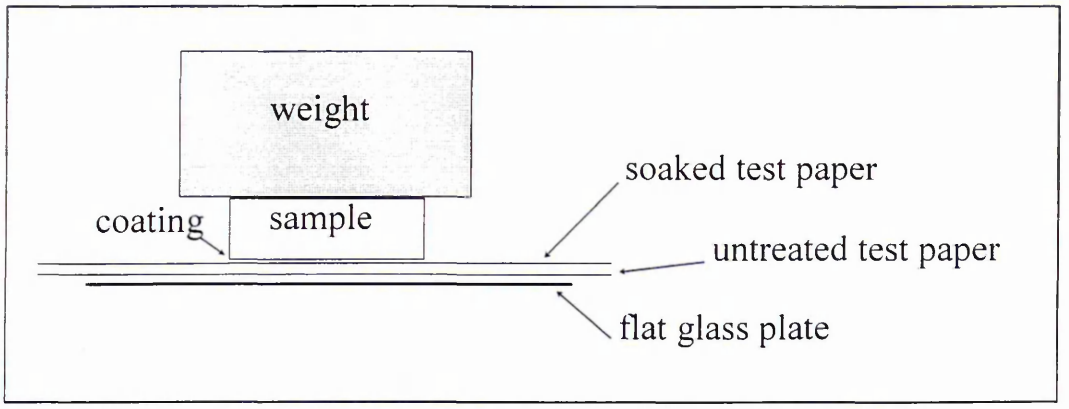

Figure 15 Ferroxyl test

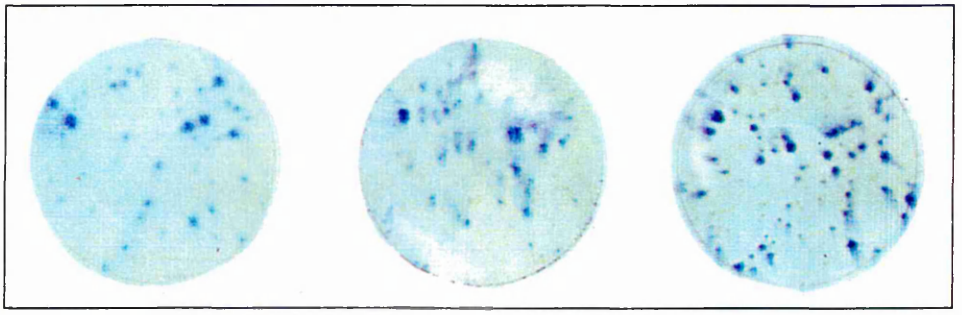

$P = 0\ N/mm^2$	$P = 0.13\ N/mm^2$	$P = 0.13\ N/mm^2$
No paper underneath test paper	No paper underneath test paper	With paper underneath freshly prepared test paper

Figure 16 Results of ferroxyl tests carried out according to ASTM B 689 1981 and BS 4758:1986

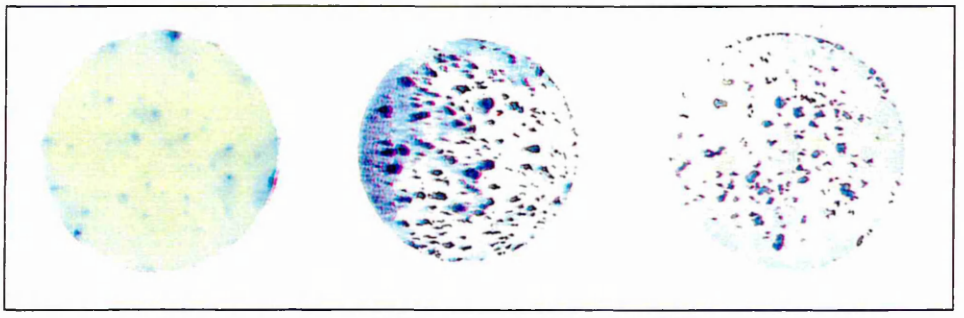

a) ASTM B 689, BS 4758:1986 Optimum conditions	b) modified ferroxyl test Test paper placed directly on the sample	c) modified ferroxyl test Sample placed directly on the test paper

Figure 17 Comparison of ferroxyl test results carried out according to ASTM B 689 1981, BS 4758:1986 and [30] on electroless nickel coatings

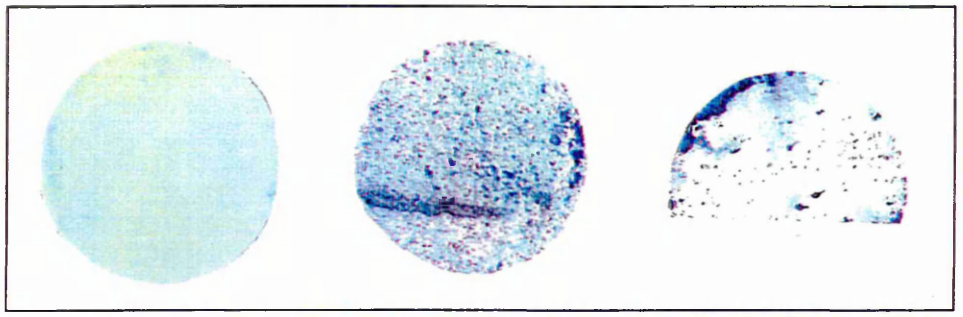

a) ASTM B 689, BS 4758:1986 Optimum conditions	b) modified ferroxyl test Test paper placed directly on the sample	c) modified ferroxyl test Sample placed directly on the test paper

Figure 18 Comparison of ferroxyl test results carried out according to ASTM B 689 1981, BS 4758:1986 and [30] on PVD coatings

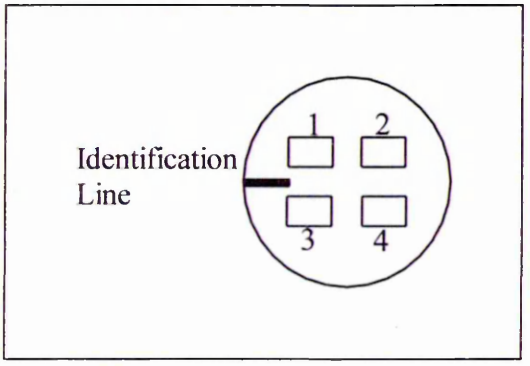

Figure 19 Illustration showing position of area frames and locations mark used on specimens to aid SEM examination of areas before and after tests

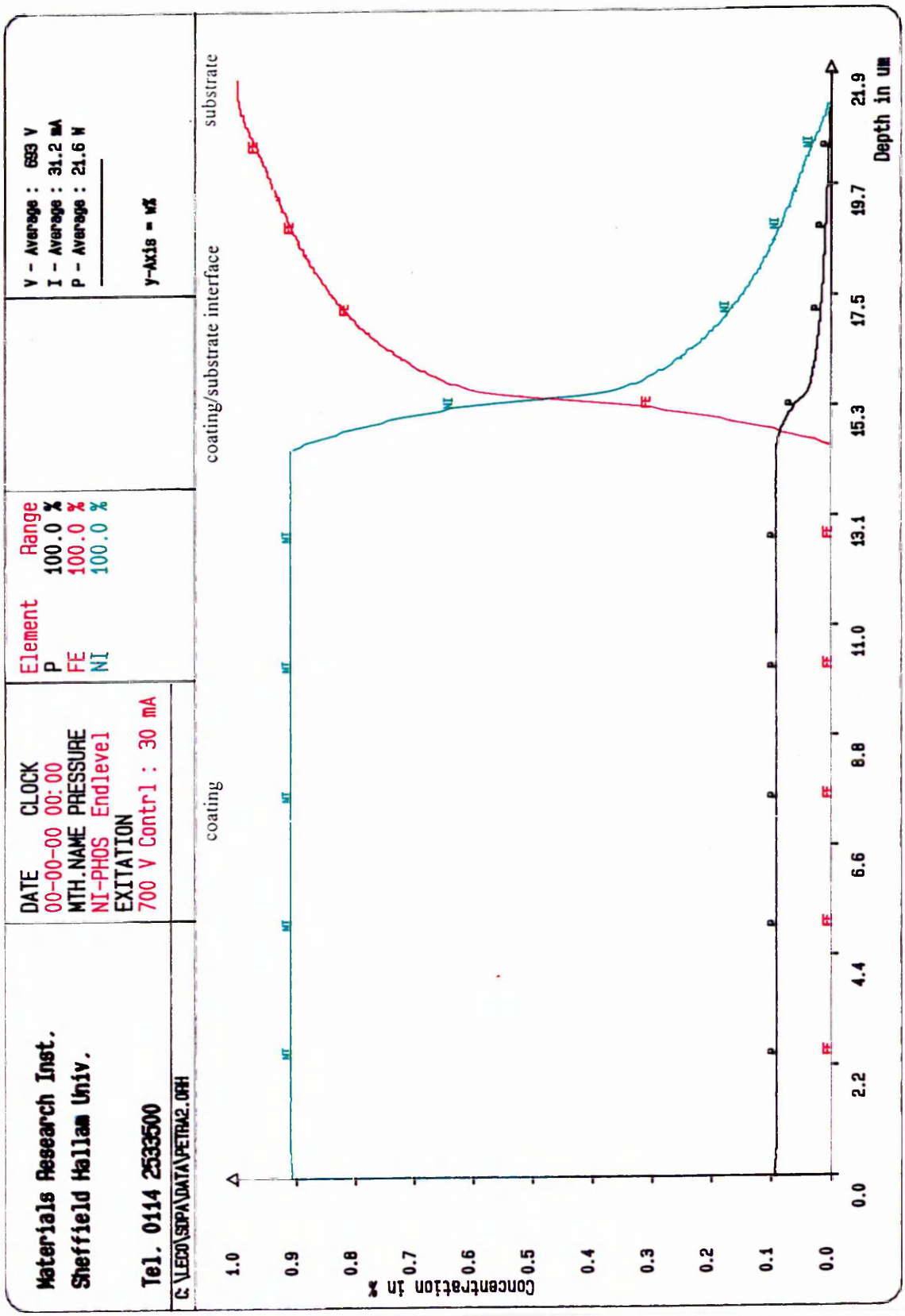

Figure 20 Elemental concentration depth profiles for a 22.1 µm electroless nickel coated sample

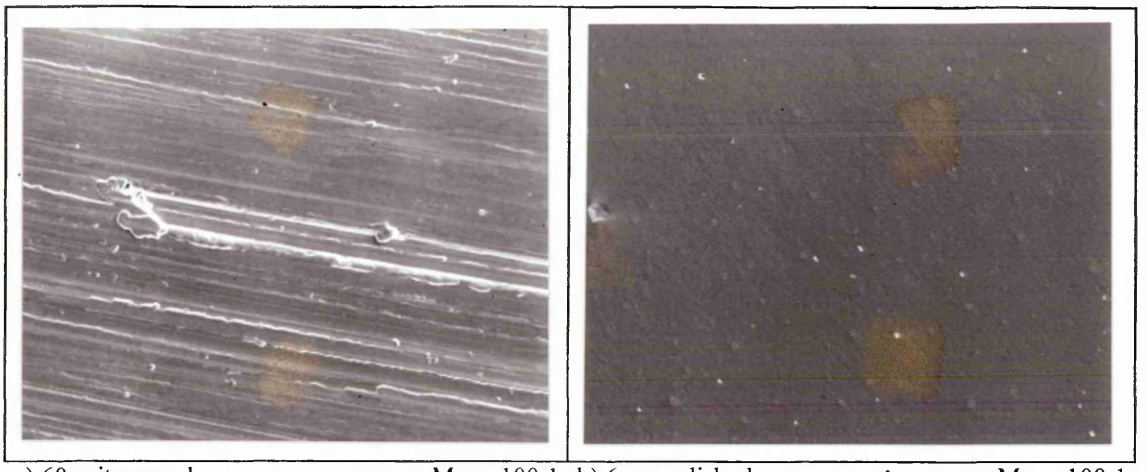

a) 60 grit ground Magn 100:1 b) 6μm polished Magn 100:1

Figure 21 The surface morphologies of 3.4 μm thick electroless nickel coated samples

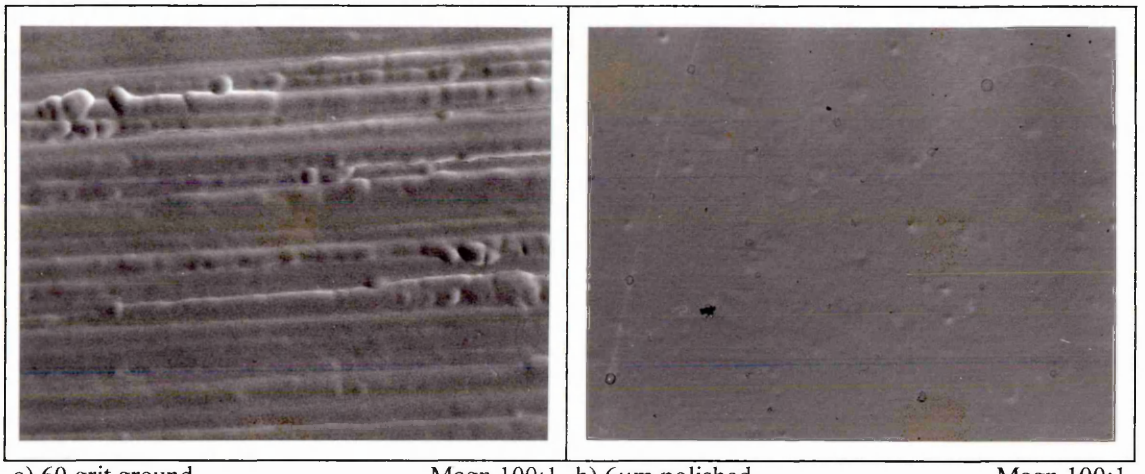

a) 60 grit ground Magn 100:1 b) 6μm polished Magn 100:1

Figure 22 The surface morphologies of 22.1 μm thick electroless nickel coated samples

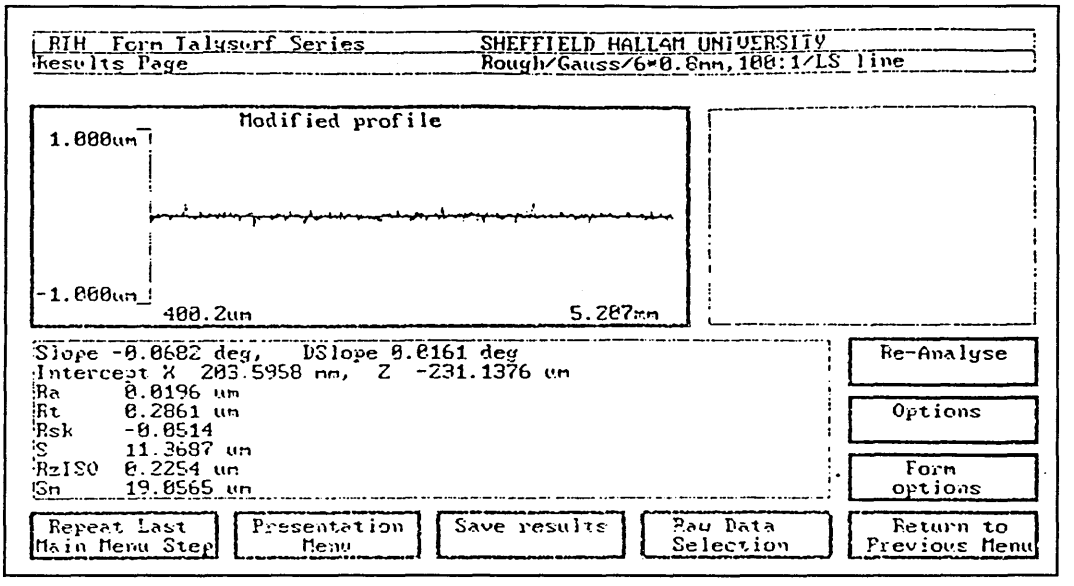

Figure 23 Surface roughness reading of a substrate (6 μm polished)

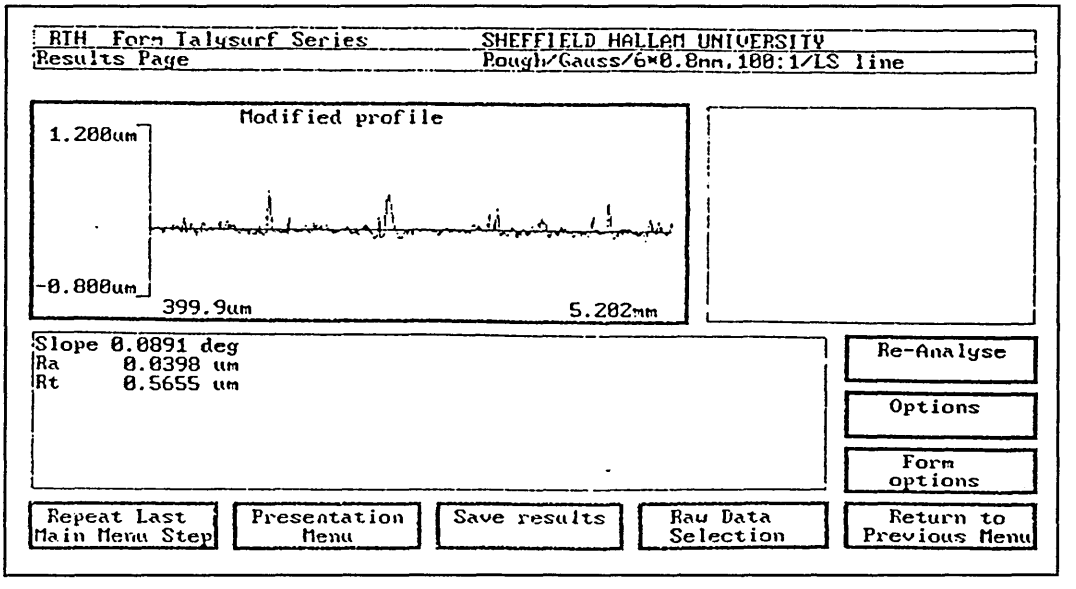

Figure 24 Surface roughness reading of a 22.1 thick electroless nickel coating (substrate 6 μm polished)

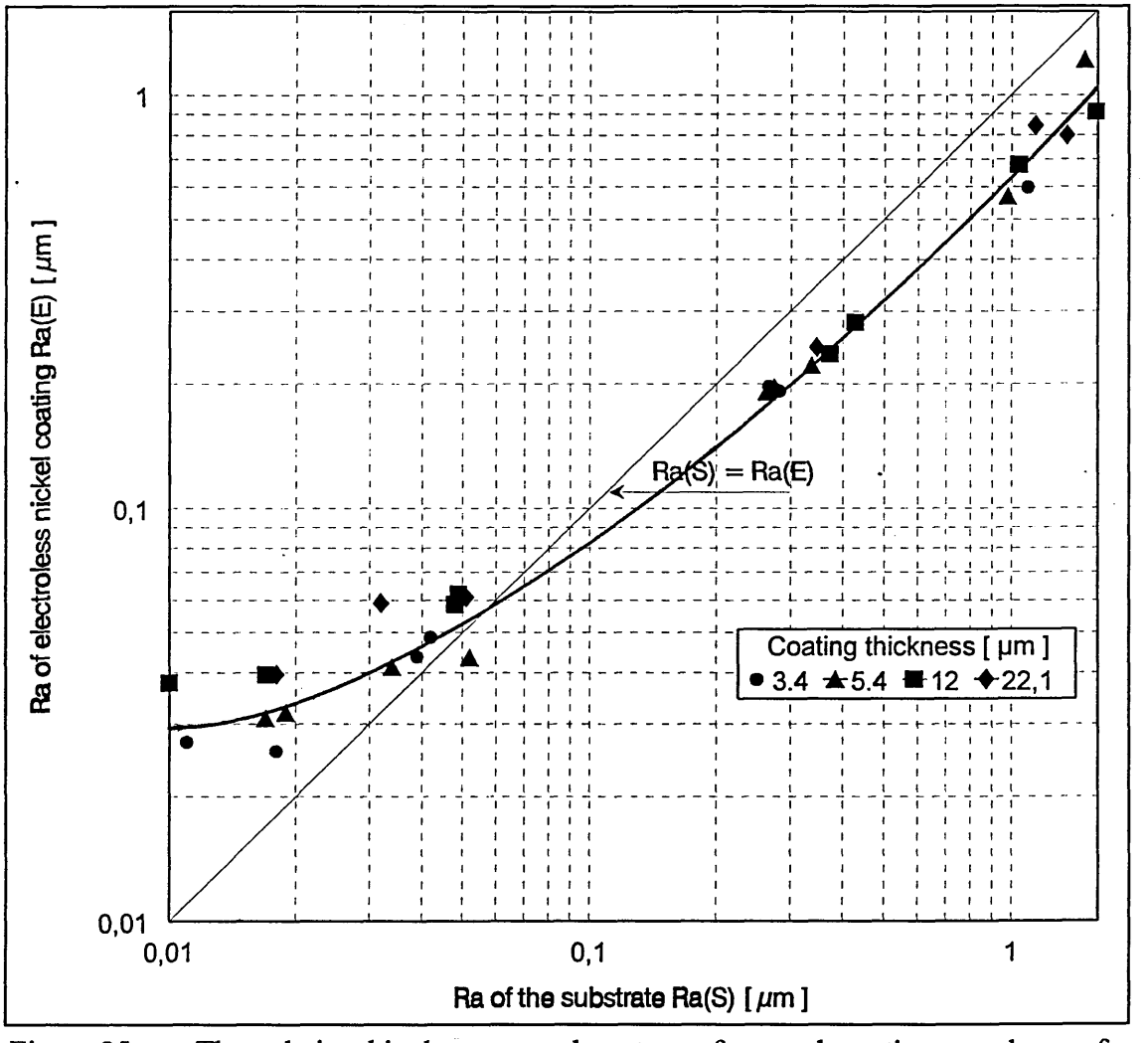

Figure 25 The relationship between substrate surface and coating roughness for electroless nickel plated mild steel

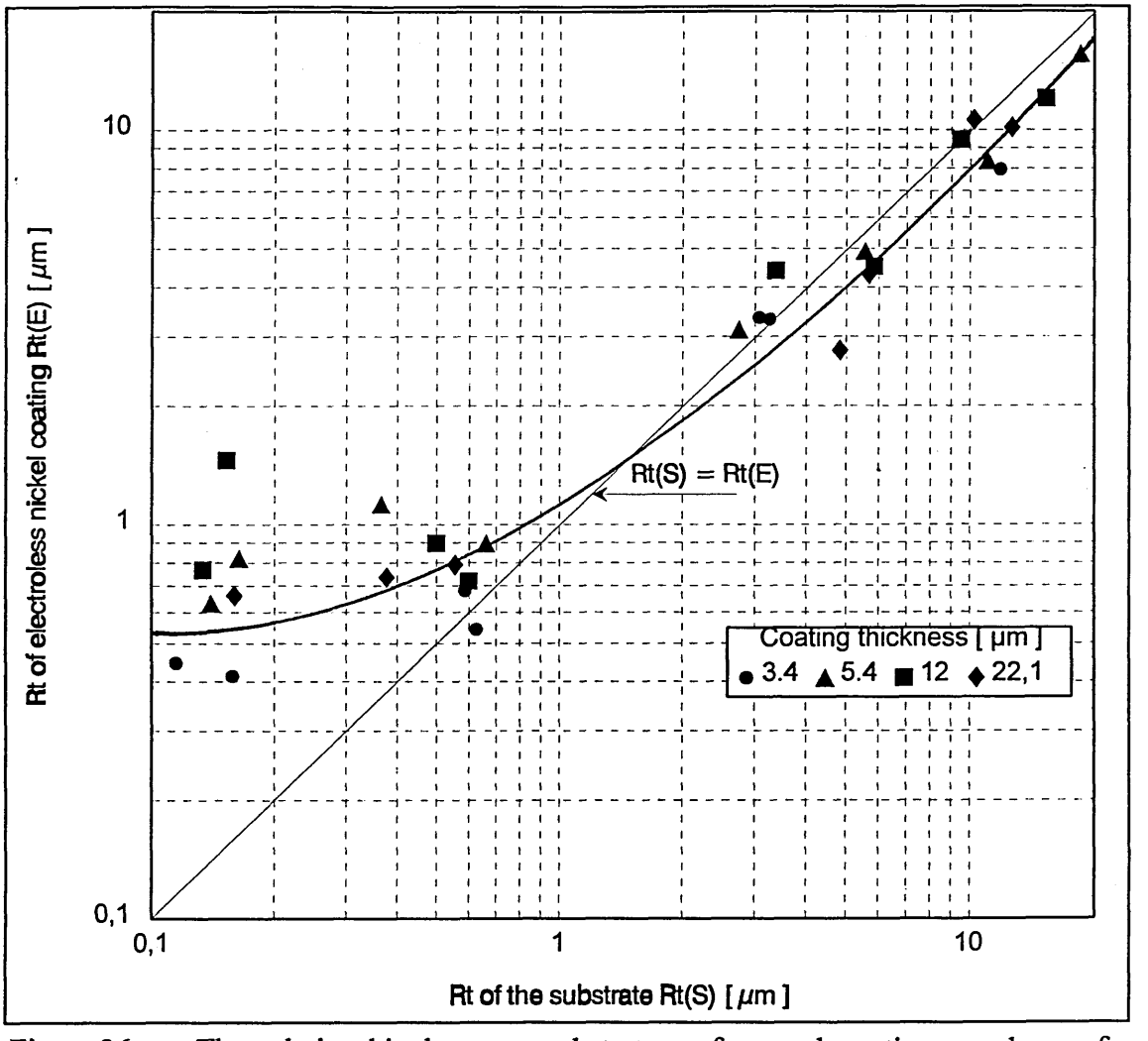

Figure 26 The relationship between substrate surface and coating roughness for electroless nickel plated steel

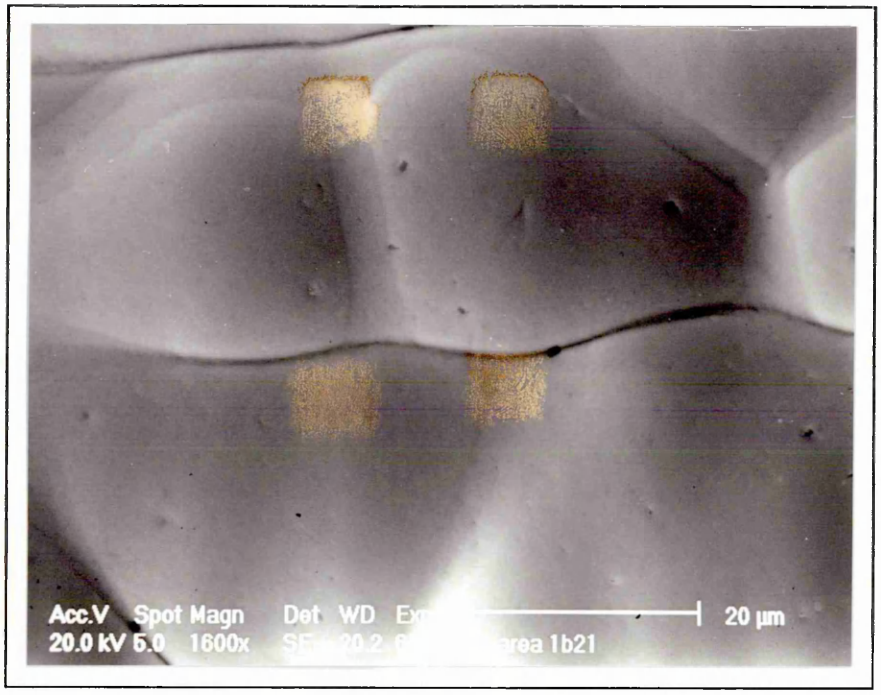

Figure 27 Surface morphology of a 22.1 µm thick electroless nickel coated sample (60 grit ground)

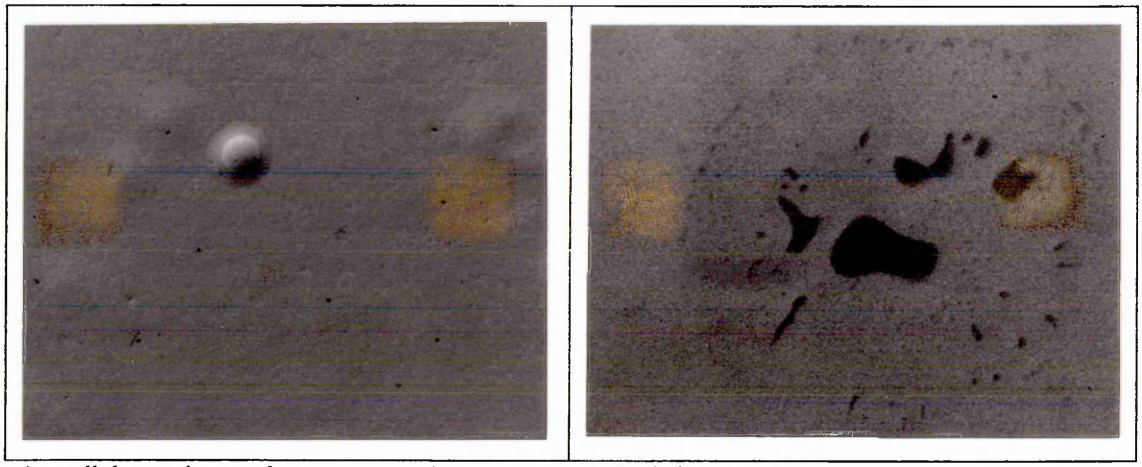

a) small depressions and 'hummocks` Magn 400:1 b) black features Magn 3400:1

Figure 28 Surface morphologies of a 22.1 µm thick electroless nickel coated sample (6 µm polished)

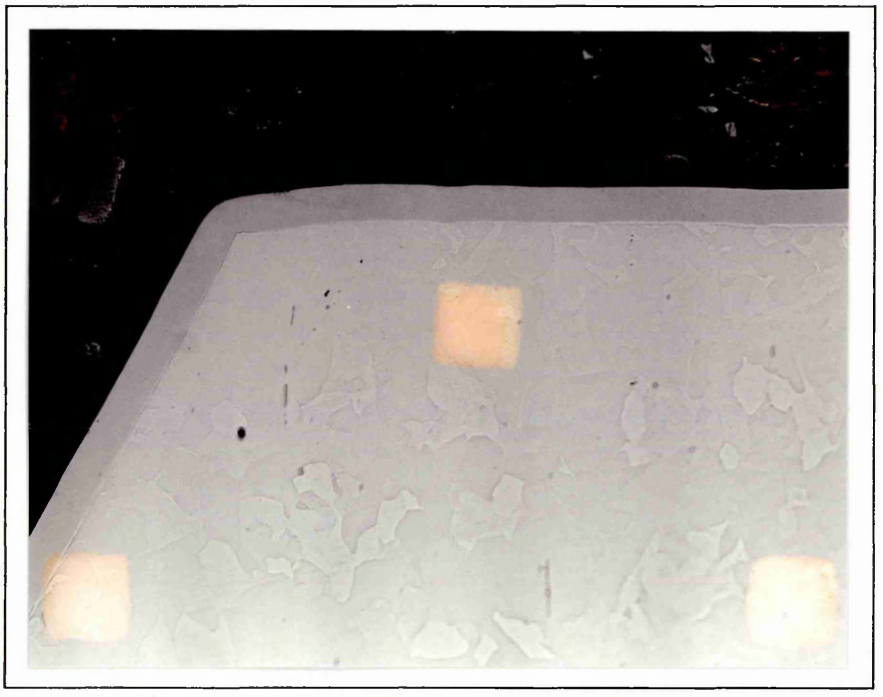

Figure 29 Cross-section of a 22.1 µm electroless nickel coated sample Magn 50:1

Figure 30 Cross-section of a 22.1 µm electroless nickel coated sample, etched in chromium acid Magn 50:1

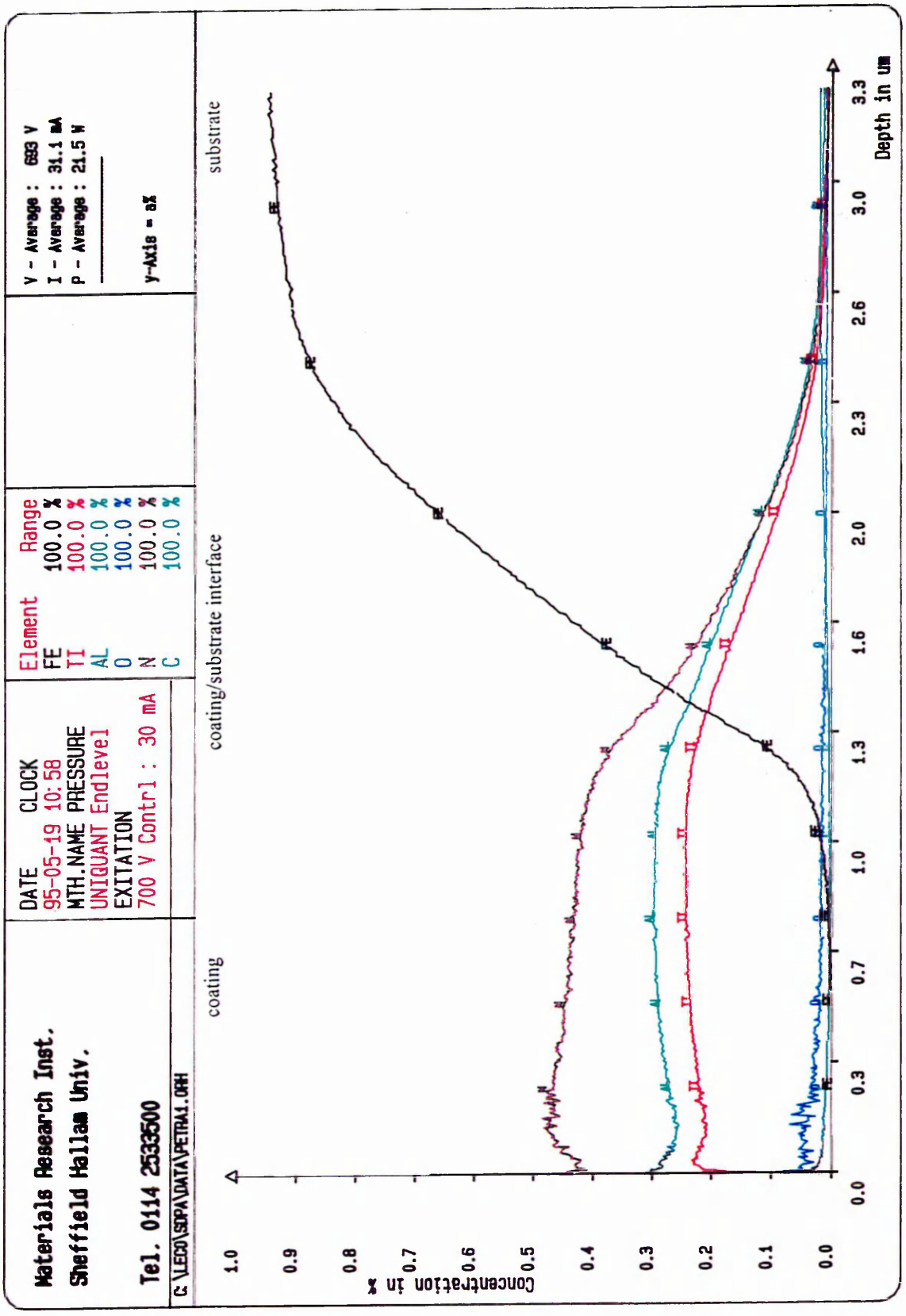

Figure 31 Elemental concentration depth profiles for (TiAl)N coated mild steel

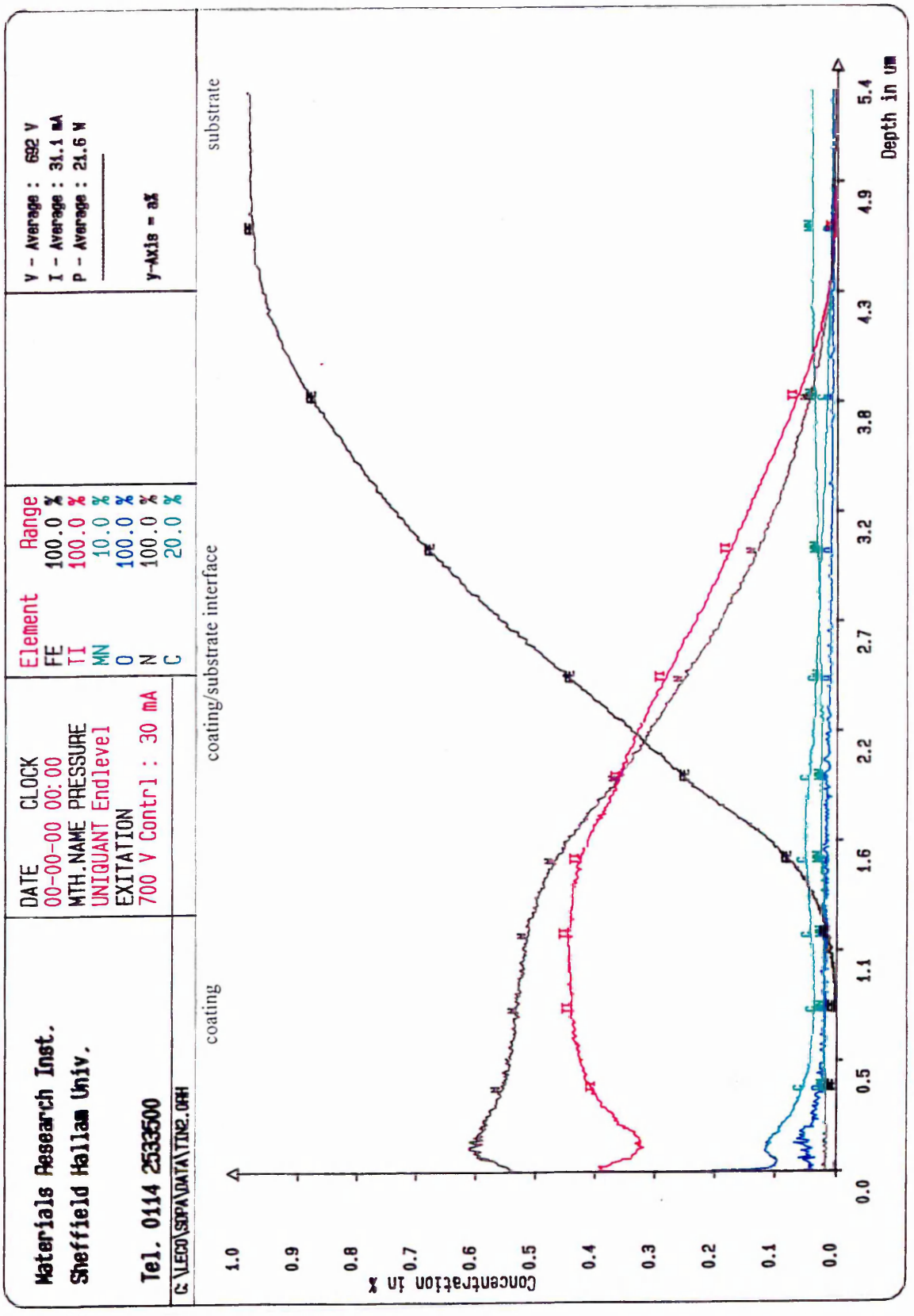

Figure 32 Elemental concentration depth profiles for TiN coated mild steel

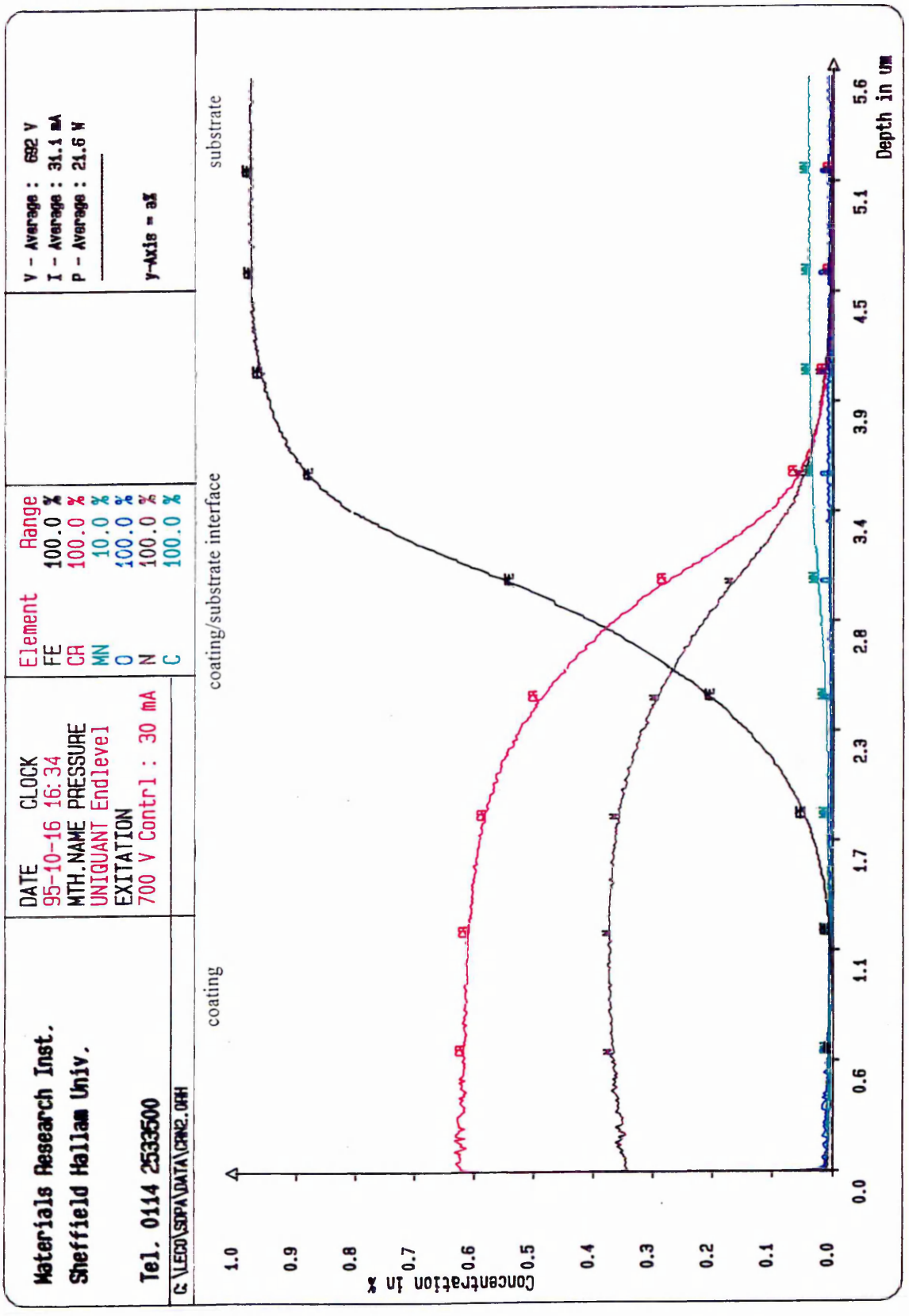

Figure 33 Elemental concentration depth profiles for CrN coated mild steel

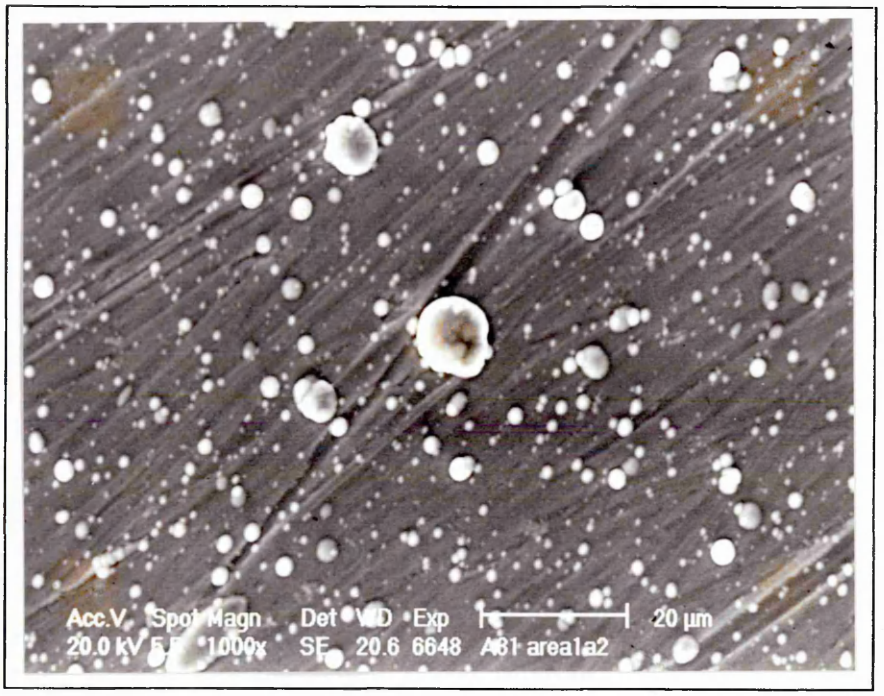

Figure 34 Surface morphology of a (TiAl)N coated sample

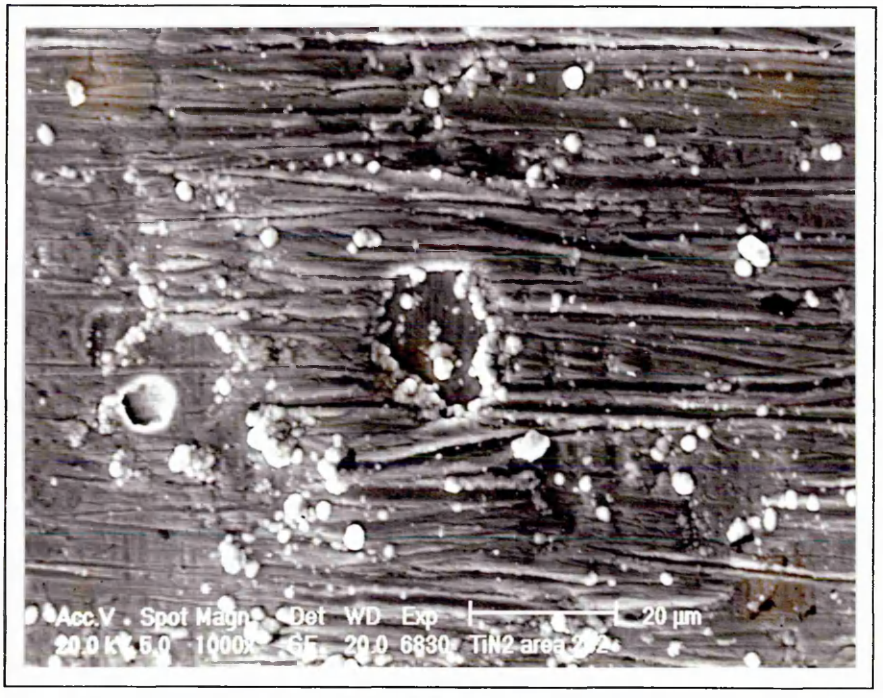

Figure 35 Surface morphology of a TiN coated sample

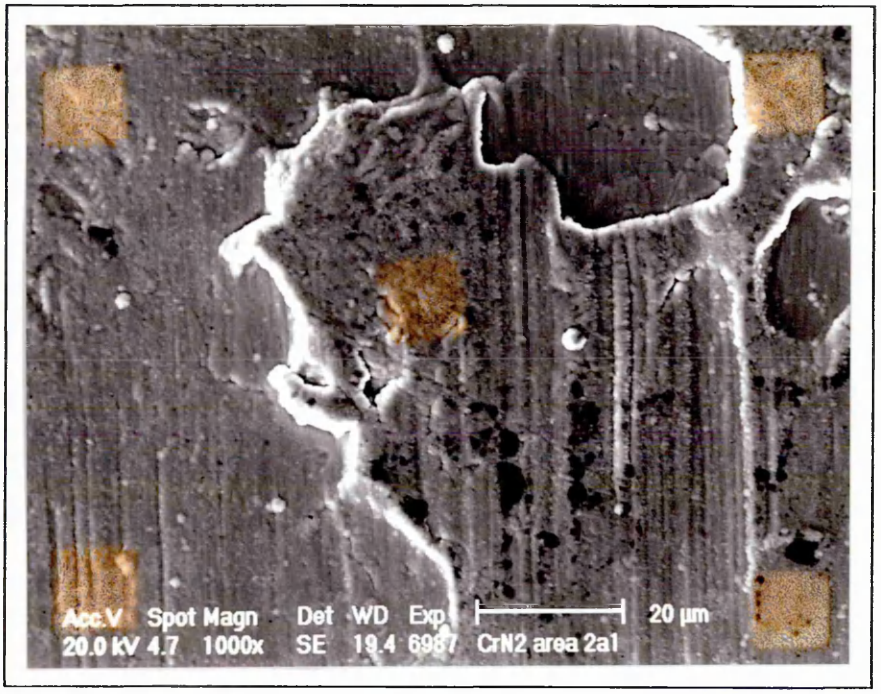

Figure 36 Surface morphology of a CrN coated sample

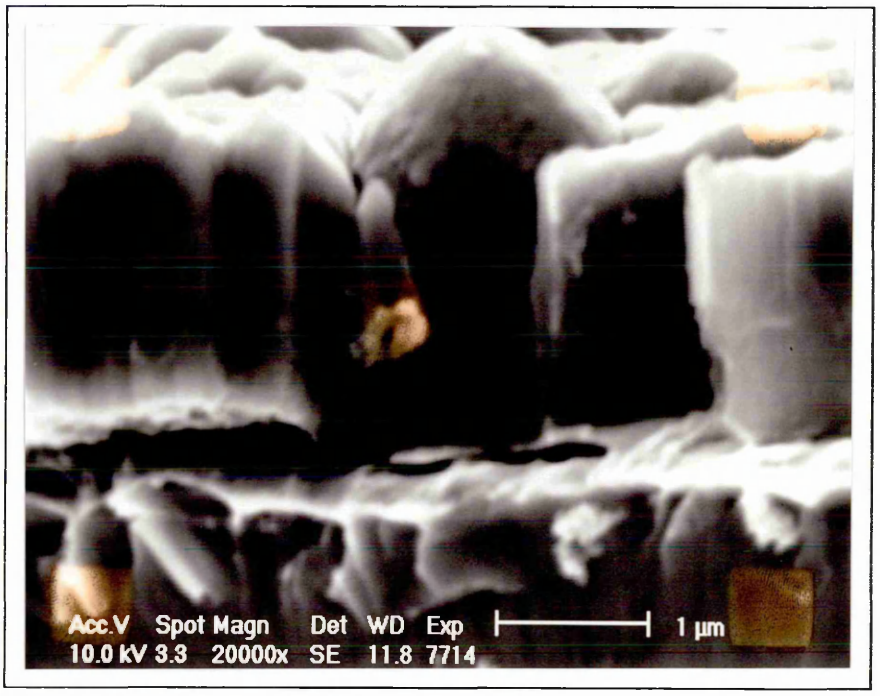

Figure 37 A fracture in a (TiAl)N coated sample

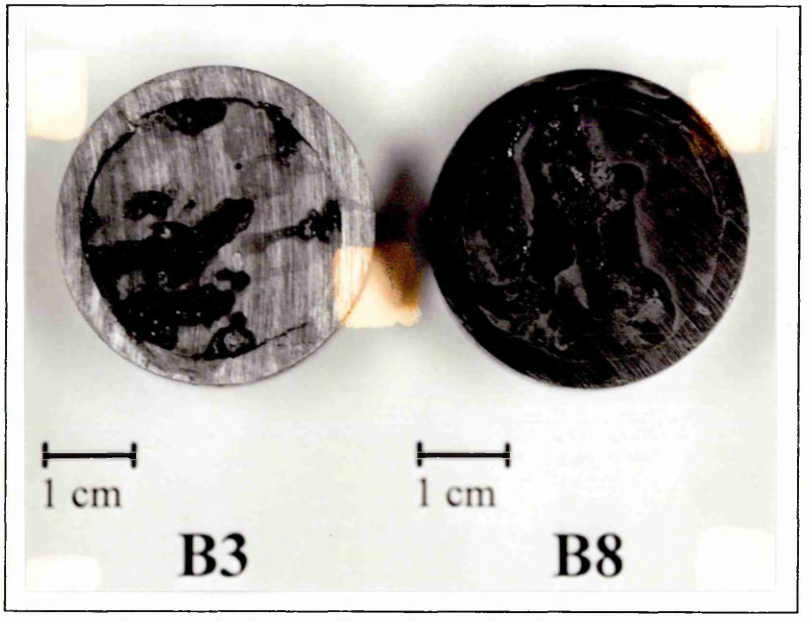

Figure 38 Electroless nickel coated samples after exposure to the NSS test

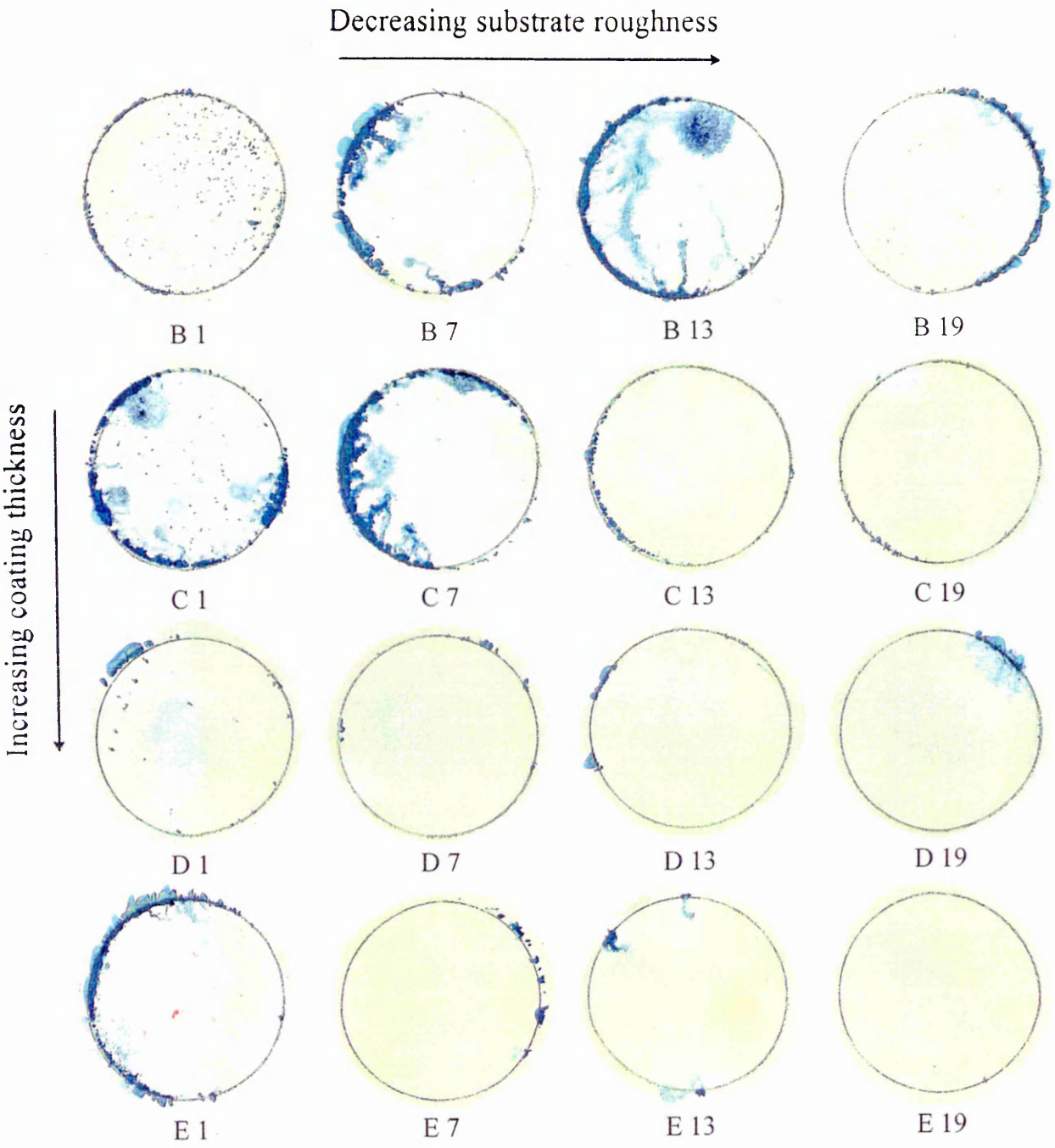

Figure 39 The results of porosity tests carried out on electroless nickel coatings using ferroxyl tests

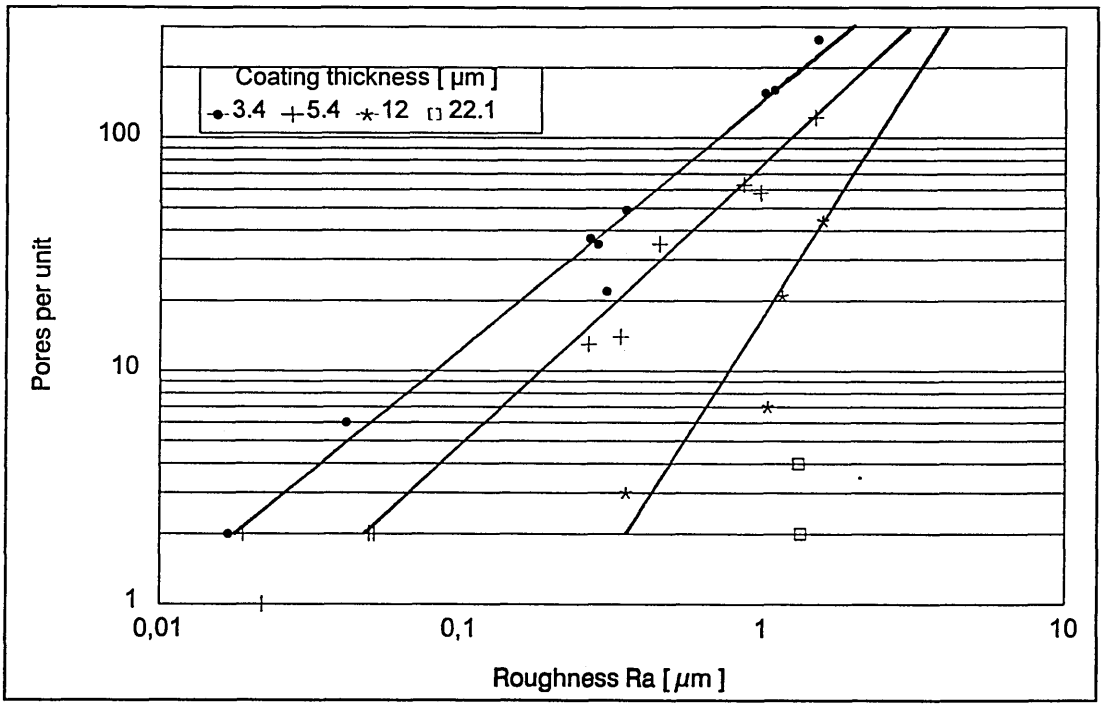

Figure 40 The relationship between porosity and substrate roughness for electroless nickel coatings

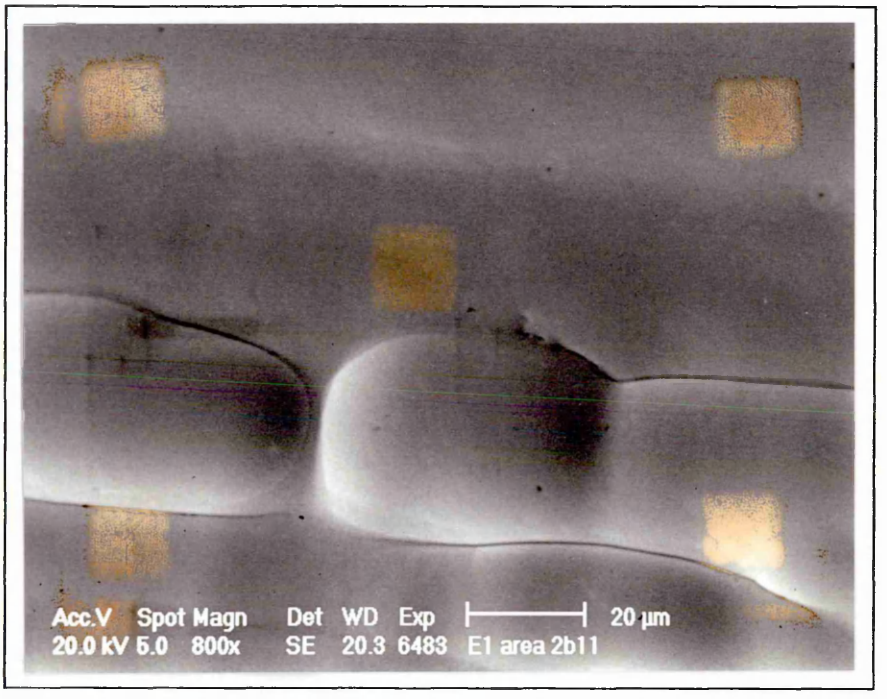

a) Electroless nickel coated sample before exposure to the ferroxyl test

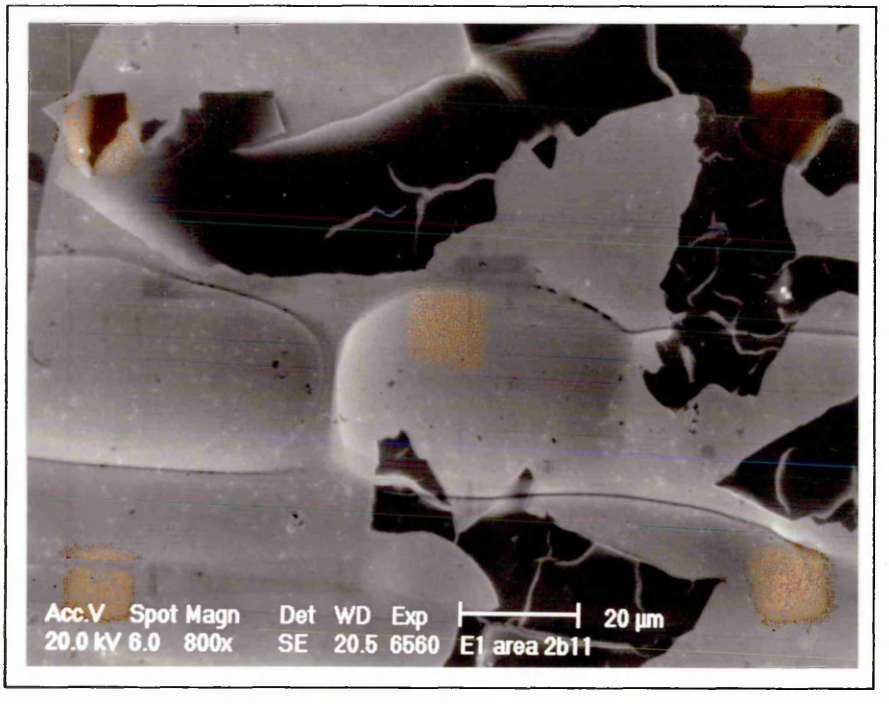

b) Electroless nickel coated sample after exposure to the ferroxyl test

Figure 41 Electroless nickel coated sample a) before and b) after exposure to the ferroxyl test

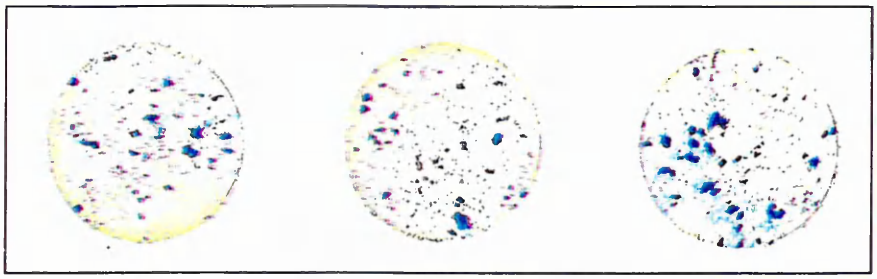

A9 A19 A31

Figure 42 The results of porosity tests on (TiAl)N coatings obtained using ferroxyl tests

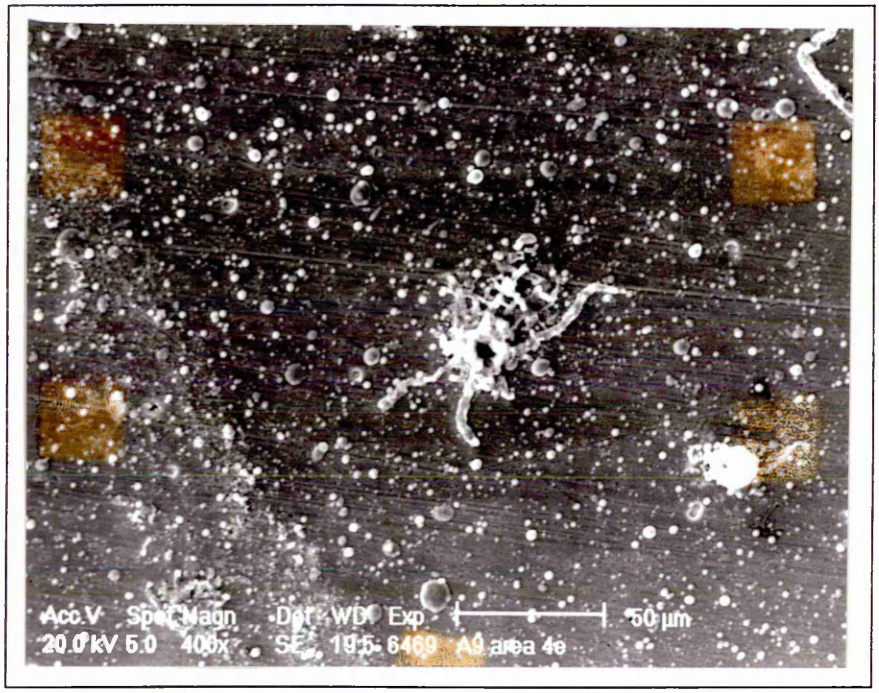

Figure 43 (TiAl)N coated sample after exposure to the ferroxyl test

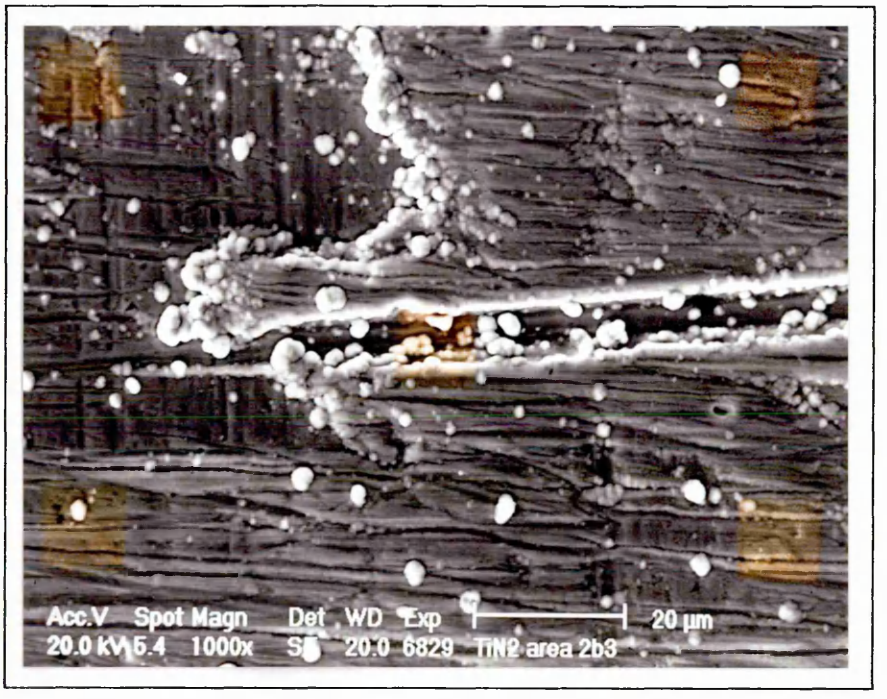

a) TiN coated sample before exposure to the ferroxyl test

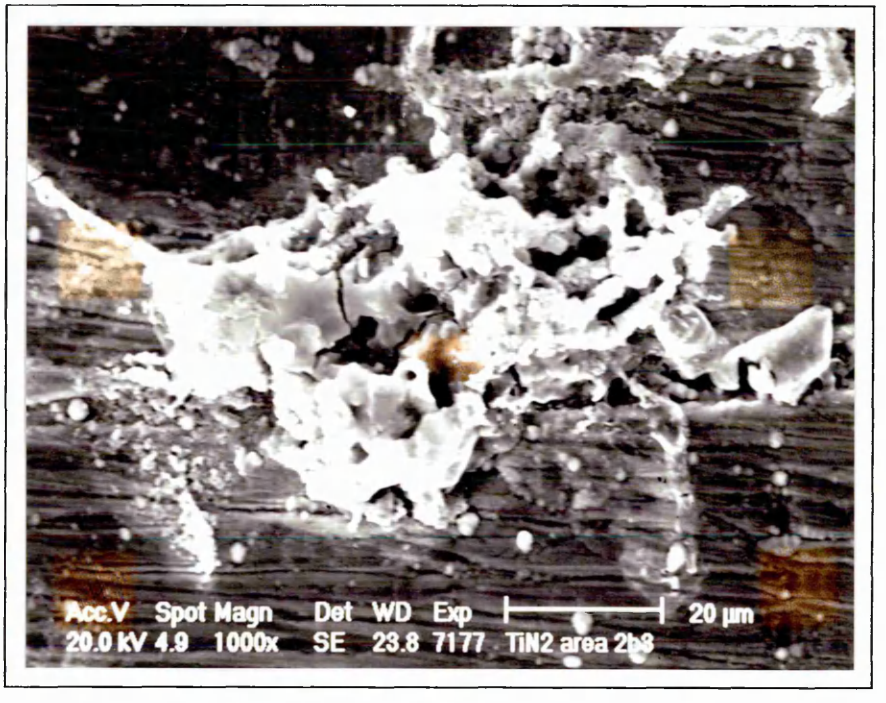

b) TiN coated sample after exposure to the ferroxyl test

Figure 44 TiN coated sample after exposure to the ferroxyl test

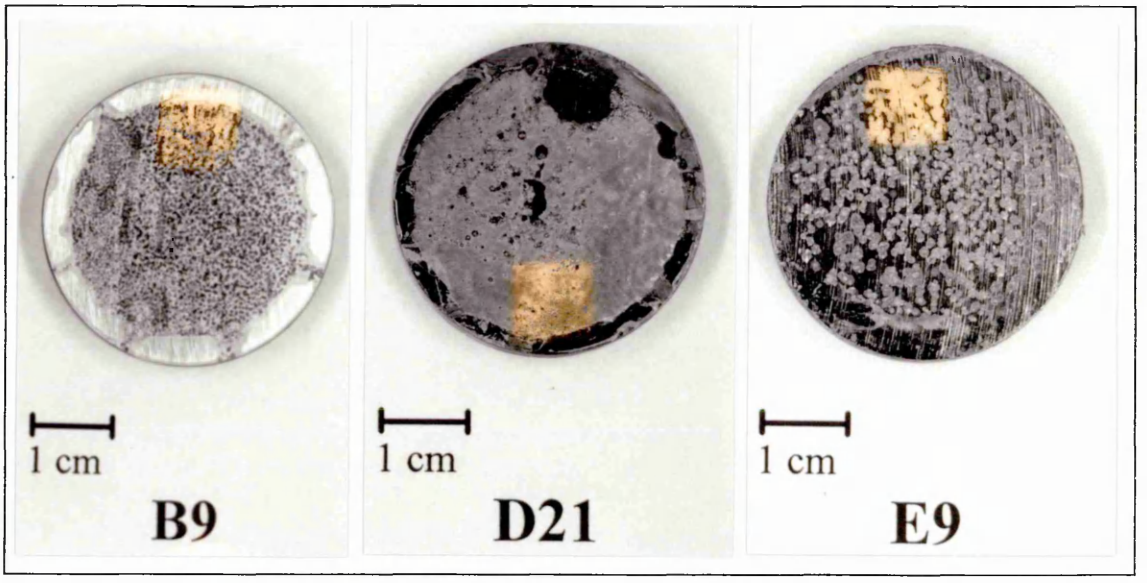

a) 24 hours b) 24 hours c) 72 hours

Figure 45 Electroless nickel coated samples after exposure to the SO_2 test for 24 and 72 hours

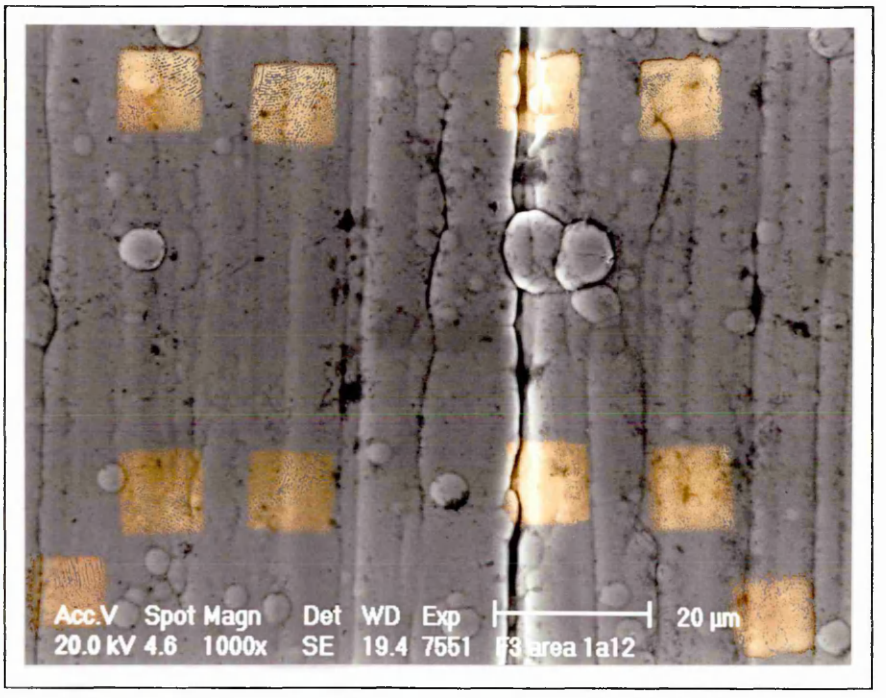

a) Electroless nickel coated sample before exposure to the SO_2 test

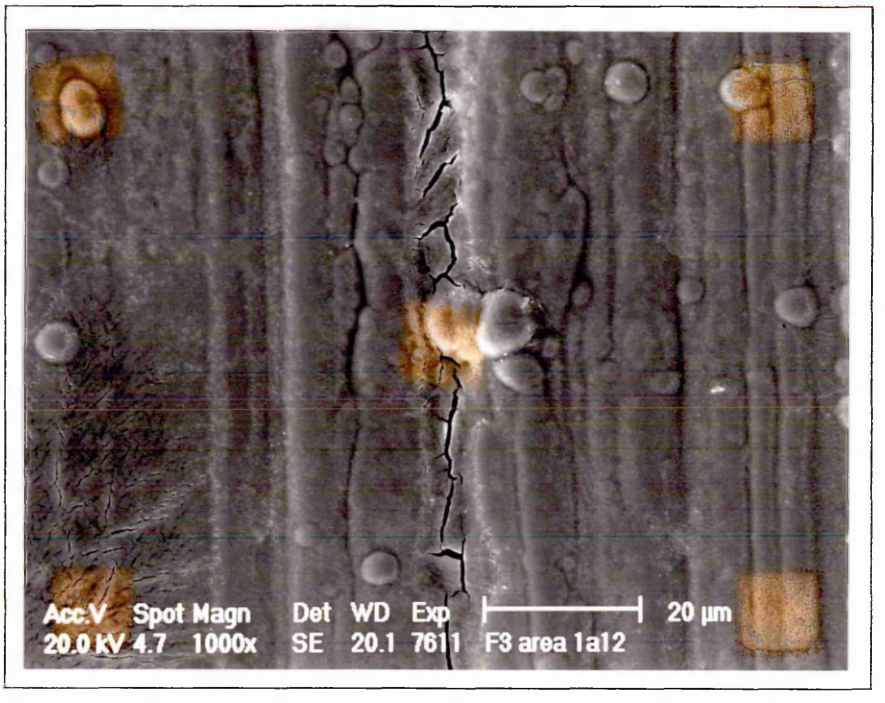

b) Electroless nickel coated sample after exposure to the SO_2 test for two hours

Figure 46 Electroless nickel coated sample a) before and b) after exposure to the SO_2 test for two hours

Figure 47 Electroless nickel sample after exposure to the SO_2 test for three hours

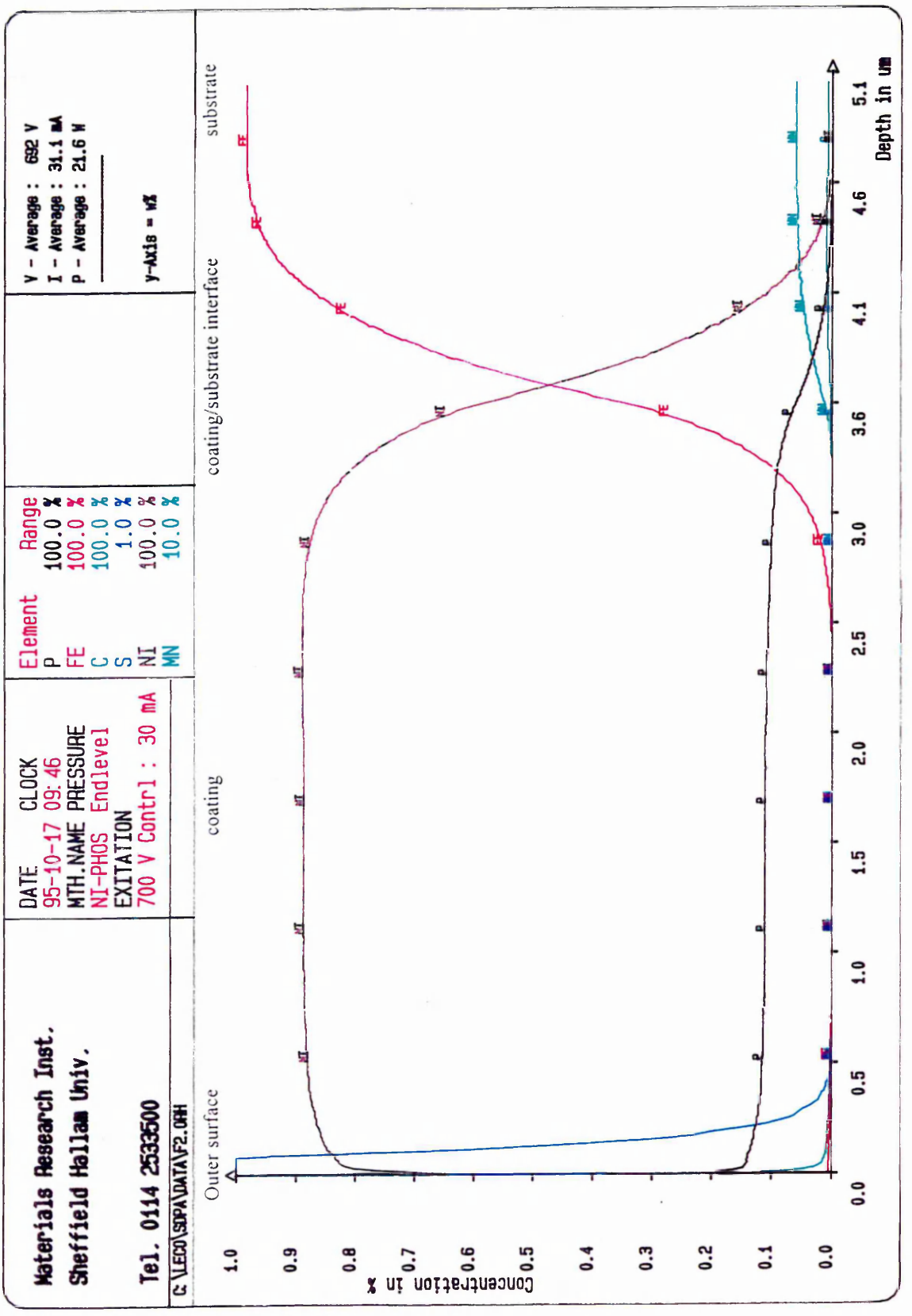

Figure 48 Elemental concentration depth profiles from an electroless nickel coated sample after exposure to the SO_2 test for three hours

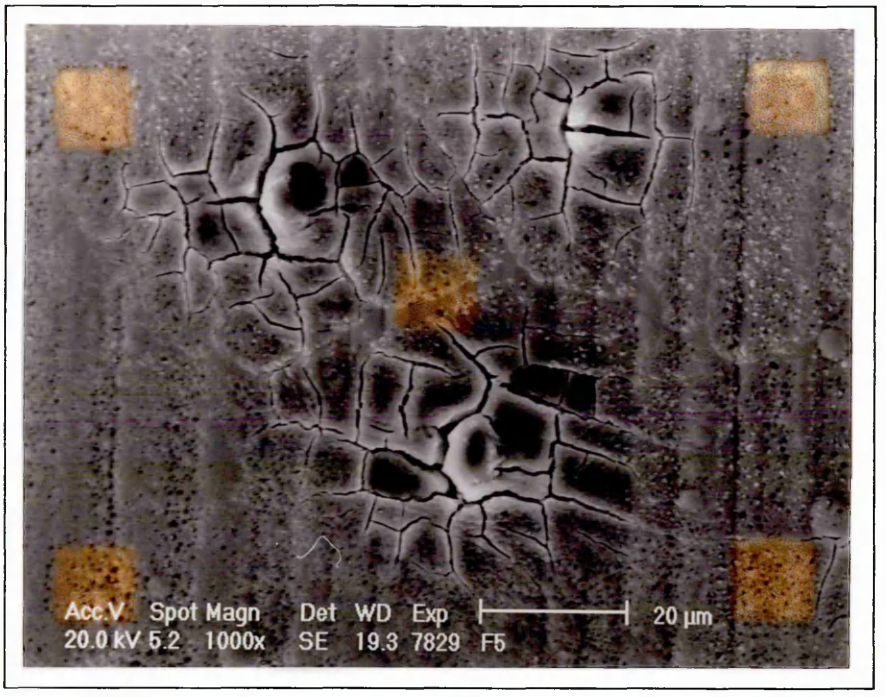

Figure 49 Electroless nickel sample after exposure to the SO_2 test for 15 hours

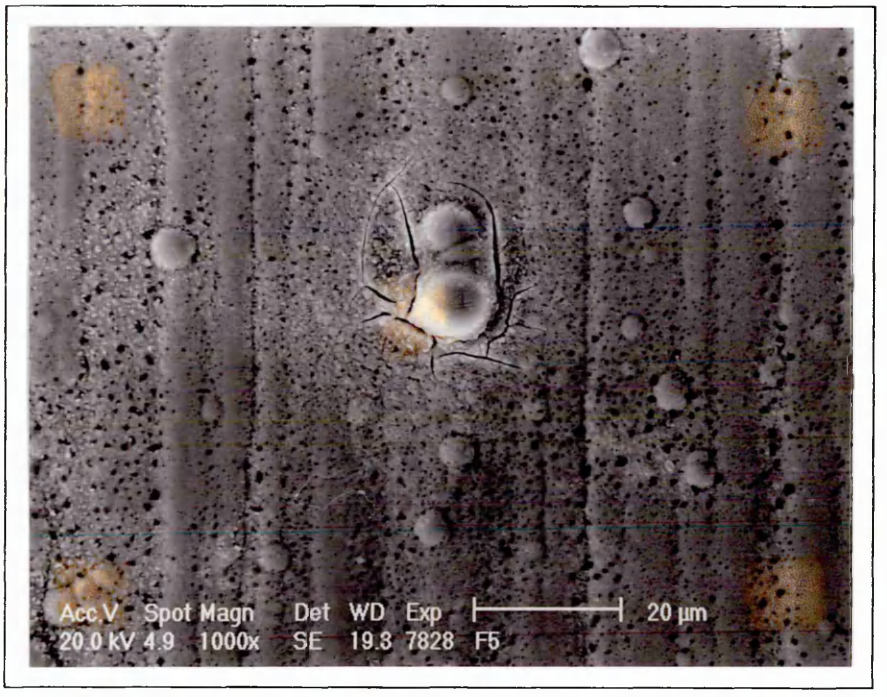

Figure 50 Electroless nickel sample after exposure to the SO_2 test for 15 hours

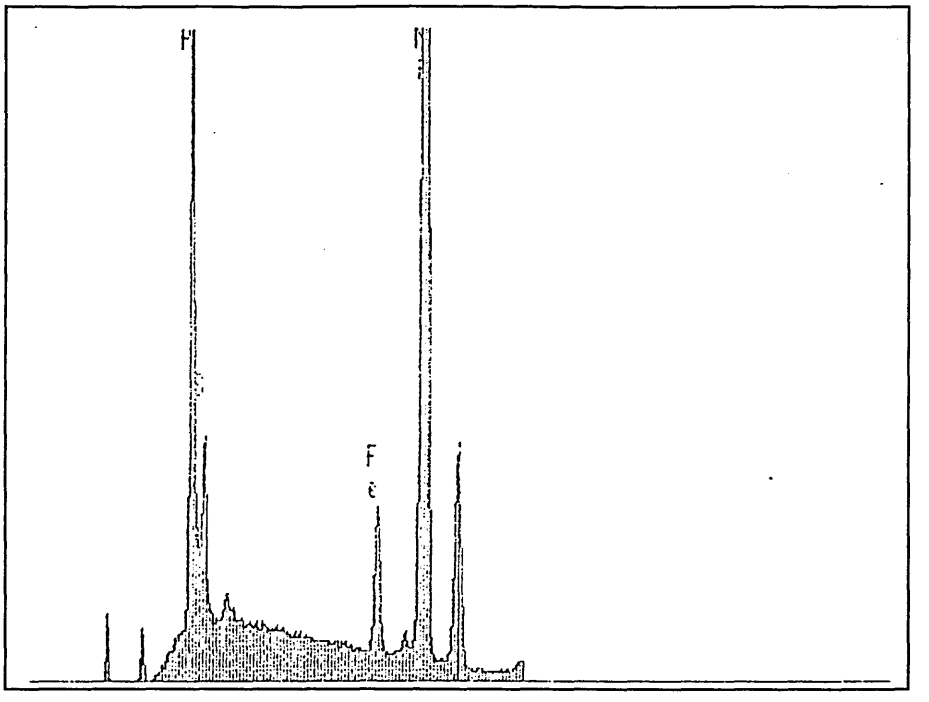

Figure 51 EDX analysis of an electroless nickel surface exposed to the SO_2 test for 15 hours

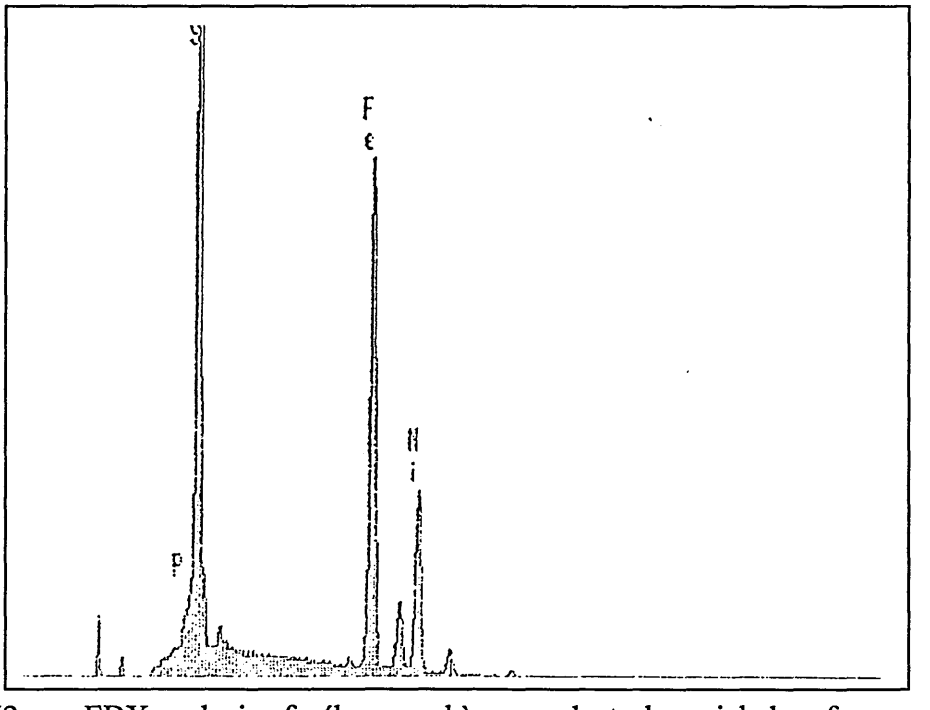

Figure 52 EDX analysis of a 'hummock' on an electroless nickel surface exposed to the SO_2 test for 15 hours

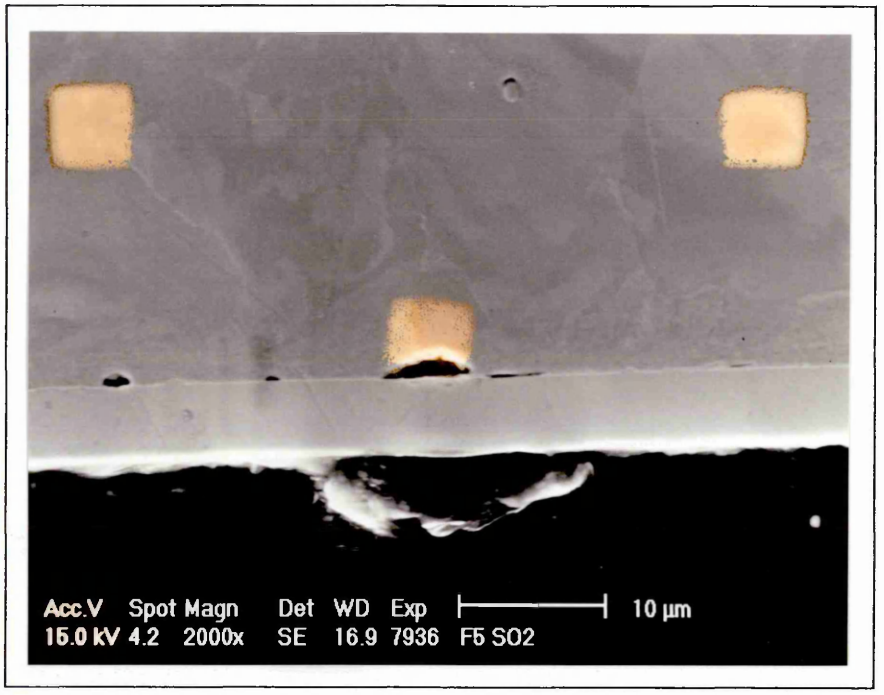

Figure 53 Metallographic cross-section of an electroless nickel coated sample after exposure to the SO_2 test for 15 hours

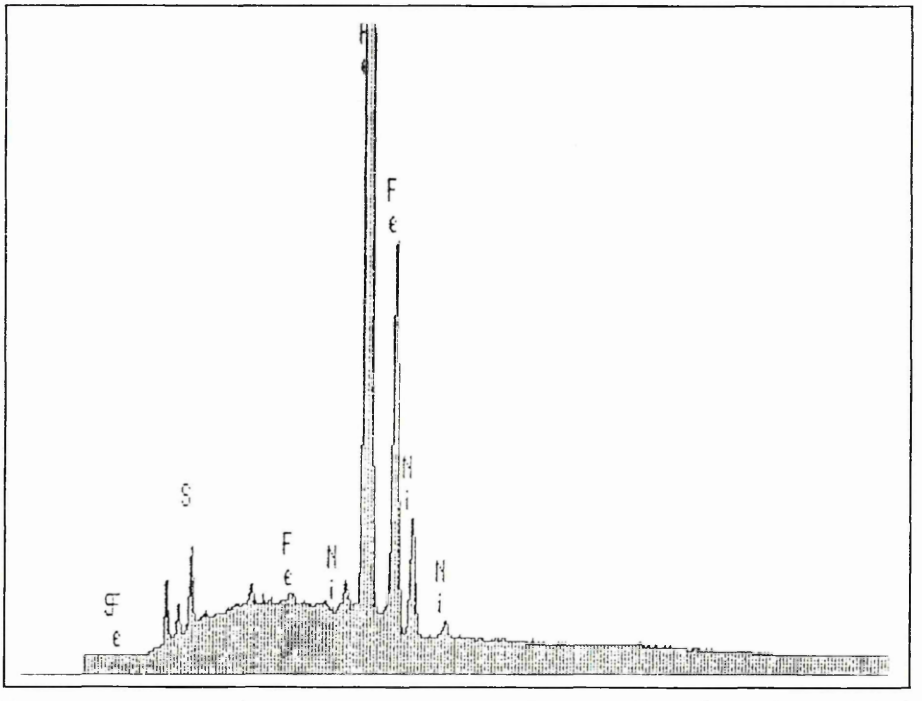

Figure 54 EDX analysis of a 'hummock' on the top of an electroless nickel coating

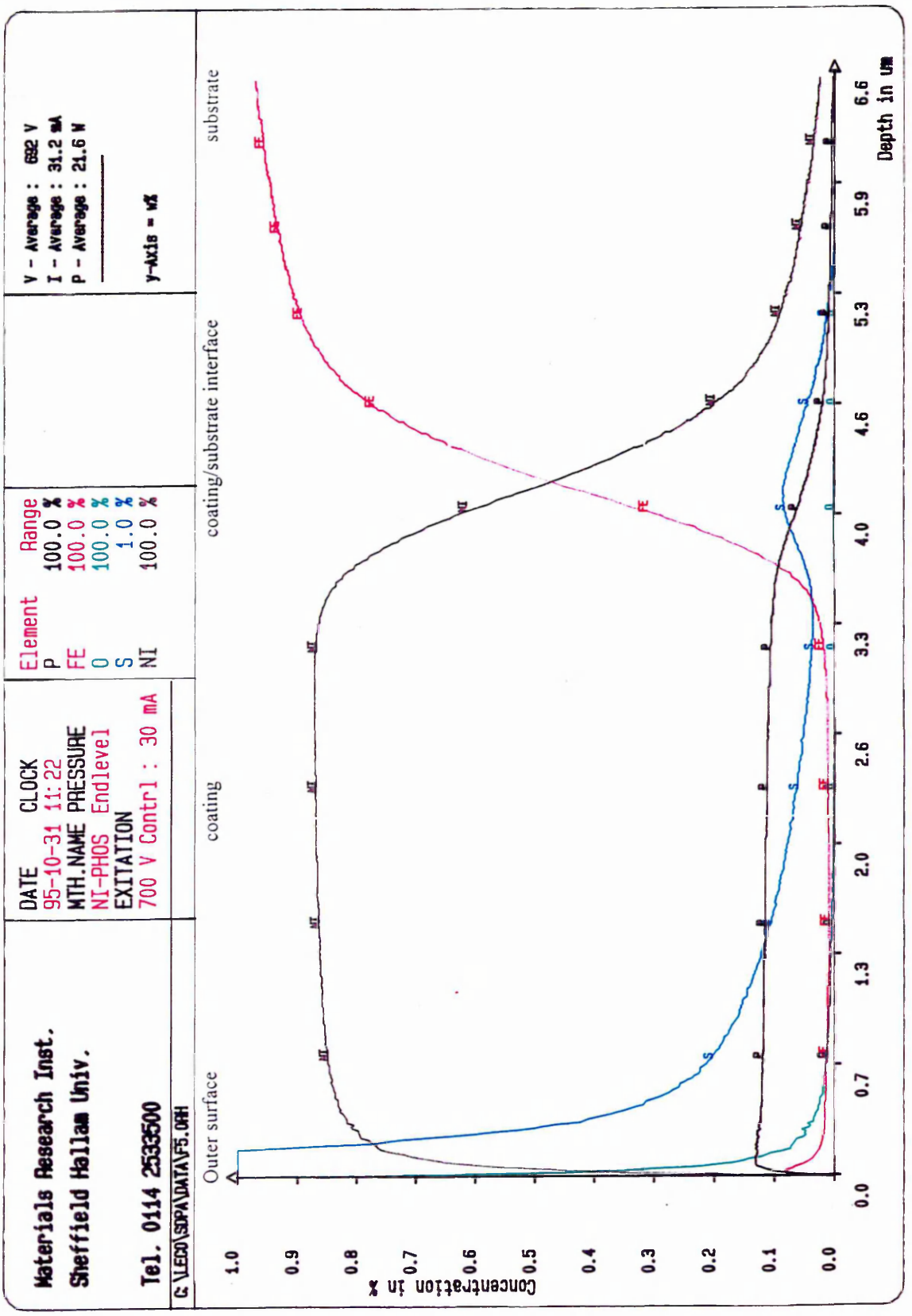

Figure 55 Elemental concentration depth profiles for an electroless nickel coated sample after exposure to the SO_2 test for 15 hours

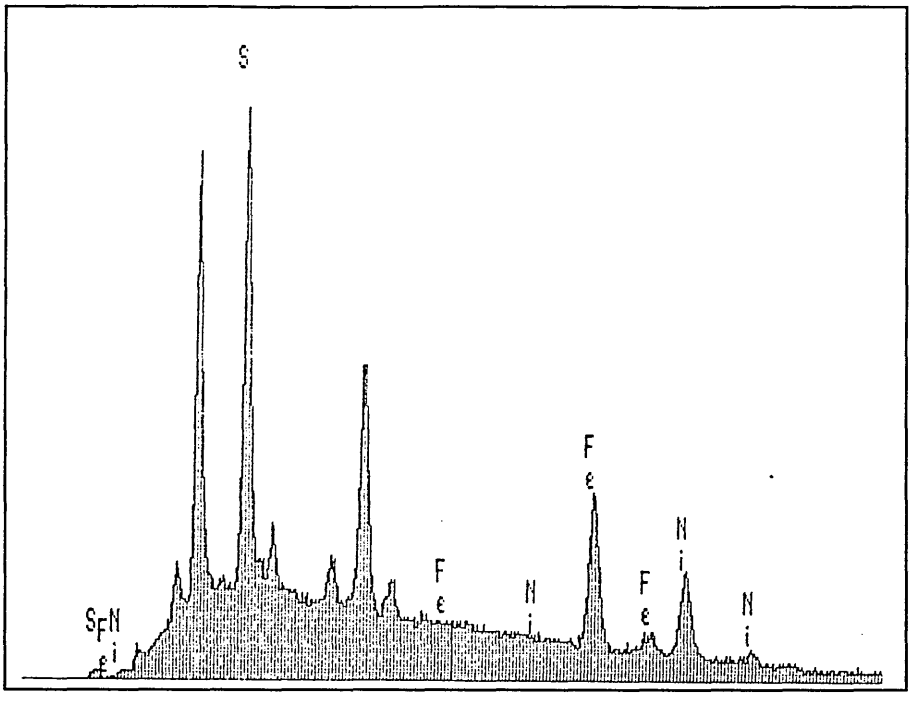

Figure 56 EDX analysis of corrosion products formed underneath an electroless nickel coating

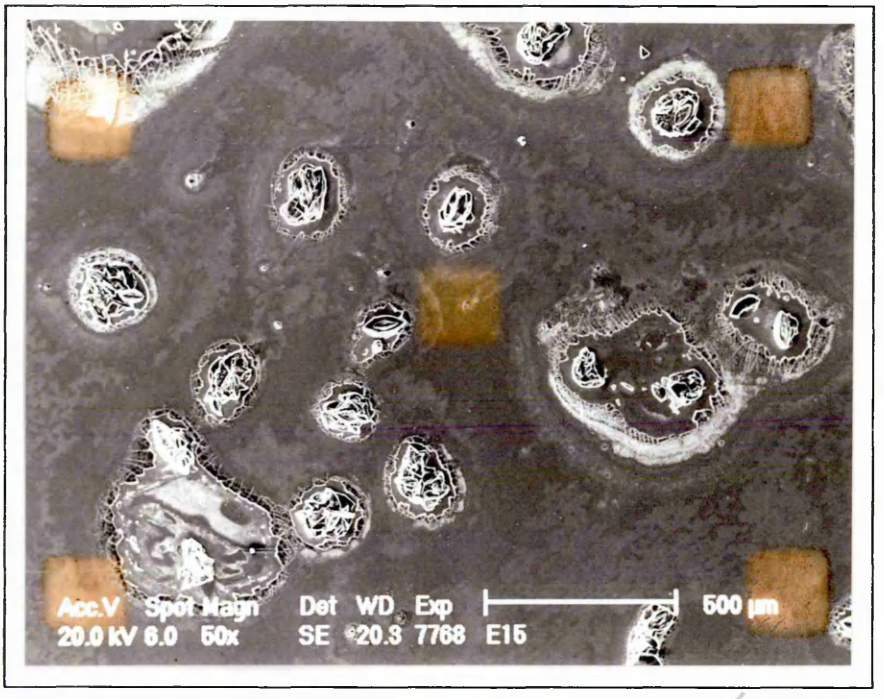

Figure 57 SEM picture of an electroless nickel coated sampel after exposure to the SO_2 test for 72 hours

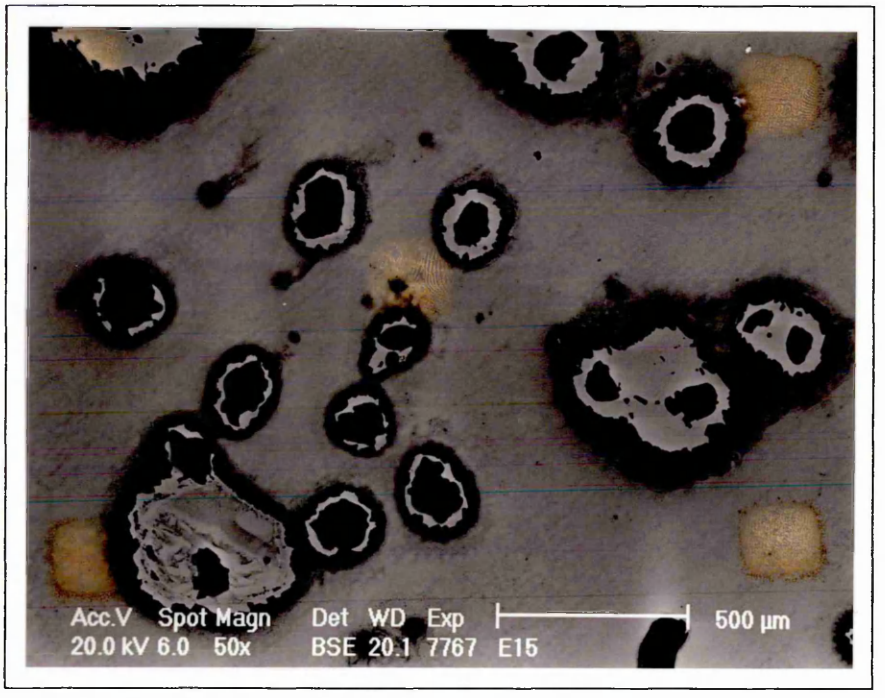

Figure 58 An electroless nickel coated sample after exposure to the SO_2 test for 72 hours (obtained using backscattered electrons)

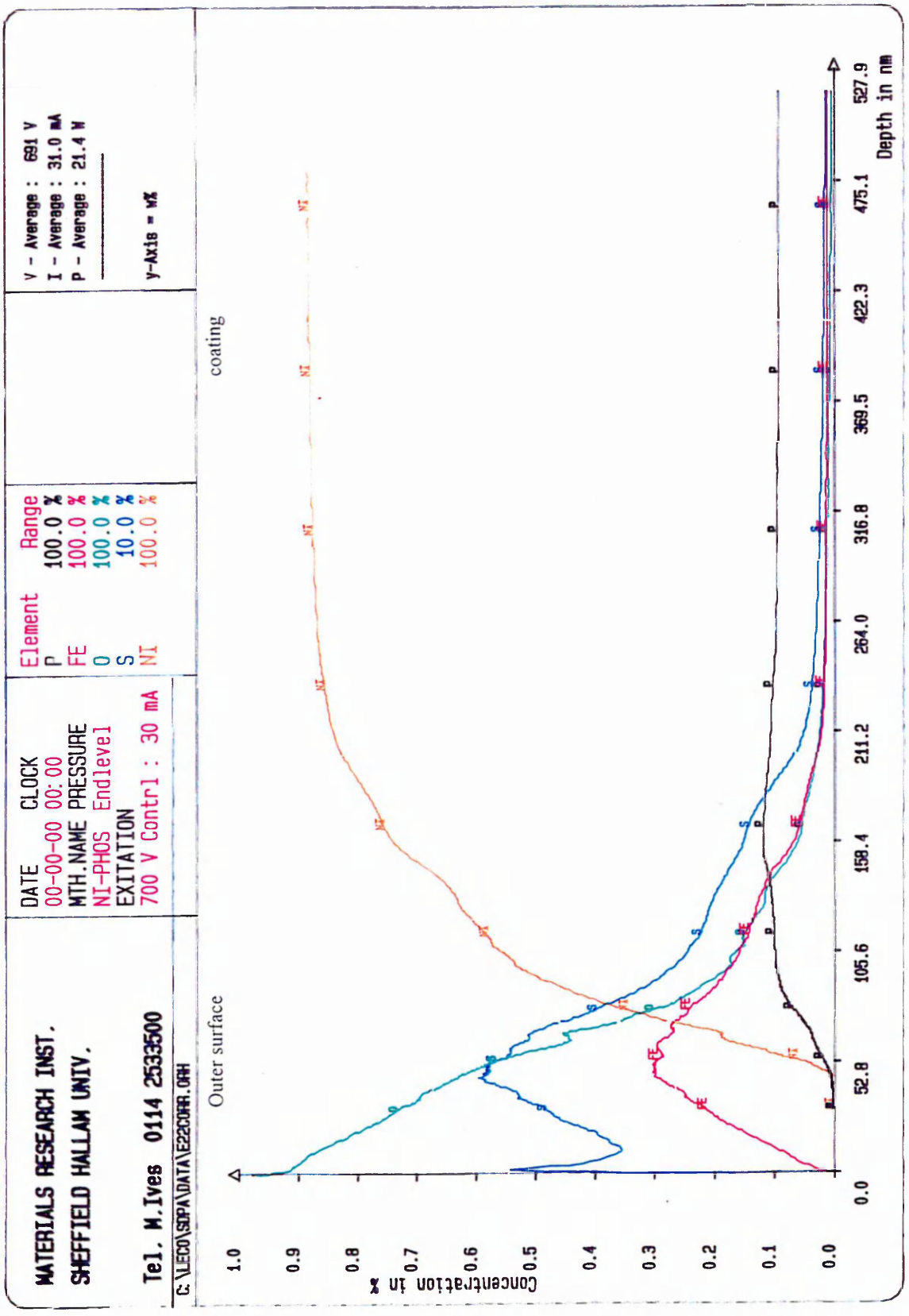

Figure 59 Elemental concentration depth profiles for an electroless nickel coated sample after exposure to the SO_2 test for 72 hours

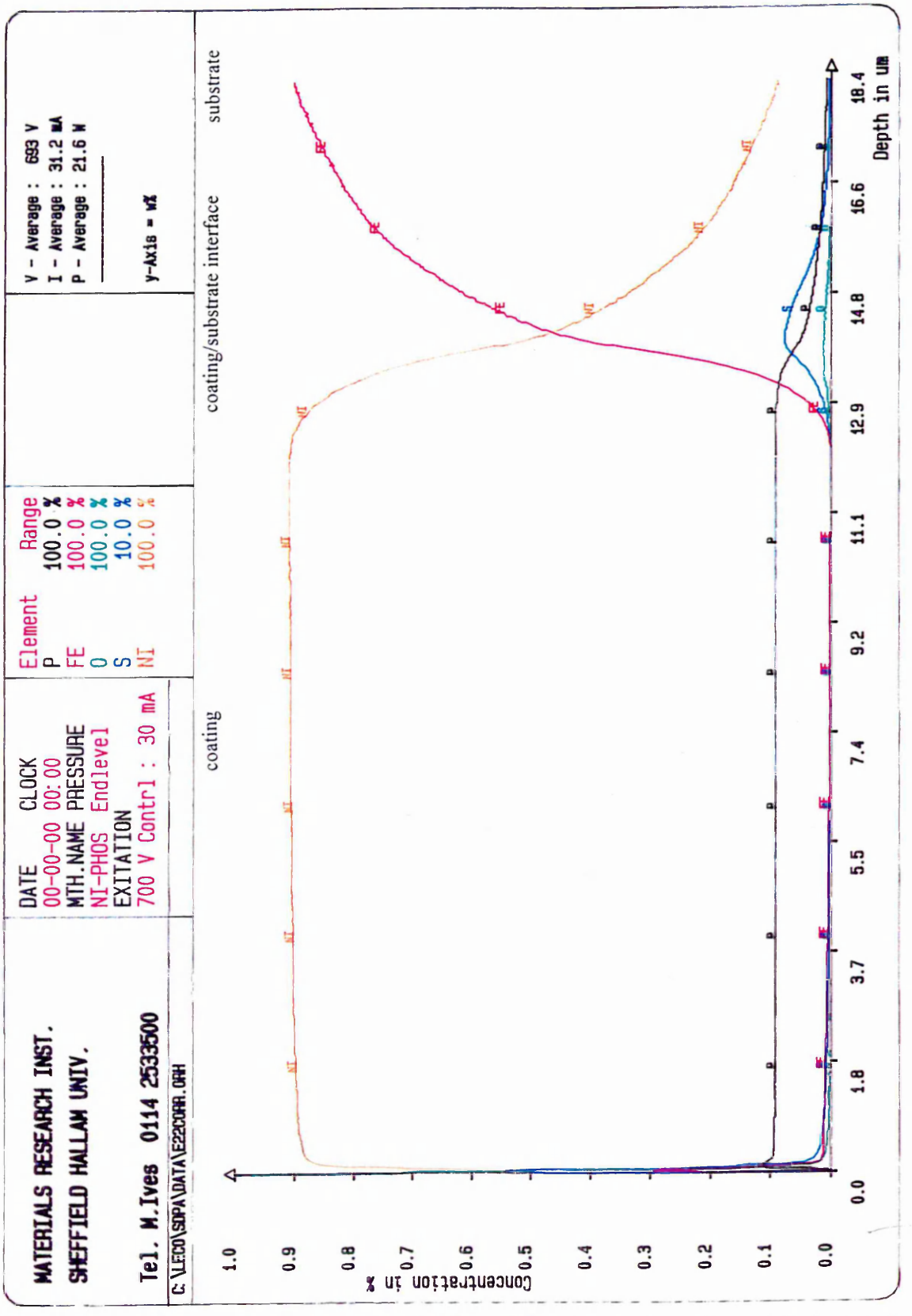

Figure 60 Elemental concentration depth profiles for an electroless nickel coated sample after exposure to the SO_2 test for 72 hours

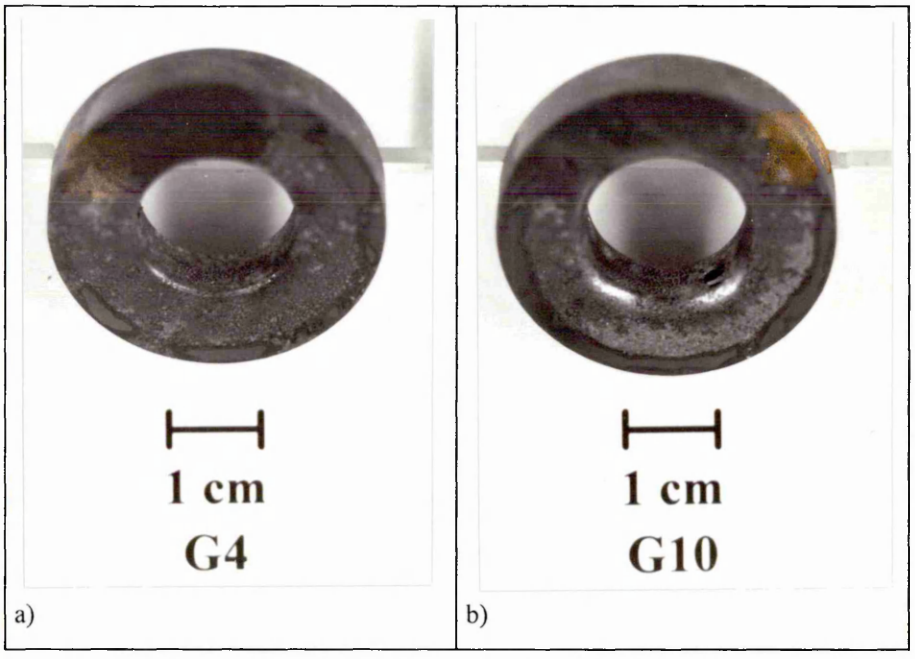

Figure 61 Electroless nickel coated samples having ´shoulders`, with a) 0.5 mm and b) 2.5 mm radii respectively, after exposure to the SO_2 test for 40 hours

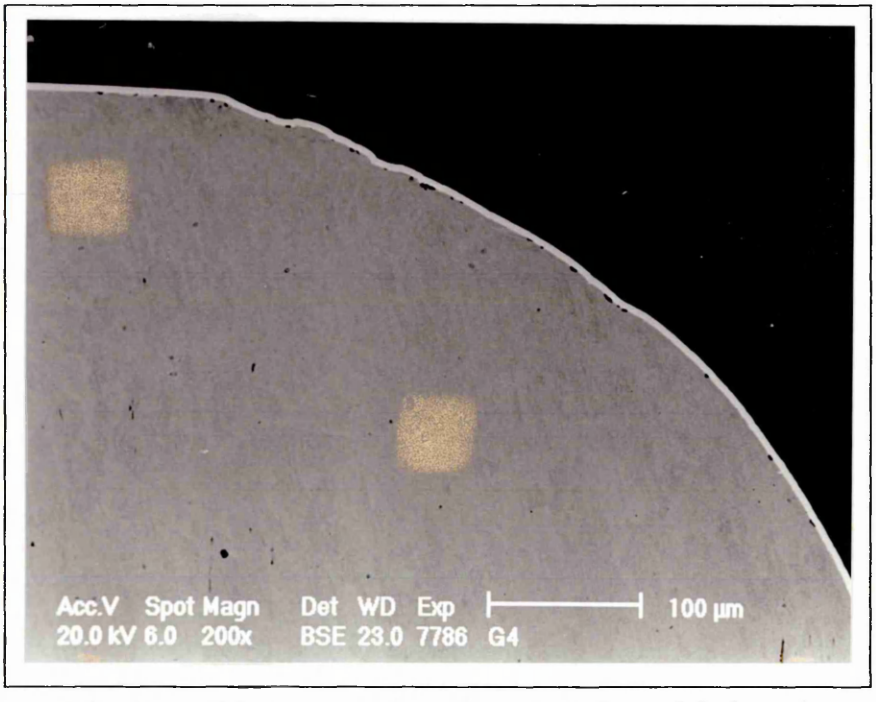

Figure 62 Metallographic cross-section of an electroless nickel coating on a surface with a ´shoulder radius` of 0.5 mm

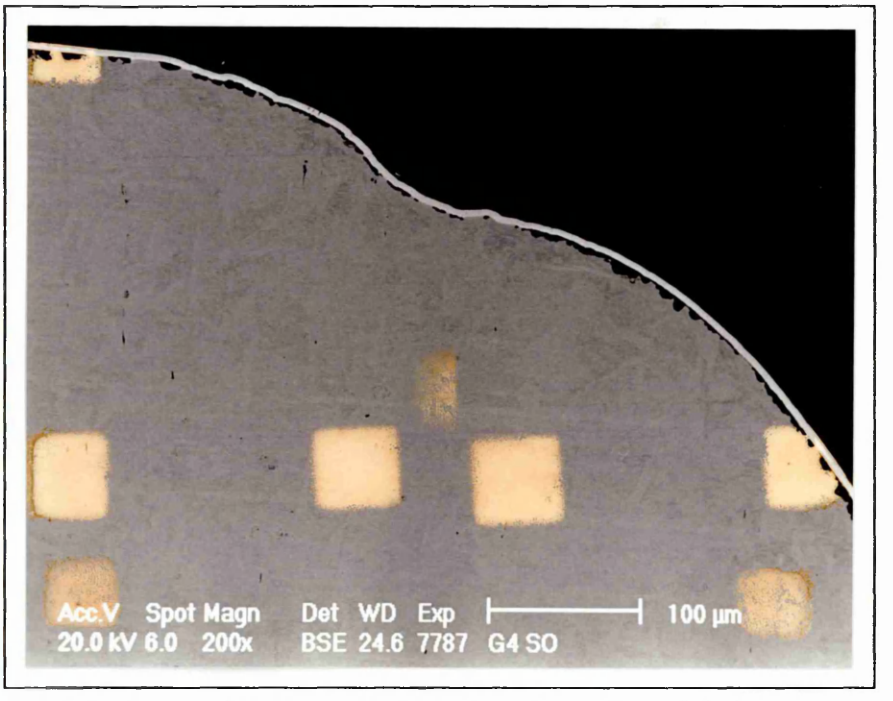

Figure 63 Metallographic cross-section of an electroless nickel coating on a surface with a ´shoulder radius` of 0.5 mm after exposure to the SO_2 test for 40 hours

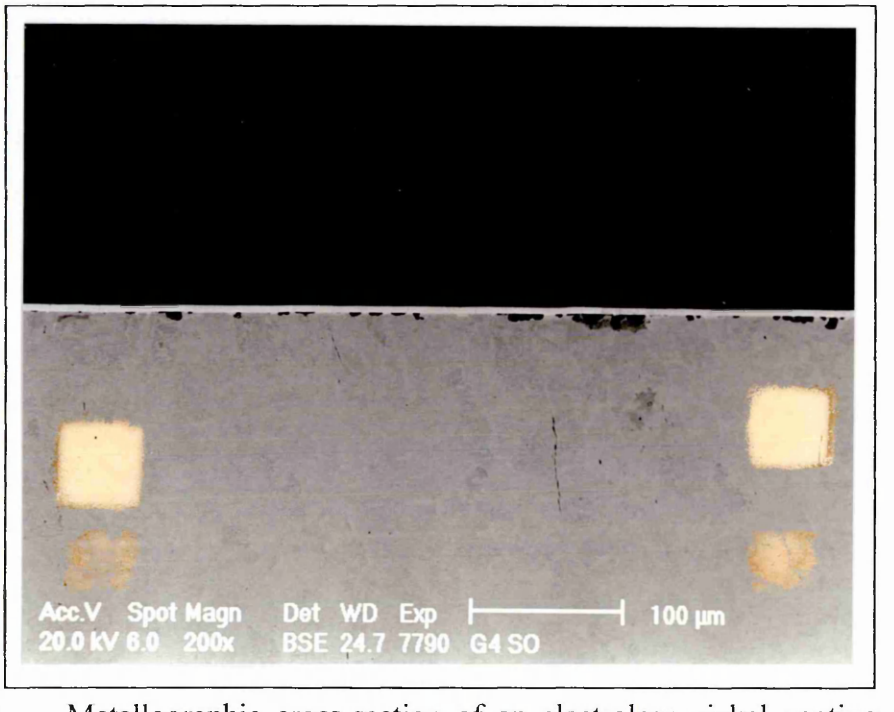

Figure 64 Metallographic cross-section of an electroless nickel coating on a flat surface after exposure to the SO_2 test for 40 hours

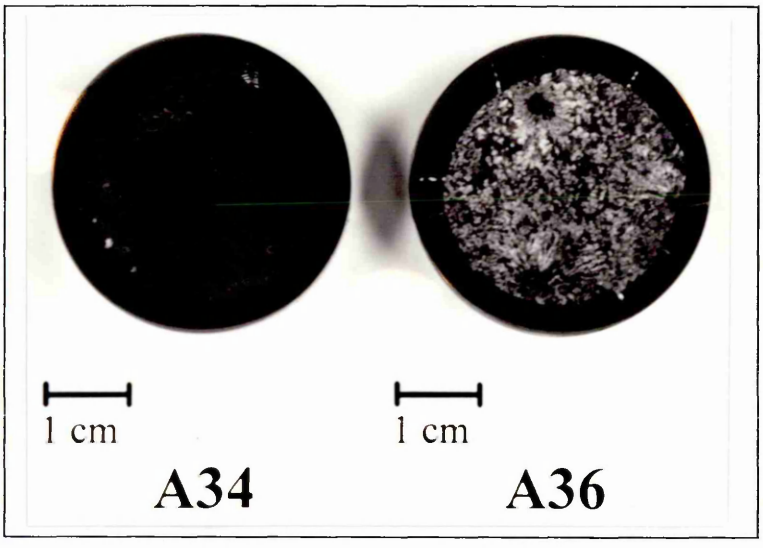

a) (TiAl)N coated sample exposed for 12 h

b) (TiAl)N coated sample exposed for 24 h

Figure 65 (TiAl)N coated samples after exposure to the SO_2 test

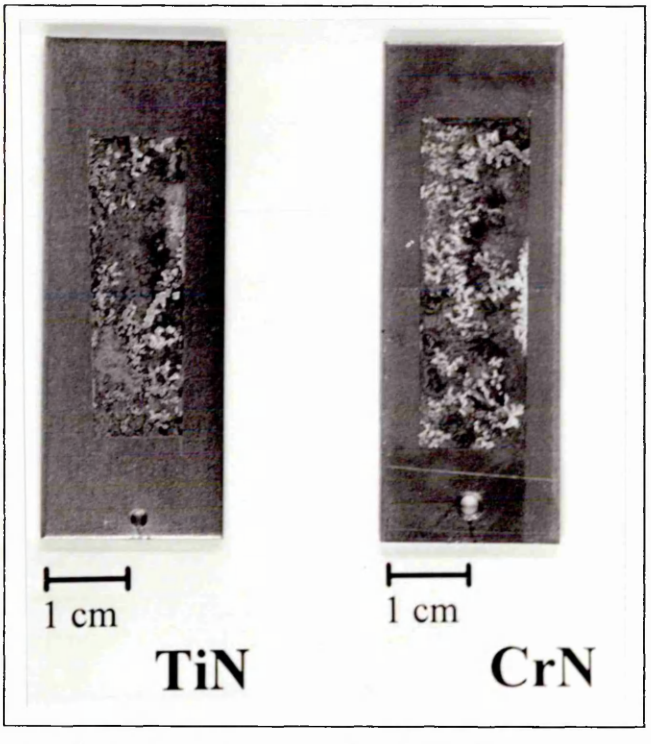

a) TiN coated sample exposed for 24 h

a) CrN coated sample exposed for 24 h

Figure 66 TiN and CrN coated samples after exposure to the SO_2 test

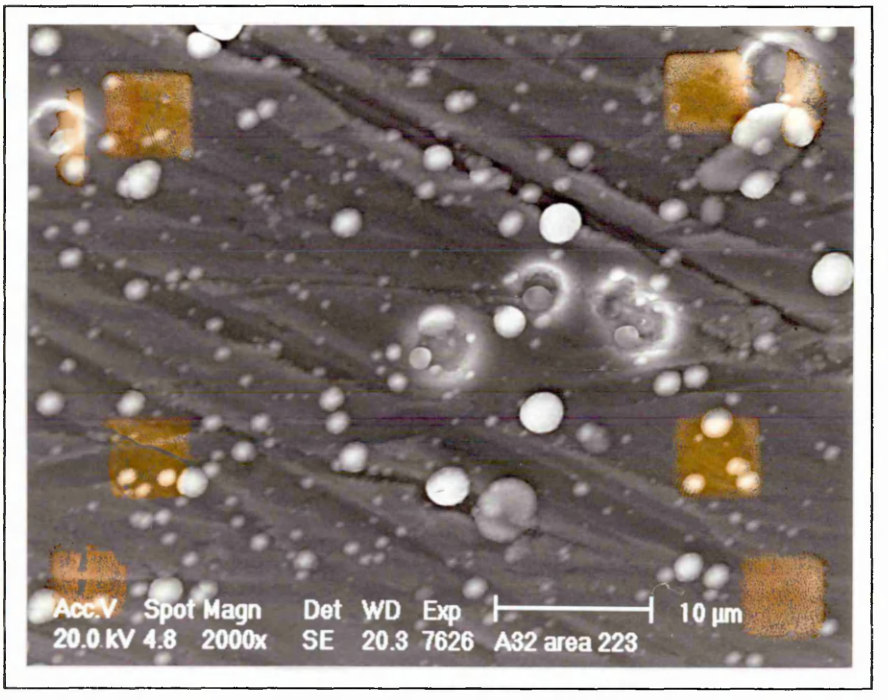

a) (TiAl)N coated sample before exposure to the SO_2 test

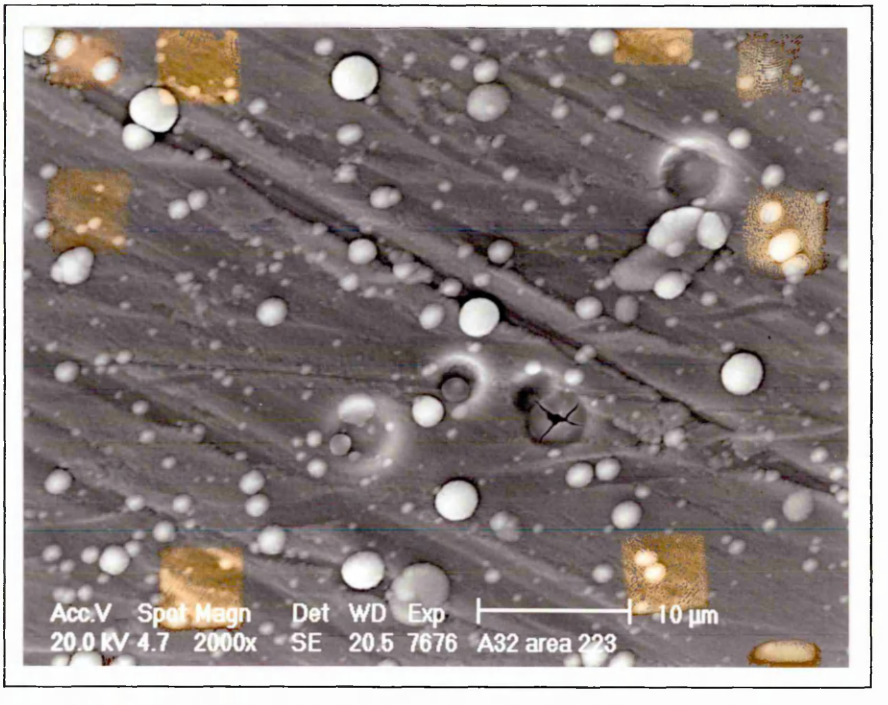

b) (TiAl)N coated sample after exposure to the SO_2 test for an hour

Figure 67 (TiAl)N coated sample a) before and b) after exposure to the SO_2 test for one hour

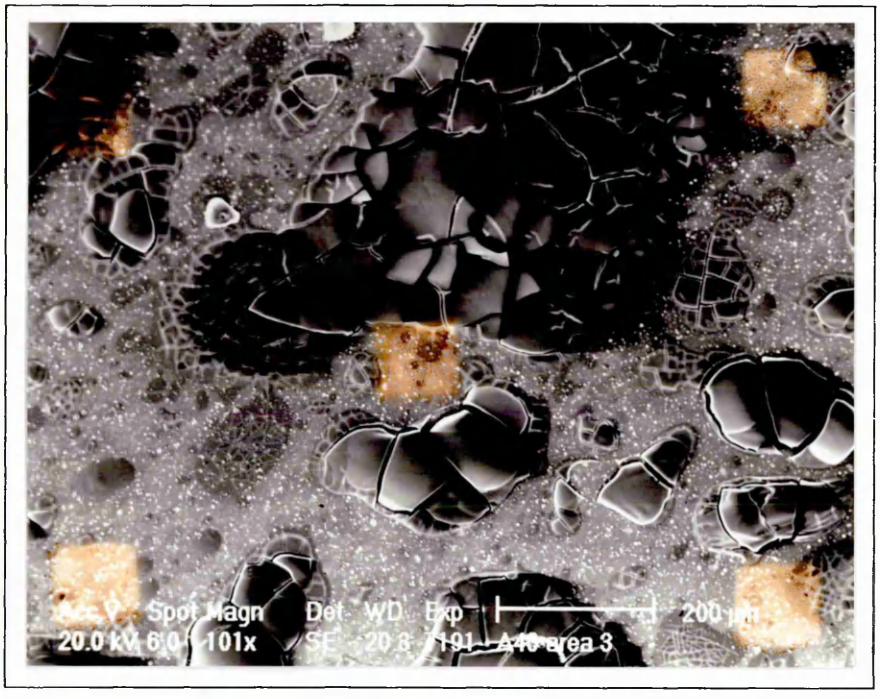

Figure 68 (TiAl)N coated sample after exposure to the SO_2 test for two hours

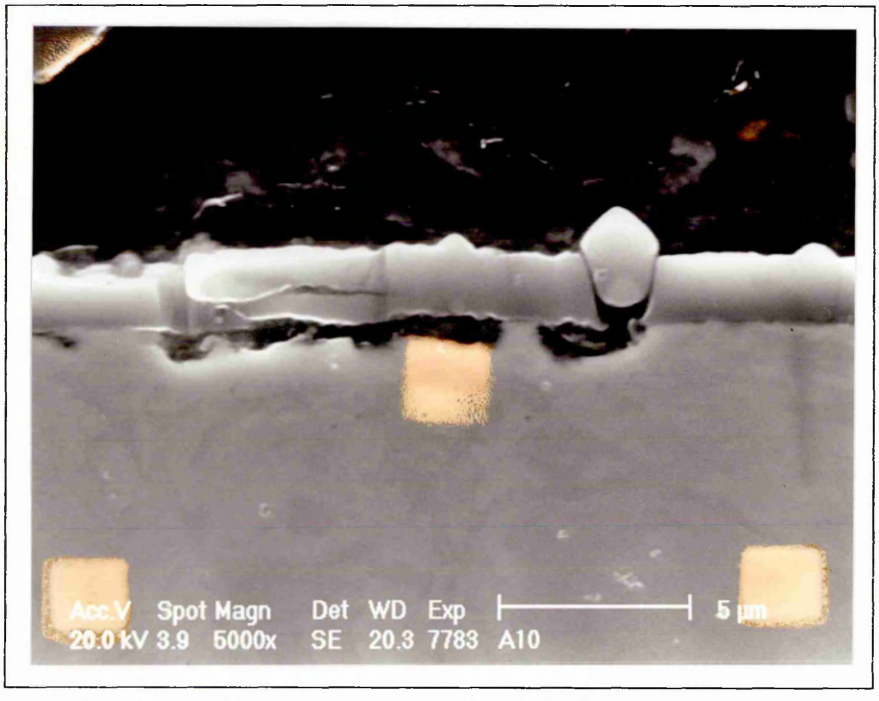

Figure 69 Metallographic cross-section of a (TiAl)N coated sample after exposure to the SO_2 test for two hours

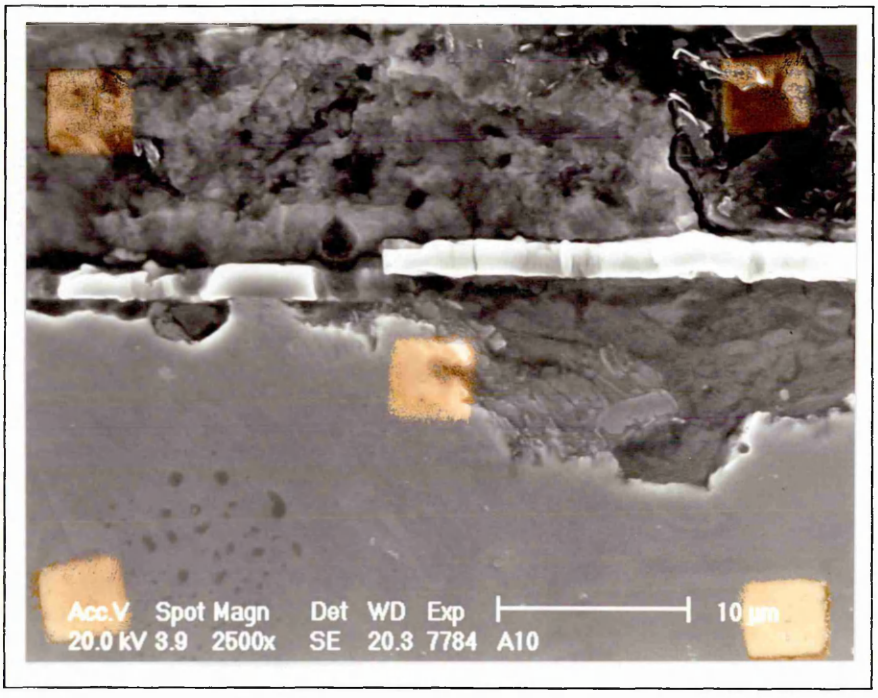

Figure 70 Metallographic cross-section of a (TiAl)N coated sample after exposure to the SO_2 test for two hours

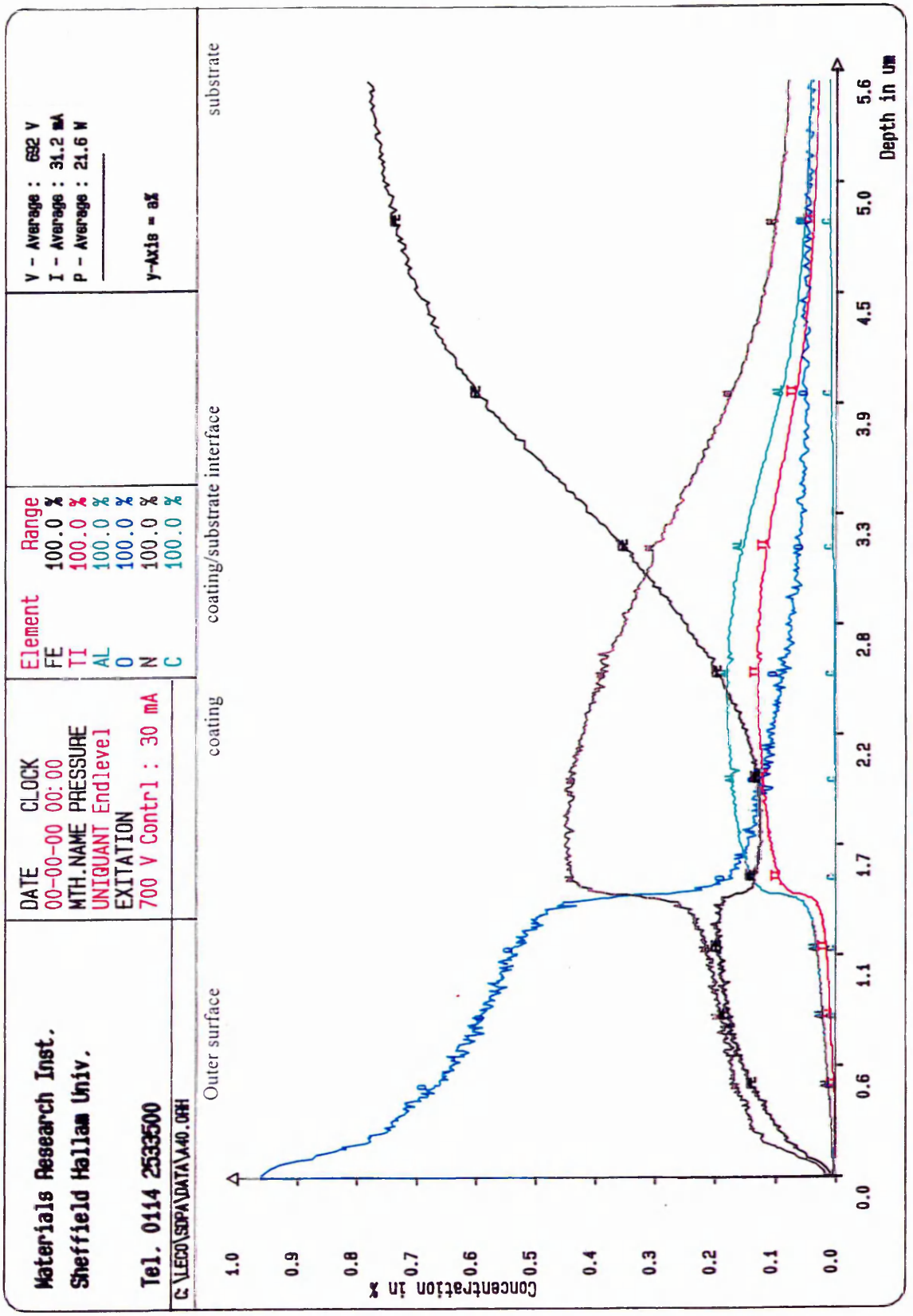

Figure 71 Elemental concentration depth profiles of a (TiAl)N coated sample after exposure to the SO_2 test for 4 hours

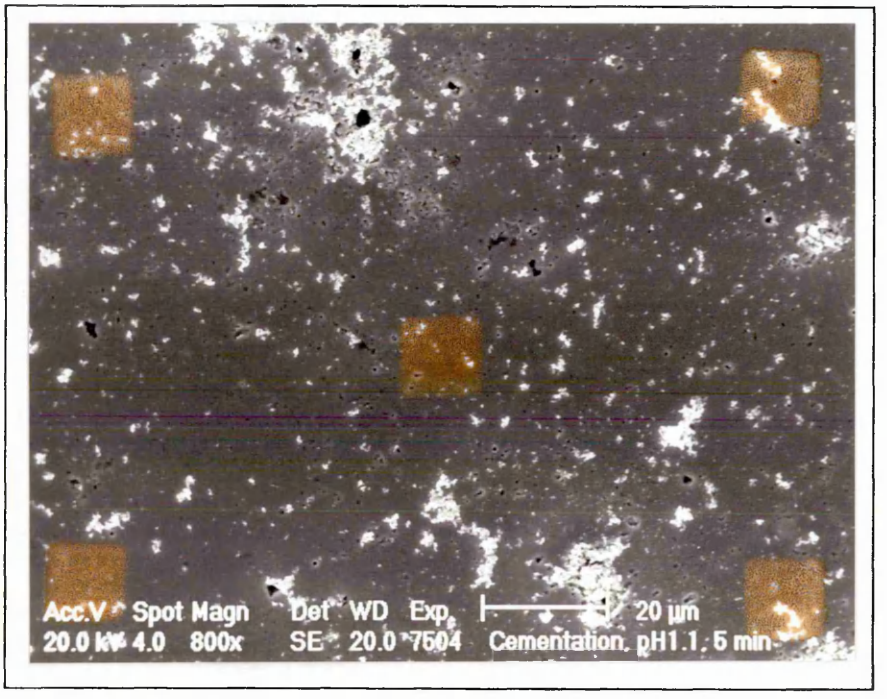

Figure 72 Mild steel after exposure to the cementation solution

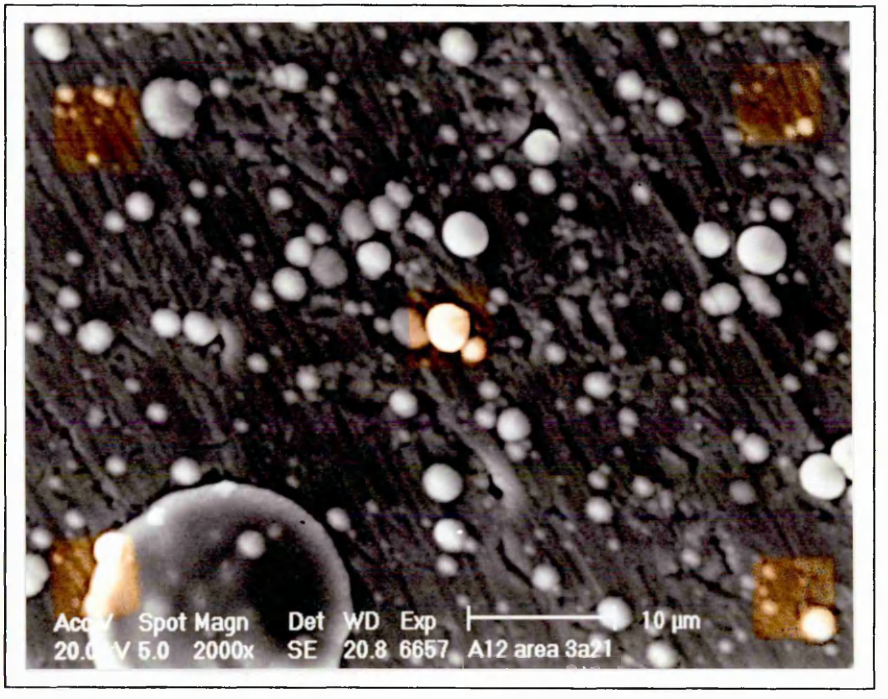

a) (TiAl)N coated sample before cementation test

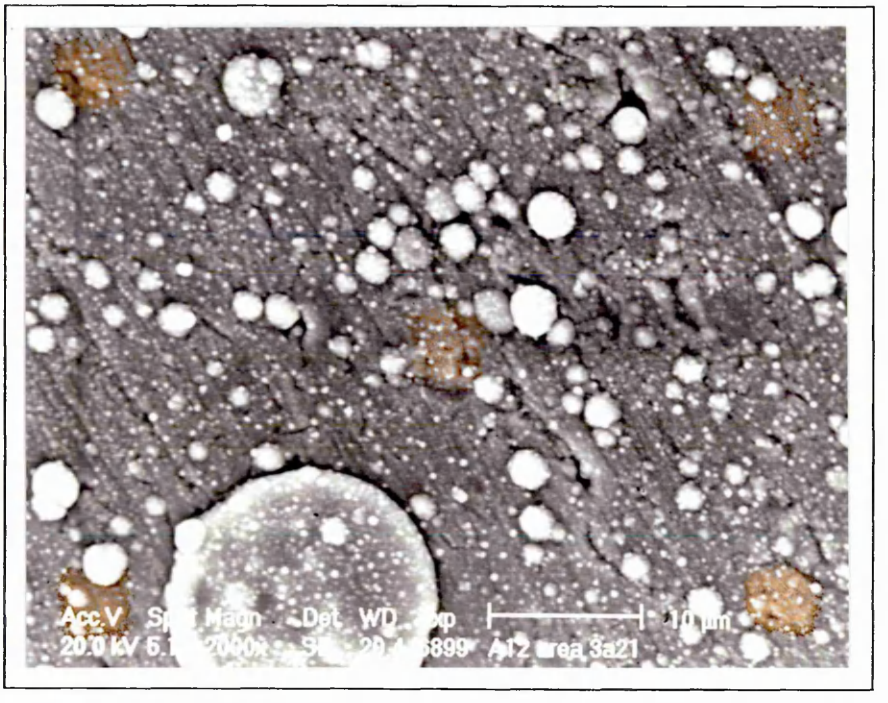

b) (TiAl)N coated sample after cementation test, pH = 1.1

Figure 73 (TiAl)N coated sample a) before and b) after cementation test, pH = 1.1

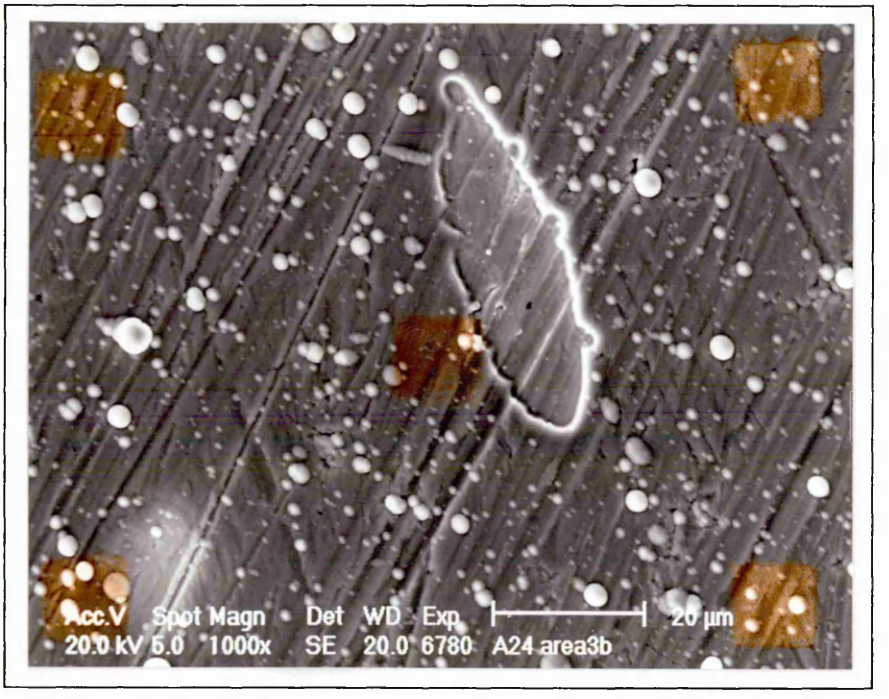

a) (TiAl)N coated sample before cementation test

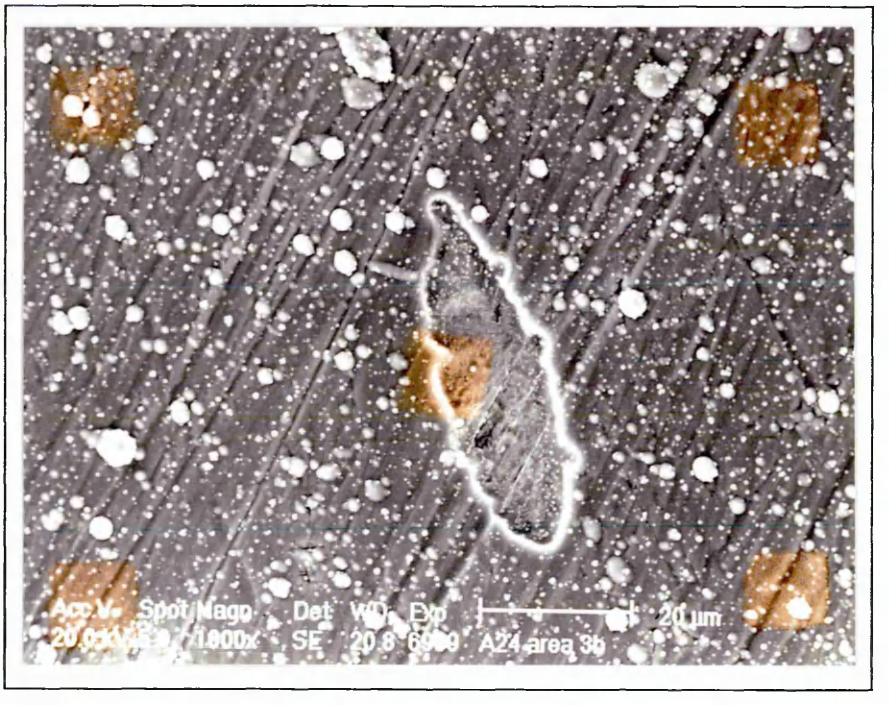

b) (TiAl)N coated sample after cementation test, pH = 5.5

Figure 74 (TiAl)N coated sample a) before and b) after cementation test, pH = 5.5

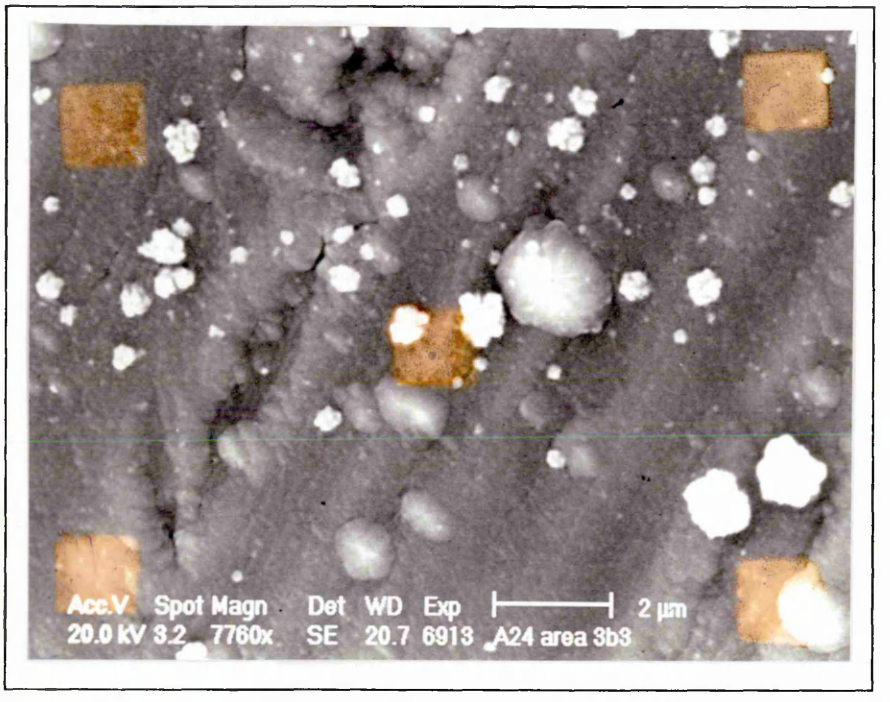

Figure 75 (TiAl)N coated sample showing ´cauliflower` like precipitates following cementation test

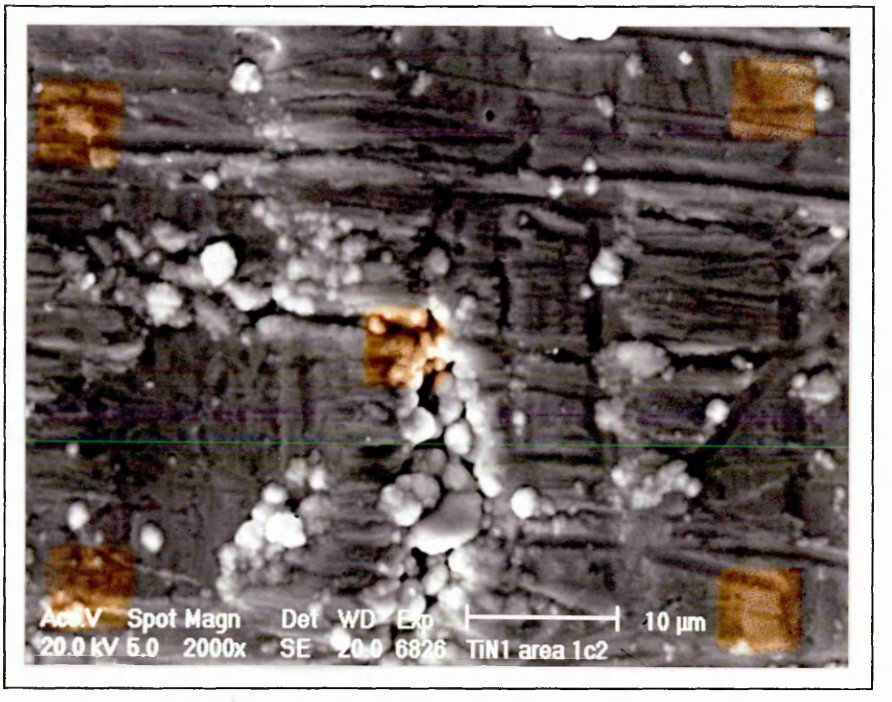

a) TiN coated sample before cementation test

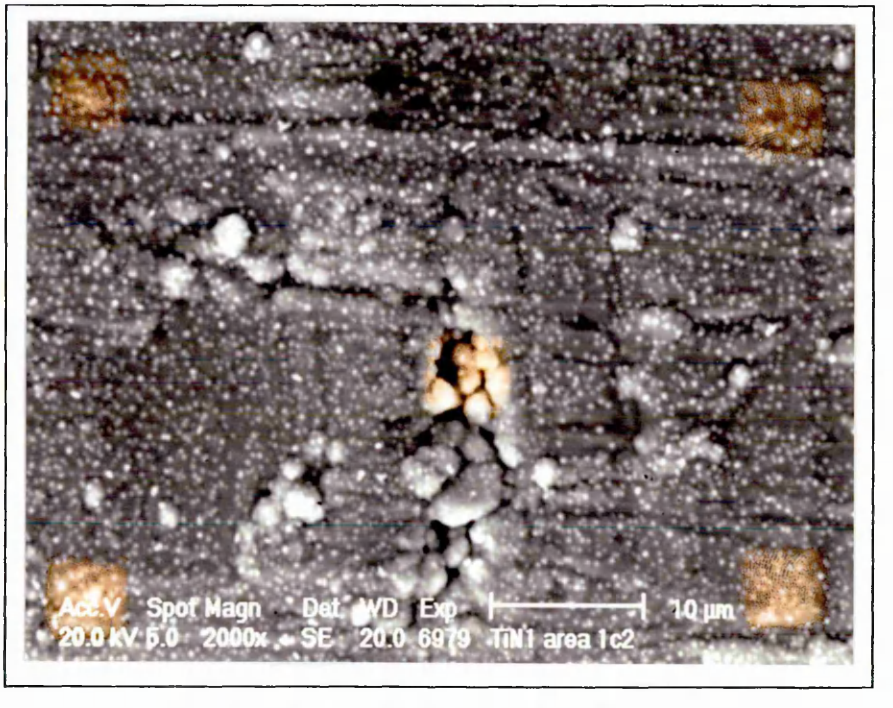

b) TiN coated sample after cementation test, pH = 1.1

Figure 76 TiN coated sample a) before and b) after cementation test, pH = 1.1

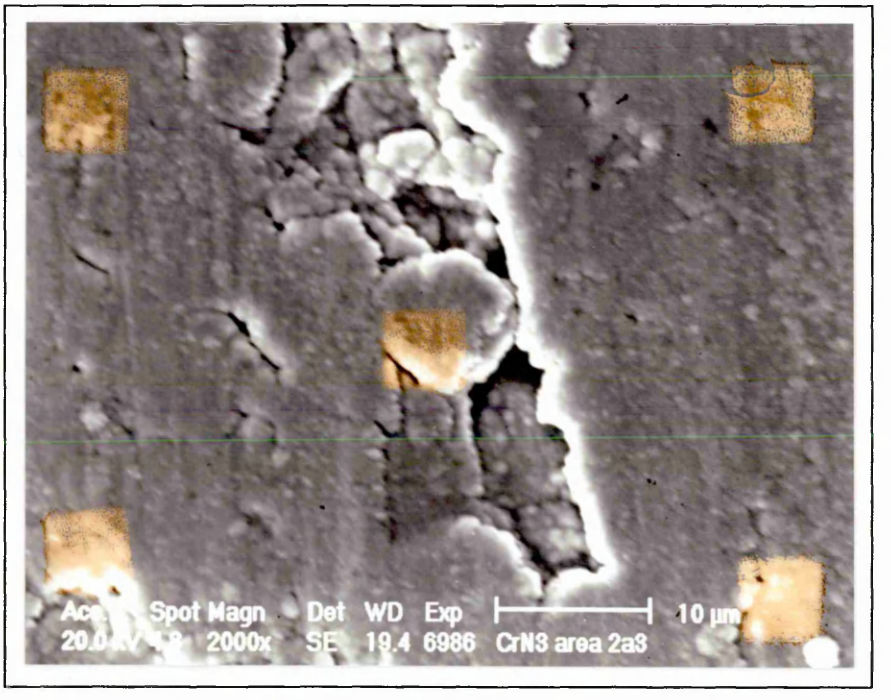

a) CrN coated sample before cementation test

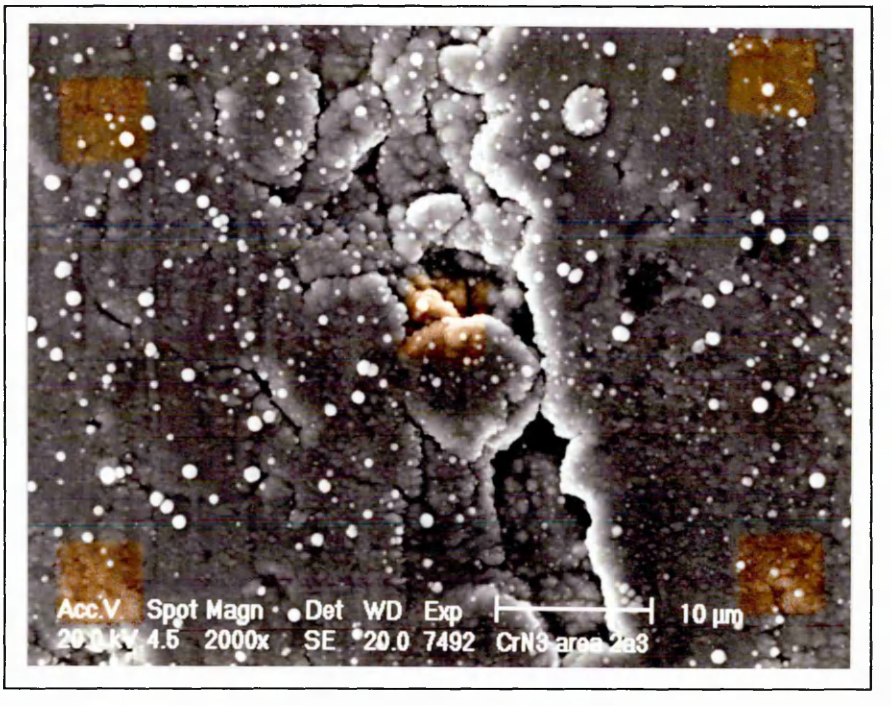

b) CrN coated sample after cementation test, pH = 1.1

Figure 77 CrN coated sample a) before and b) after cementation test, pH = 1.1

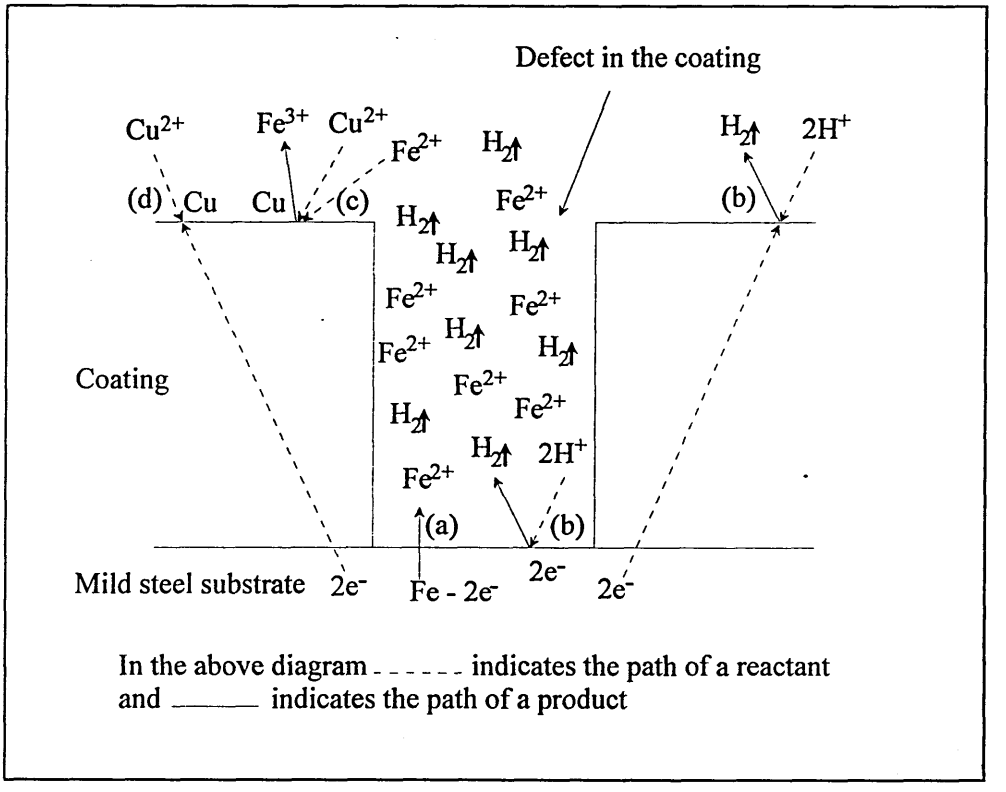

Figure 80 Schematic diagram of modified cementation process at a defect in a coating surface